Biotechnological strengthening of flood embankments.

Including applicability based on experiments, and concepts close to industrial application

Date: **January 2013**

Report Number: **WP04-01-12-12**
Version Number: 2_0_Pn

Deliverable Number: D4.1
Due Date for Deliverable: 31/05/12
Actual Submission date: 24/01/13
Task Leader: Maaike Blauw, Deltares

FloodProBE is co-funded by the European Community Seventh Framework Programme for European Research and Technological Development (2009-2013)
FloodProBE addresses "Technologies for Improved Safety of the Built Environment in Relation to Flood Events"
Start date: PU November 2009, duration: 4 Years

Document Dissemination Level PU

PU = **Public**	
PP = **Restricted to other programme participants (including the Commission Services).**	CL restricted = **Classified with the mention of the classification level restricted "Restraint UE"**
RE = **Restricted to a group specified by the consortium (including the Commission Services).**	CL confidential = **Classified with the mention of the classification level confidential "Confidential UE"**
CO = **Confidential, only for members of the consortium (including the Commission Services).**	CL secret = **Classified with the mention of the classification level secret "Secret UE"**

Document Information

Title	Report on bio-technological strengthening of flood embankments, including the applicability based on experiments, and concepts close to industrial application
Lead Author	Maaike Blauw, Marien Harkes
Contributors	Vera van Beek, Andre Koelewijn, Miranda van Wijngaarden, Geeralt van den Ham.
Distribution	Public
Report Number	WP4-R-12-12

Document History

Date	Version	Prepared by	Organisation	Approved by	Notes
24/09/2012	1_0_Pn	Maaike Blauw, Marien Harkes	Deltares	Rutger de Graaf	
05/12/2012	2_0_PN	Maaike Blauw	Deltares	Mark Morris	

Acknowledgement

The work described in this publication was supported by the European Community's Seventh Framework Programme through the grant to the budget of the FloodProBE project, Grant Agreement Number 243401.

Summary

This report describes the results of activities executed for FP7 FloodProBE task 4.1 to develop and test cost-effective and sustainable construction technologies to increase the flood resilience of the built environment, with a focus to improve the performance of existing and new flood defences. The sustainable construction technology tested for the feasibility of increasing flood resilience is the bio-based in situ strengthening technique called BioGrout. The application of BioGrout technology is tested and optimized to prevent, permit retrofit and to repair geotechnical failure mechanisms in flood defences.

For urban flood defences, internal erosion, involving the removal of sand, forms an important potential type of failure that eventually leads to inundation of the hinterland. Internal erosion occurs when groundwater velocity, driven by a hydraulic head difference across the flood defence during a flood, exceeds a critical value. If internal erosion below a point structure is suspected to threaten the stability of the structure, this can only be investigated by means of extensive and, hence, costly leak detection monitoring techniques (e.g. tracer, temperature or self-potential methods). Alternatively, traditional measures for mitigating (potential) internal erosion problems, such as reduction of the groundwater flow velocity by means of installation of sheet piles or local grout injection can be adopted. These, however, are also often costly or otherwise undesired, for example, when the water defence has certain historical value.

BioGrout is an innovative technology for *in situ* strengthening of unconsolidated sediments using bacteria. This technique enables sustainable improvement of the erodibility of sandy soils by building calcium carbonate bridges between the sand grains through microbial processes. Contrary to traditional grout injection methods, BioGrout can be applied without a significant reduction of the permeability of the sand. The feasibility of BioGrout has been tested through lab experiments. Small-scale experiments and Hole Erosion Tests (HET) have shown the possibility of using BioGrout to prevent backward erosion. Also the effectiveness of BioGrout for preventing backward erosion has been investigated with both small-scale and medium-scale experiments, and computer models have been used to determine the implications for practice.

The main conclusion from this research is that BioGrout is a technology that is suitable to prevent backward erosion in flood defences. By applying BioGrout the critical head required to initiate internal erosion is increased at least three times, sufficient to withstand higher water levels in rivers and a rise in sea level. A key advantage of BioGrout is that it can be applied in situ with light material, causing no disturbance in the surroundings and can hence be used at locations where access is limited. . However, the costs to apply BioGrout are substantial, making it a high grade technology. Also the production of ammonium chloride means that large volumes of BioGrout should not be used; it will be mainly used at locations where other techniques cannot offer an acceptable solution.

However, in the future, more and more flood defences (and multifunctional dikes) will be built or raised. These structures, and in particular where a hard structure is built into a dike (i.e. transitions), are locations with a higher risk for erosion. These point locations, where erosion might occur, could be treated very well by using BioGrout.

Contents

Tables

Figures

1 Introduction

Global warming is expected to lead to more severe storm and rainfall events as well as to increasing river discharges and sea level rise. This means that flood risk is likely to increase significantly. Furthermore, 80 % of the population will live in urban areas by 2020 and the economic values in these areas are constantly growing. This means that flood risk in urban areas will increase disproportionately. Improved identification and upgrading of weak links in flood defence systems will increase the cost-effectiveness of flood protection investments significantly. The principal aim of FloodProBE is to provide cost-effective means for flood risk reduction in urban areas. One of the key principles of the FloodProBE project is “Improving the performance of urban flood defences”. Urban flood defences comprise both soft soil embankments and hard structures. Failures are very often caused by internal erosion processes, particularly at transitions between defence types. Complex combinations of defence types are typical in urban areas. Since flood defence systems are only as strong as the weakest links, these have to be identified, assessed and strengthened. In FloodProBE methods, tools and technologies are developed for all three aspects.

The objective of FloodProBE Task 4.1 is to develop and test cost-effective and sustainable construction technologies to increase the flood resilience of the built environment, with a focus to improve the performance of existing and new flood defences. The sustainable construction technology tested for the feasibility of increasing flood resilience is the bio-based in situ strengthening (increased erosion resistance) technique called BioGrout. In FloodProBE, the application of BioGrout technology has been tested and optimized to prevent, allow retrofit and to repair geotechnical failure mechanisms in flood defences. This report (deliverable D4.1 Bio-technological strengthening of flood embankments, including the applicability based on experiments, and concepts close to industrial application”, contains results of experiments and computer models to test the feasibility and applicability of BioGrout on flood embankments for preventing internal erosion. The cost-effectiveness for industrial application of BioGrout is also taken into account by combining knowledge gained from field tests (not executed in the FloodProBE-project) and lab-experiments performed in FloodProBE.

For urban flood defences, internal erosion involving the removal of sand forms an important potential type of failure that eventually may lead to inundation of the hinterland. Especially transitions between soft embankments and hard structures (e.g. sluice, foundations) appear to be weak spots. However, prediction of internal erosion at these transitions is often problematic, as potential leakage paths are difficult to identify. Prerequisites for internal erosion are the presence of an unfiltered exit, erodible soil and a sufficiently high hydraulic gradient, resulting in increased seepage flow. Where internal erosion below a point structure is suspected of threatening the stability of the structure, this suspicion can only be refuted by means of extensive and hence, costly leak detection monitoring techniques (e.g. tracer, temperature or self-potential methods). Alternatively, traditional measures for mitigating (potential) internal erosion problems can be adopted. These measures mainly involve an increase in the potential leakage path or blocking of the (potential) internal erosion channels by means of construction of berms, filter constructions, installation of sheet piles or (local) grout injection. They are, however, often costly and include sometimes undesired effects, for example, when the water defence has certain historical value or there is lack of space (for berms).

Several modes of internal erosion in or below flood defences can be distinguished; the most important are (1) backward erosion, (2) suffusion and (3) erosion by concentrated leakage through pre-existing paths and (4) contact erosion (D3.1.1). With respect to transitions between soft embankments and hard structures mode (1) and (3) are most relevant. Due to its dominant influence on the safety of a flood defence system, preventing internal erosion is still a challenging research field. It is the reason for assessing the feasibility of BioGrout technology as a new measure for preventing internal erosion. BioGrout is a method to adapt the soil properties and is induced by bacteria when flushing the soil with specific nutrients.

BioGrout may prevent internal erosion by cementing the grains to each other while the water flow is hardly influenced. The latter aspect is an especially important advantage compared with (traditional) grout injection techniques, since reduction of the permeability of the treated soil will often lead to transference of the internal erosion problems to adjacent, untreated parts of the soft embankment, instead of solving the erosion problem. Furthermore, in urban areas a non-destructive flushing technique is an advantage compared to traditional internal erosion prevention techniques that will substantially hinder and damage the existing area, due to, for example, settlement, excavations or vibrations. Several successful large-scale tests and pilots have been carried out with BioGrout, from 1 m^3 up to 400 m^3 with different types of permeable soils (sand and gravels). These tests were performed to assess the applicability of upscaling BioGrout.

The main goal of the research done in the FloodProBE-project for Task 4.1, and described in this report, was to evaluate the suitability of BioGrout as an alternative internal erosion prevention technique. First the state of the art of BioGrout is described, to identify gaps and needs in knowledge to determine whether BioGrout is a suitable alternative method for preventing internal erosion underneath flood defence systems. The process and state of the art of BioGrout are described in chapter two (summary of report WP04-01-10-09). An experimental plan, based on the gaps and needs identified in chapter 2, was set up. With small and medium scale lab-experiments and computer models the possibility and feasibility of BioGrout as internal erosion prevention technique is assessed. The experimental plan is presented in chapter 3. The methods of the laboratory experiments are described in chapter 4 and the results are discussed in chapter 5. The computer modelling to apply BioGrout in the field is discussed in chapter 6, followed by a description of the industrial application of BioGrout in chapter 7.

2 State of the art of BioGrout

2.1 BioGrout Process

BioGrout is an innovative biotechnology for sandy soil improvement in terms of mechanical strength and stiffness. From a PhD study at Murdoch University in Australia (Whiffin 2004) the feasibility of the *in-situ* strengthening of sand was shown. Deltares has developed the BioGrout technology in terms of knowledge and applicability. The technology is based on Microbial In situ Carbonate Precipitation (MICP). There are several (M)ICP methods in development worldwide. At Deltares two different methods have been studied, urease-based and denitrification-based. BioGrout principles and production for both methods are described by Van Paassen (2010). Currently, the denitrification-based BioGrout process is in a fundamental research phase and not ready to be applied in the field. For this reason, this study focuses on the urease-based BioGrout method. With urease-based BioGrout (referred from now on as BioGrout), carbonate is produced through the hydrolysis of urea. *Sporosarcina pasteurii*, an ureolytic bacterium, able to produce large amounts of the intracellular enzyme urease, hydrolyzes urea, producing carbonate and ammonium ions:

$$CO(NH_2)_2 + 2H_2O \rightarrow CO_3^{2-} + 2NH_4^+$$

In the presence of calcium (injected as a salt e.g. calcium chloride), the carbonate precipitates forming calcium carbonate crystals that bond the sand particles together (Figure 1):

$$Ca^{2+} + CO_3^{2-} \leftrightarrow CaCO_3(s)$$

The result of this process is an increase in mechanical strength and stiffness of the soil, whilst keeping a significant portion of the original materials' permeability. The waste product is ammonium chloride, which has to be removed and treated.

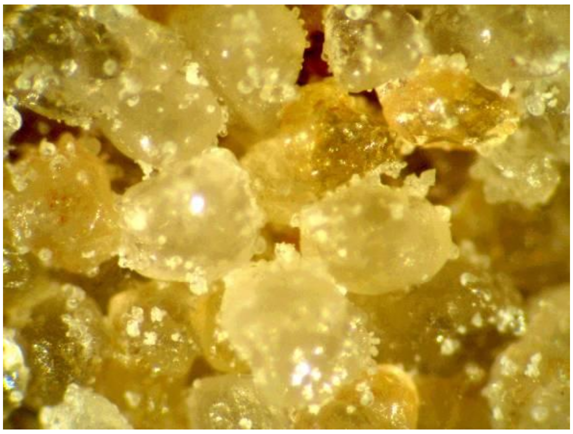

Figure 1 Picture of BioGrout treated sand grains

2.2 BioGrout development

Since 2005, BioGrout technology has been developed with the aim "Can BioGrout be applicable at field scale to obtain ground improvement by means of an in situ process". This paragraph, describes the state of the art of BioGrout urease-based process and is based on the results of laboratory experiments and upscale experiments performed between 2005 and 2009.

Optimization of the growth of ureolytic bacteria Sporosarsina pasteurii

Sporosarsina pasteurii is the key of the BioGrout process as it provides the urease, but the optimal growth conditions of the bacteria are not similar to the optimal conditions for synthesis of urease. Therefore, it is investigated under which growth conditions (medium, temperature, pH) the maximum rate of urease production occurs (Whiffin et al., 2007).

Obtaining a controllable process: optimization of applying BioGrout

For field application, the BioGrout process should be controllable. Therefore, for optimizing the BioGrout process the following topics were investigated:

1. Homogenous strengthening of the treated soil:
   Bacteria can be distributed homogenously over the sand column, by using a fixation solution, achieving a homogenously strengthened sand volume. This is described in more detail by Whiffin et al. 2007 and Harkes et al. 2009.
2. The correlation between strength and amount of calcite formed:
   The strength is adjustable between 200 kPa and 30 MPa (concrete). A correlation between the amount of precipitated $CaCO_3$ and the mechanical parameters strength and stiffness of the treated material has been determined (Harkes et al. 2008) (Figure 2).
3. Permeability: the permeability of the treated soil decreases maximal with 30% when increasing the strength up to 15 MPa. The soil becomes impermeability with strengths above 15 MPa.
4. Effects of different parameters on the BioGrout process:
   Temperature, pressure, pH, salinity varies between sites. Enzymes are sensitive to external conditions, which can enhance, and (partially or fully) inhibit the rate of the reaction. Hence, the influence of extreme environmental and chemical conditions on the process has been studied.
   - Temperature: process is not hindered with temperatures between 5-70 °C.
   - Pressure: process is not hindered with pressure up to 80 bar.
   - Salinity has no effect on the bacterial activity or on the calcium carbonate precipitation.
   - pH: calcite dissolves in an acidic environment. This occurs significantly around pH 4, which is not reached ordinarily in the soil. Furthermore, most soils are buffered at pore level and the precipitated calcium carbonate will constitute the main buffer after the BioGrout process.

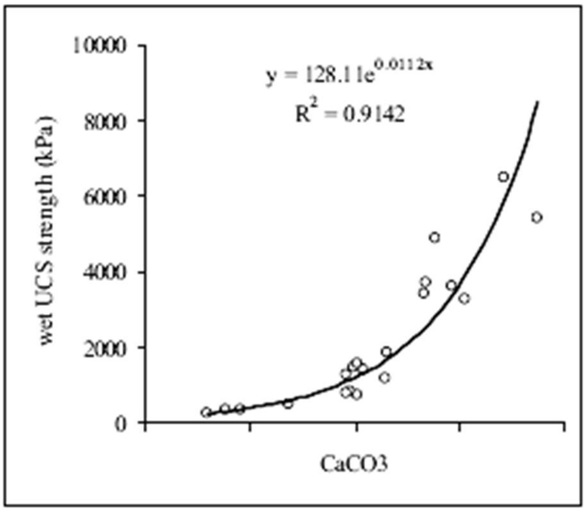

Figure 2 Correlation between strength and calcium carbonate content (Harkes et al. 2008)

Pilot scale development

The feasibility of BioGrout to improve strength and stiffness of sandy soil in the range of 300 kPa up to 20 MPa was demonstrated at laboratory scale on 16 cm sand columns (1D-flow). Later, the bio-cementation of a sand column over a distance of 5 meter have been performed (Whiffin et al. 2007).

Scale up from 1D to 2D (1m3)

The next step in the up-scaling process of BioGrout was a 2-dimensional (radial symmetric) flow experiment. By placing an injection point in the middle of a 1m^3 container from which injection took place towards the edges of the cube. A more-or-less spherical sand zone was consolidated (Figure 3).

Figure 3 Picture of the results of the cube experiment

Scale up from 2D to 3D (100 m^3)

Subsequently, a 100 m^3 container experiment was performed. A concrete container of 8 x 5.6 x 2.5 m was filled with loose sand to simulate a field application of BioGrout, but maintaining a closed system. The injection of the reagents and extraction of the effluents produced was carried out through three injection wells separated by a distance of ca 5 meters from three extraction wells (Van Paassen et al. 2010). 40 m^3 of sand was biologically cemented (Figure 4), which corresponded to the treated portion of the sand. There was a strong correlation between the final density of the cemented sand and strength.

Figure 4 40 m3 of biocemented sand strengthened with the BioGrout process

Field test: strengthening gravel for horizontal drilling

In 2010, the first BioGrout field test was executed to strengthen gravel for horizontal drilling, with positive results (figure 5). It is possible to apply BioGrout in the field, extracting and treating all the ammonium chloride, and commercial production of the bacteria (Van Paassen, 2010b).


Figure 5 **Cementing gravel for the horizontal drilling pilot near Nijmegen 2010.**

2.3 Boundary conditions BioGrout

Every location has its specific physical and chemical conditions that determine the feasibility of the application of BioGrout. The following boundary conditions have to be considered before applying BioGrout.

Soil permeability

Because the technique involves flushing of soil, the material to be treated must be sufficiently permeable (hydraulic conductivity >10^{-5} m/s). The application of BioGrout concerning permeability also depends on the depth BioGrout is applied. At larger depths the change on heave decreases, making it possible to apply high injection pressures, meaning that lower permeability's can be overcome. BioGrout has been successfully applied at lab and pilot scale in:

- Sand (>10^{-5} m/s)
- Sandy-soils, sand containing (low) amounts of gravel, peat, shells or clay
- Gravel

Soil conditions

The temperature in the soil and ground water must be between 5 – 70 ˚C, the maximum pressure in the soil 80 bar, and the pH above 4.

Saturation

BioGrout has only been applied, up to now, in saturated soils. It is unknown if it is possible and how homogenous the BioGrout would be for strengthening unsaturated soils. For application in unsaturated areas, additional research is needed.

Waste product

The BioGrout process produces concentrated ammonium chloride. This waste product needs to be extracted from the soil and treated before being discharged or re-used. The amount of ammonium chloride is proportional to the volume of treated soil and the required strength. Therefore, a maximum volume of soil can be treated. This volume depends not only on required strength, but also on regulations, location of waste water plant etc.

Costs

The main costs for applying BioGrout is the production of bacteria, the treatment of ammonium chloride and costs for urea/ calcium chloride. The costs depend per application (e.g. location, size, required strength), but are in the range of high-grade technologies (500 - 1000 €/ m^3).

2.4 Advantages of BioGrout

BioGrout has many advantages when compared to conventional techniques:

- Applied in situ, without soil displacement and influencing constructions in the surrounding areas.
- Large injection distance, at least 5 m between injection and extraction wells.
- Fast process: within 5-10 days, sufficient strength is obtained.
- Strength and stiffness are adjustable between 0.2 MPa and 50 MPa.
- Permeability is more or less maintained up to 10 MPa, hardly influencing the (ground) water flow.
- Light application material, making it usable for difficult to reach locations.
- Only calcite, a natural mineral, is left in the soil.

3 Research motivation

3.1 Applicability of BioGrout in general

In considering the advantages of BioGrout (§2.3 and §2.4) it can be concluded that BioGrout (urease-based method) is a high-grade technology and therefore a niche product. Mainly due to the production and subsequent treatment of ammonium chloride the cost for applying BioGrout is relatively high. Since ammonium chloride must be treated at a wastewater plant, a limited volume of ammonium chloride may be produced, limiting the volume of treated soil (max. 1000 m^3). The required strength also plays an important role in the minimization of ammonium chloride production. BioGrout should be applied in areas where a small increase in strength or stiffness is sufficient, to keep the production of ammonium chloride low.

In summary: BioGrout is best applicable (more favourable), with the following conditions:

- Volumes treated soil < 1000 m^3
- Small increase in strength < 3 MPa
- Maintaining soil permeability and no disturbance on surroundings.

3.2 Applicability of BioGrout as a method for the prevention of internal erosion

One of the key principles of the FloodProBE project is improving the performance of urban flood defences. Urban flood defences comprise both soft soil embankments and hard structures. Internal erosion, particularly at transitions between soft embankments and hard structures, is an important potential type of failure, which eventually leads to inundation of the hinterland. There are several forms of internal erosion; the most important are backward erosion, erosion by concentrated leakage and suffusion. With respect to transitions between soft embankments and hard structures, backward erosion and concentrated leakage are most relevant. Traditional measures for mitigating or preventing (potential) internal erosion are banks, sheet piles and grout injection. However, these measures have their disadvantages e.g. need space (bank) or cause a nuisance to the surroundings. Hence BioGrout offers an additional, alternative method for preventing internal erosion.

The hypothesis

BioGrout will stop/prevent internal erosion and will transfer the problem to adjacent areas.

Research goal

Assess the possibility and effectiveness of BioGrout as an alternative method for preventing internal erosion.

Gaps in Knowledge

The following gaps in knowledge need to be assessed, to determine whether BioGrout offers an alternative method for internal erosion prevention.

1. Possibility and effectiveness of BioGrout:
   a. Does BioGrout stop/prevent internal erosion?
   b. What is the minimal strength needed to stop erosion?
   c. What is the effect of heterogeneity in the soil to the BioGrout process?
   d. Optimal shape and dimensions of the treated soil
2. Applicability at a field scale:
   a. Optimal location for BioGrout to prevent internal erosion;
   b. How to apply BioGrout in a flood defense system?
   c. What is the durability of BioGrout?
   d. Costs for BioGrout as a prevention method for backwards erosion?

3.3 Research plan

In Task 4.1 of the FloodProBE-project the research focus concerning BioGrout will be on preventing backward erosion. This is because there is much experience in research on backward erosion. Therefore, much knowledge is gained on this mechanism, making further research in the applicability of a new prevention method more reliable. With backward erosion, water flow causes particles to be transported from the downstream part of the levee, thereby forming pipes at the interface of the cohesive top layer and the sand. When the pipes have developed towards the riverside, on-going erosion and widening can result in failure of the levee or dam. This procedure and focus has been consulted and discussed with partners from FloodProBE WP3 (where research has been undertaken into internal erosion processes)

The above mentioned gaps of knowledge are the basis of the research plan. The research plan consists out of two parts: laboratory experiments (chapter 4: Materials and methods; chapter 5: Results) and computer modelling for applying in the field (chapter 6).

The laboratory experiments consist of:

1. Investigate suitability, effectiveness and optimal application methods for BioGrout in a flood defence system
   a. Hole erosion test (HET)
   b. Box experiments
      i. Small scale backward erosion experiment
      ii. Medium scale backward erosion experiment
2. Durability and sustainability of BioGrout
   a. Mechanical
   b. Chemical

The computer modelling:

1. To calculate the required shape, location and minimum strength of the treated soil for preventing/stopping internal erosion;
2. To calculate the optimal application method for BioGrout in a flood defence system.

4 Materials and Methods

4.1 Introduction

First, the possibility of BioGrout as an internal erosion prevention method was evaluated with small-scale backward erosion experiments and the minimum strength improvement has been assessed by means of Hole Erosion Tests. Subsequently, the effectiveness of BioGrout and the optimal geometry for the BioGrout volume to prevent backward erosion was determined by means of small and medium scale backward erosion experiments and by using computer models. Uncertainties existed with respect to the effectiveness of BioGrout near clayey layers. Backward erosion is a failure mechanism that can take place anywhere, however, it is most common along a transition pathway. One of these transitions can be sand-clay. Clay may have an effect on the BioGrout process, thus the effectiveness of BioGrout at this boundary is tested. Finally, the durability of BioGrout was tested in the laboratory by looking at the mechanical (cyclic loading) durability and chemical (percolating rain water) durability.

4.2 General BioGrout

Bacterial suspension

For each experiment, the urease positive bacteria *Sporosarcina pasteurii* (DSMZ33) was used. The medium for cell culturing contained per liter: 20 g yeast extract, 10 g ammonium chloride and 10 µM nickel chloride. The medium was autoclaved for 20 minutes at 121°C. After sterilization the pH was adjusted to 9.The organism was grown at 25°C in Erlenmeyer flaks under shaking conditions (300 rpm) to late exponential phase before harvest and stored at 4°C prior to use. The optical density and urease activity of the bacterial suspension were determined immediately before use. The optical density at 600 nm of the bacterial suspension varied between 4 and 6 and urease activity was around 2 mS/cm/minute.

Monitoring parameters for bacterial growth

- Urease activity was determined using the conductivity method described in Harkes et al. 2009.
- The optical density was used as an indication of biomass concentration. Optical density was measured using a spectrophotometer at a wavelength of 600 nm.

Characteristics of sand used in the experiments

All of the experiments have been carried out with Itterbeck sand (125µm – 250µm), a river sand with grain size characteristics d_{10} = 129 µm, d_{50} = 179 µm, d_{90} = 219 µm (Smals, The Netherlands).

4.3 Hole erosion test

The aim was to obtain a correlation between the strength of the sand material and the erosion resistance. In order to verify the erodibility of treated sand, a series of Hole Erosion Tests were executed by Cemagref.

Preparation of sand columns

First, six sand pack columns have been cemented with three different strengths (1, 2 and 3 flushes). The setup consisted of a standard PVC tube (length: 20cm; internal diameter: 6.5cm), filled with sand, and closed with a top and a bottom (inlet and outlet) to flush the sand sample with the reagents.

The following process was applied in order to cement the sand samples:

- **Bacteria placement**:

Injection of a bacteria suspension (approximately one pore volume) followed by the injection of an equivalent volume of 50 mmol/l $CaCl_2$ in order to immobilize the bacteria in the sand (Van Paassen 2006).

- **Bio-consolidation**
  Injection of one pore volume of an equimolar urea and $CaCl_2$ solution with a pre-defined concentration, followed by a pause to let the reaction running until all the urea is hydrolyzed.

- **Cleaning**
  Flushing the cemented sand column with three pore volumes of water

The characteristics of the grouted samples which have been tested are shown in table 1.

Table 1 Injection procedure for HET test BioGrout samples

Column	1A&1B	2A & 2B	3A & 3B
Solution 1	bacteria	bacteria	bacteria
Solution 2	$CaCl_2$ (50mM)	$CaCl_2$ (50mM)	$CaCl_2$ (50mM)
injection 1	U/Ca (1M) 24h	U/Ca (1M) 24h	U/Ca (1M) 24h
injection 2	demi water	U/Ca (1M) 24h	U/Ca (1M) 24h
injection 3		demi water	U/Ca (1M) 24h
injection 4			demi water

bacteria = 300 ml suspension directly followed by $CaCl_2$ 50 mM 100 ml
U/Ca + 24h = 1M 300 ml + 24 hours wait
demi water= 600 ml ; U/Ca=urea/calcium chloride solution

Internal erosion resistance assessment
The erodibility of cohesive soil, like clay, can be analyzed by a hole erosion test (HET). This method has not yet been standardized and different versions have been developed. The HET version developed by Cemagref (France) consists of applying a constant water flow rate through a preformed lengthways hole in a soil column and measurement of the pressure drop versus time. In order to verify the improvement in resistance to erosion of BioGrout treated sand, a series of hole erosion tests were carried out. This requires that the HET test is suited to this type of soil and can provide reliable parameter values of the erodibility: the coefficient of erosion k_{er}, and the critical shear stress τ_c (Bonelli et al., 2006). Both parameters are directly related to the critical head difference for backward erosion over a structure.

The aim of this test was to assess the internal erosion of artificially formed pipes (holes) under different flow velocities through the pipe and hydraulic pressure. The HET is commonly used for quantifying the rate of backward erosion in a soil, and for finding the critical shear stress corresponding to initiation of backward erosion.

Samples labelled A were tested in June 2010 and samples labelled B were tested in September 2010 in order to verify the reproducibility of the test results. In each sample, a hole with diameter of about 6 mm was drilled in the centre along its entire length. Then, the sample was installed in the HET device. At the end of the test, the sample was removed out of the device and a moulding of the final hole was made with paraffin wax. Samples of series A were destroyed to retrieve the solidified wax while the series B samples were left unchanged.

4.4 Box experiments

Figure 6 shows the small-scale experiment set-up as well as how this set-up represents a sand layer under a dike. With these experiments the suitability, effectiveness and optimized shape of BioGrout-treated sand was determined.

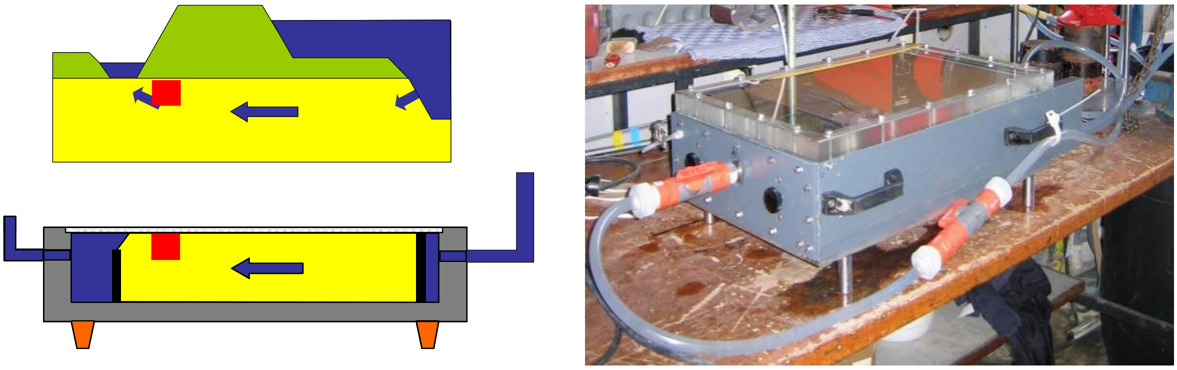

Figure 6 Small-scale experiment set-up for BioGrout prevention of backward

Eight small-scale experiments, 0.006 m^3 (6 liter), and one medium-scale experiment, 0.51 m^3 (510 liter), were performed. In the experiments, a sand sample was prepared in a PVC box with a transparent cover. All experiments, but two, contained clay linings along the sides. A part of the sand sample was treated using the BioGrout technique described above. The goal of the two experiments without clay lining was to determine whether BioGrout is suitable as a backward erosion prevention technique. The experiments with clay lining were performed to investigate the effectiveness of BioGrout between the sand and the clay layer.

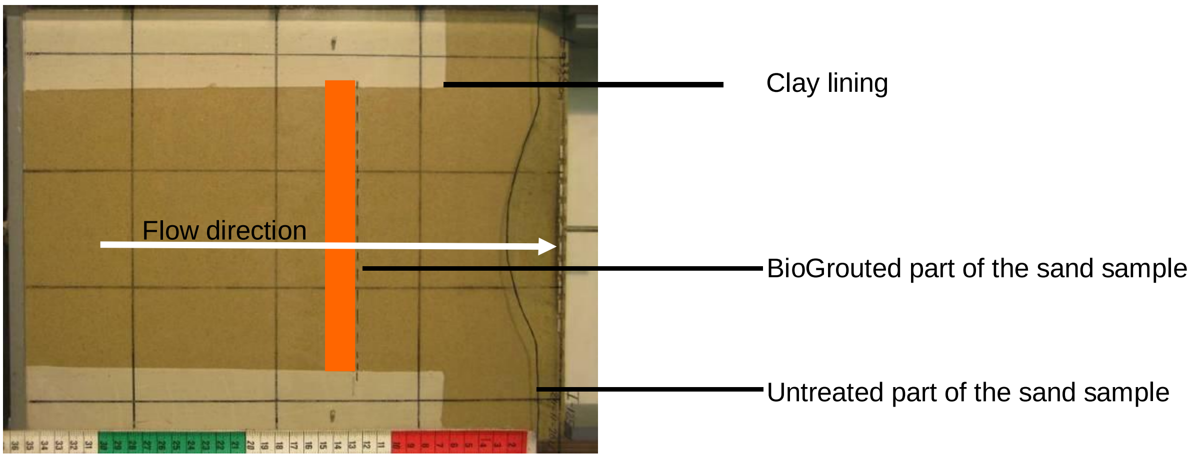

Figure 7 Top view of small-scale backward erosion experiment (experiment I_125).

Table 2 shows an overview of the different experiments. The width of the clay lining was increased in experiment I-127 to force the pipe develop along the clay lining. Experiment I-128 differed from experiment I-129 in the type of BioGrout treatment. In experiment I-128 the sand sample was treated over the full-depth and 9 cm BioGrout was subsequently removed to ultimately obtain a thickness of 1 cm. However, when removing a part of the BioGrout calcite dust is formed, that remains in the sand sample causing a decrease in permeability. In experiment I-129, just 1 cm sand was treated with BioGrout. After treatment, sand was added to the set up. In all experiments, a relative density of around 90% was achieved.

Table 2 Overview experiments

Experiment no.	Clay lining	Treatment	Depth BioGrout
B95	No clay	BioGrout	full depth: 0.1 m
B98	No clay	BioGrout	0.02 m
I-124	5 cm at each side	None	n.a.
I-125	5 cm at each side	BioGrout	full depth: 0.1 m
I-126	5 cm at each side	BioGrout	full depth: 0.1 m
I-127	15 cm at one side, 5 cm at the other	BioGrout	full depth: 0.1 m
I-128	15 cm at one side, 5 cm at the other	BioGrout	0.01 m
I-129	15 cm at one side, 5 cm at the other	BioGrout	0.01 m
Itt-15-MS-BG	no clay lining	BioGrout	0.04 m

Box parameters

The small-scale and medium-scale boxes were made of PVC with a transparent Perspex cover. The dimensions of the small-scale box was 10 cm deep, 20 cm wide and the flow length from upstream to downstream was 30 cm. The dimensions of the medium scale box were 40 cm deep, 88 cm wide and the flow length from upstream to downstream was 145 cm (figure 8).

Figure 8 Medium scale experiment set-up BioGrout for backward erosion prevention

Sand

The sand was packed by tamping to a dry density of approx. 1.7 g/cm^3 (porosity around 36%). Packing was performed under water to avoid the inclusion of air pockets. The box was connected to a system in which the flow rate was regulated by changing the water level.

Treatment

A part of the sand in the box was treated with BioGrout. In all tests, BioGrout was applied over the full width of the box. Approximately a quarter of the treated pore volume was injected with the bacterial suspension immediately followed by the same volume fixation fluid (50 mM $CaCl_2$). Immediately after the fixation fluid was fully injected the cementation fluid containing 1M of calcium chloride and urea was flushed through. After approx. 24 h reaction time, a second flush with 1M cementation fluid was injected. The hole erosion tests proved that a double flush gives sufficient strength against erosion.

Experiment

During the experiment, the water flow was made visible by using coloured water. Experiments were performed with and without a BioGrout-block in the middle of the box. During the test, a top view video was made.

4.5 Mechanical durability of BioGrout

Materials

Tests on the mechanical durability of BioGrout were conducted on samples obtained from the second container experiment (2009). After cementation, ten cores were drilled, from which five samples were taken for cyclic triaxial tests. The dimensions of the samples are in shown in table 3. The samples were cut in such a way from the drilled cores to obtain maximum homogeneity in each sample.

Table 3 Dimensions and properties of tested samples (S1-S5)

		S 1	S 2	S 3	S 4	S 5
h	[cm]	13.55	13.69	12.68	13.23	12.78
d	[cm]	6.27	6.4	6.41	6.39	6.38
m_{sat}	[g]	860.33	911.8	868.24	899.31	840.86
Vi	[cm3]	418.37	440.41	405.12	424.28	408.57
ρ_{sat}	[g/m^3]	2.056	2.070	2.143	2.12	2.06
ρ_{dry}	[g/m^3]	1.693	1.867	1.836	1.794	1.669
ϕ_{dry}	[%]	36.36	29.82	30.72	32.55	36.12
K_i		2.45E-05	1.43E-05	1.84E-05	1.85E-05	9.96E-06
$CaCO_3$cont.	[mg/cm^3]	39.99	40.12	56.26	51.67	50.49

Cyclic tri-axial loading

The samples were fully saturated by applying a backpressure until the B-value reached at least 0.96 according to standards. Throughout the course of the test, a constant effective confining pressure of 50kPa was applied. The tests were performed under undrained conditions. The frequency of the load-unload cycle was set on 0.2 Hz, with a total test duration of approximately 72 h, reaching ca. 52,000 cycles. The load-unload cycles were chosen to alternate initially between 10 and 100kPa with an increase of the maximum load amplitude by doubling to 200, 400 and 800 kPa until a final load amplitude of 1400kPa was reached and kept constant during the test (table 4). During cyclic loading the vertical applied force, vertical displacement, pore pressure as well as cell pressure was continuously measured with a sampling rate of 0.37 seconds, attaining 13 sample points per cycle.

For samples that did not fail within 72h, the cyclic loading was stopped and monotonic loading was applied until failure. The monotonic loading was conducted in the same triaxial cell, to prevent disturbance of the samples.

An overview of the test procedures and details of the properties of the samples is given in the following part. It is important to say that sample 5, which was tested as the first one did not undergo the exact same procedure as the other samples. The time scheme of all tested samples is described in table 4. Initially maximum load amplitude of 100kPa was chosen corresponding to forces applied in civil engineering applications. After 70h testing of S5, no major effects were observed. Therefore, the load amplitude was increased until maximum amplitude of 1400kPa. The following samples were carried out with the same starting load amplitude, but the increase in loads was doubled each hour during the initial 4h of the test until maximum load amplitude of 1400kPa was reached.

Table 4 Time scheme [minutes] of increasing loads for all tested samples

	Stress	S 1	S 2	S 3	S 4	S 5
Step 1:	100 [kPa]	0 - 60	0 – 70	0 - 60	0 -60	0 - 4165
Step 2:	200 [kPa]	60 - 120	70 – 156	60 - 120	60 – 120	4165 - 4566
Step 3:	400 [kPa]	120 - 180	156 - 216	120 - 183	120 – 183	4566 - 4641
Step 4:	800 [kPa]	180 - 223	216 - 240	183 - 245	183 – 249	4641 - 4676
Step 5:	1400 [kPa]		240 - 2584	245 - 4320	249 – 3150	4676 - 5929
time of failure [h,min]		**3h, 43 min**	**43h, 4min**	**72h**	**52h, 30 min**	**98h, 49min**

Table 5 Details of cyclic tri-axial tests performed on BioGrout samples, including estimation of peak strength

		S 1	S 2	S 3 *	S 4	S 5 *
q_{est}	[kPa]	902	2,564	2,129	1,655	781
q_{cyc}	[kPa]	800	1,400	1,400	1,400	1,400
q_{max}	[kPa]	800	1,400	2,447	1,400	657
N_f	[-]	2,660	30,530	51,840	37,800	71,148

***** did not fail during cyclic loading

Table 5 shows the maximum cyclic load q_{cyc}, the monotonic strength q_{max}, and number of cycles N_f upon failure. It also contains the predicted monotonic strength q_{est}, which was calculated for the samples according to the correlation of Van Paassen (2009). Important to notice: this correlation cannot hold for the cyclic loading since the type of load application is distinctive for the behavior of the material tested. This is seen in S5. During cyclic loading, S5 was able to withstand load amplitude of 1400kPa over approximately 20h of cyclic loading. However, during subsequent monotonic loading the sample failed at a load of approximately 660 kPa.

4.6 Chemical durability

Materials

Five PVC tubes with Itterbeck sand were treated with BioGrout according to the procedure stated by Harkes et al. (2009), to test the chemical durability of BioGrout. Details of the samples are described in Table 6. The sand was treated with four batches of 1 M of $CaCl_2$ and urea. During the reaction phase, the ammonium concentration in the effluent was measured at different times to calculate the conversion rate of $CaCO_3$. The ammonium concentration was determined by adding 2 ml effluent in a cuvet containing 100µl of Nessler reagent. After 1 min, the optical density of the sample was measured in a spectrophotometer at 425nm.

Table 6 Details of packed sandstone columns for chemical durability tests

column	height	mass of sand	volume	dry density	matrix volume	pore volume	porosity	height precipitated
	h	m	V	ρ_{dry}	V_{matrix}	V_{por}	φ	$h_{perc.}$
	[cm]	[g]	[cm^3]	[g/cm^3]	[cm^3]	[cm^3]	[%]	[cm]
CR 1	16	844.4	539.13	1.57	324.77	214.36	39.76	11.5
CD 2	16	879.0	539.13	1.63	338.08	201.05	37.29	12.0
CD 3	16	894.9	539.13	1.66	344.19	194.94	36.16	12.2
CR 4	16	865.1	539.13	1.60	332.73	206.40	38.28	11.8
CB 5	16	876.5	539.13	1.63	337.12	202.01	37.47	13.5

Flushing procedure

As previously stated all five columns were treated in an identical way to obtain similar properties. One column was not flushed, but used as a blank, to compare its strength with the strength of the flushed columns.

The flushing of the columns with artificial rain (Boschloo, D.J., Stolk, A.P. 1999) and demineralised water was done from top to bottom with a flow rate of 200ml/h, reaching 1PV/h (pore volume/ hour) for 10 days. Each column was flushed with 260 pore volumes. Samples of the influent as well as the effluent were taken twice a day to measure the conductivity, pH and $CaCO_3$ content. For practical reasons the flow rate was decreased to half the speed during weekends.

The demineralised water was sparged with nitrogen to prevent dissolution of carbonate into the fluid, therefore maintaining the concentration in the influent minimal. The composition of the artificial rainwater is shown in Table 7. The pH of water was kept between 5 and 6 throughout the experiment. Artificial rainwater was stored in a conventional vessel with a loose lid during flushing, to imitate rainwater travelling through the atmosphere and percolating through the soil.

Table 7 Composition of the artificial rain water

Salts	mg/l
$(NH_4)_2SO_4$	8.8268
$MgCl_2$	1.5044
$CaNO_3$	0.6665
KNO_3	0.6125
$NaHCO_3$	0.4550
NaCl	1.3189
K_2HPO_4	0.7481
NH_4Cl	0.0523
$NaNO_3$	7.8413

4.7 Freezing-thawing cycles

When used as a ground improvement material in the shallow subsurface, BioGrout treated soil might encounter effects of changing weathering conditions that might alter its compressive strength. There are three physical processes that influence negatively the strength of building materials, thus likely also BioGrout: heating-cooling, wetting-drying, and freezing-thawing. In Hale and Shakoor (2003), the effects of heating and cooling as well as wetting and drying were not found to reduce the strength of their tested sandstones. Only the freezing and thawing cycles showed significant effect on the degradation of strength. Hence, in the following only the effect of freezing and thawing cycles on BioGrout was examined.

Yearly cycles in temperature between below and above 0°C can cause cycles of freeze and thaw of the pore fluids. This expansion and subsequent contraction of pore fluids may cause cracks inside a material, weakening it. This degradation of strength can be crucial for the application of BioGrout as a ground improvement material.

Material

The freeze-thaw cyclic experiment was conducted on samples from the second container experiment. The cores were drilled from the same block as the samples for cyclic loading tests.

Procedure
To determine the strength of the cores the correlation of Van Paassen (2009) was used. Prior to the freeze-thaw cycles, the samples were stored in water to maximize the water content in the samples and subsequently wrapped into foil to prevent loss of water and sand grains from the surface of the cores during testing.

The freezing- thawing treatments were carried out in a conventional freezer at a constant temperature of -18°C. The thawing cycles were conducted in a warm water bath at 20°C. Both samples were subjected to 26 freeze- thaw cycles, with duration of 16h and 8h respectively. After completion of this part, the unconfined compressive strength of the samples was investigated. S06 broke in half during handling and therefore was tested with a 1:1 ratio, S10 stayed intact and was tested with standard 1:2 ratio.

5 Results

5.1 Hole erosion test

A collapse of sample 1A was observed in the beginning of the test (figure 9). Samples 2A and 3A appeared relatively non-erodible even at high flow rates generating significant shear stresses. The cemented soil samples did not show the typical measurements usually observed for cohesive soil samples (turbidity pulse and progressive decrease of the pressure drop), little erosion occurred and sand accumulated on the downstream outlet of the sample during the test.

After removal out of the HET device, a significant expansion of the initial conduit was observed. This enlargement seemed more pronounced for sample 2A. In both cases, the amount of erosion was heterogeneous as shown by the photographs of both paraffin cores 2A and 3A (figure 9). Results of the second series (B) are comparable to the results of series A, showing the reproducibility of the tests.

The samples BioGrouted with one flush were poorly resistant to erosion and a low hydraulic stress was sufficient to break most of the cemented contacts in almost the entire sample. The samples grouted by two or three flushes were relatively resistant to erosion. Unfortunately, it was not possible to measure the erodibility coefficients for these samples, because the difference in pressure between the upstream and downstream was extremely small (an order of magnitude below typical values for cohesive soil) with a very noisy signal due to the inherent fluctuations of the flow rate during the test. The signal to noise ratio was too bad for the interpretation model to be used.

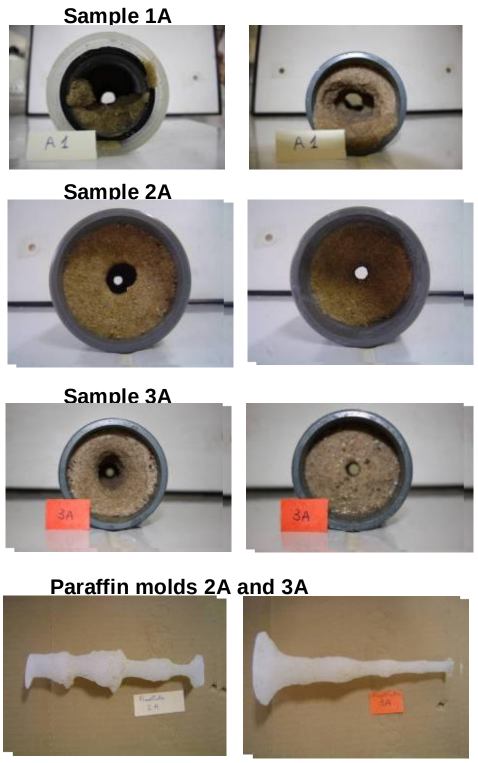

Figure 9 Hole Erosion Test results samples A

The paraffin moulds show that the samples are inhomogeneous eroded (Fig. 9). The shapes of the moulds reveal the existence of four layers compacted after each other during preparation of the sand sample.

The cementation was heterogeneous too, because stronger and softer areas were identified during drilling of the hole in the cemented sample. A final remark: due to the irregular shape of the hole, the interpretation model that is based on the assumption of a roughly cylindrical hole can probably not be used. The small pressure drop along the hole during erosion was unexpected. A hypothesis is that the erosion observed here is not constant over time and not uniformly distributed on the inner surface of the hole as is usual for cohesive soils. Sand mass loss would rather be due to several successive instabilities, quasi-instantaneous and localized in the most vulnerable areas of the sample (Van et al., 2011).

5.2 Box experiments

Results of lab experiments

Table 8 shows links for videos of the different experiments which are available on YouTube.

Table 8 Links to videos of the different performed experiments.

Experiment	**YouTube** reference
I-124	http://www.youtube.com/watch?v=Ev_vFHqexaA&feature=relmfu
I-125	http://www.youtube.com/watch?NR=1&v=zgqkeGwlYbw&feature=endscreen
I-126	http://www.youtube.com/watch?v=3qewVnImnE4&feature=relmfu
I-127	http://www.youtube.com/watch?NR=1&v=3JP5xAWtg4I&feature=endscreen
I-128	http://www.youtube.com/watch?v=I6FVRQDrGrw&feature=relmfu
I-129	http://www.youtube.com/watch?v=L7zjOV49tqI&feature=relmfu
Itt-ms-15-bg	http://www.youtube.com/watch?v=Y4nbk9kokuM

Figure 10 shows stills of the resulting video at four moments in time of experiment B95. In figure 10A, the backward erosion channel has already been formed from the right site towards the BioGrout block. From still A to B the coloured water is visible from the upstream left site of the box to the BioGrout block. In figure 10B, the coloured water is mainly in the 5 cm wide and 10 cm deep BioGrout block. Figure 10C shows that the coloured water is at the end of the block and in the backward erosion channel. Finally figure 10D shows the final stage where the backward erosion channel is clean water and some coloured water still remains in the downstream area where no backward erosion channel occurs.

Both tests, B95 and B98, show that the BioGrout layer was almost equally permeable as the sand layer and that the backward erosion process was fully stopped at the left upstream site of the block. The test was executed in the presence of two different types of BioGrout block sizes; both over the full 20 cm width, but one 10 cm deep and 5 cm long, and the other 2 cm deep and 2 cm long. Both BioGrout experiments resulted in at least a factor of two increase of the critical head, i.e. the water head required for the development of a complete backward erosion channel.

The reference test in the program was I-124, where the sand sample was not treated with BioGrout. After increasing the water head, a pipe started to form at the downstream side of the sand sample, and progressed towards the upstream side without further increasing of head. The pipe did not grow along the clay linings, but remained in the middle of the sample. The observations in this test were similar to those previously performed backward erosion tests described in Van Beek and Förster (2012).

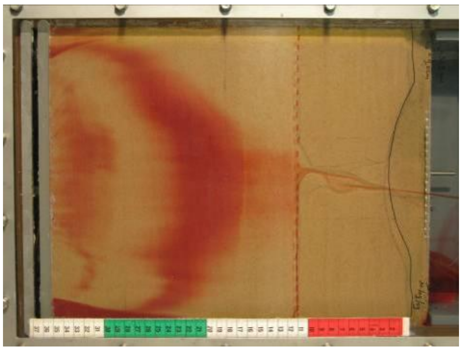
A
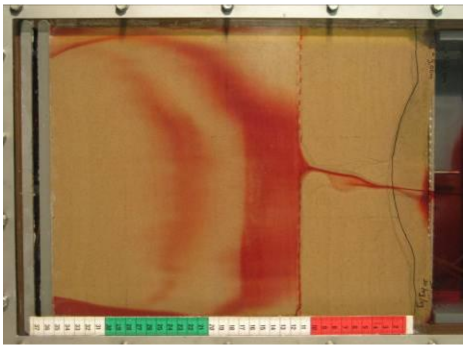
B
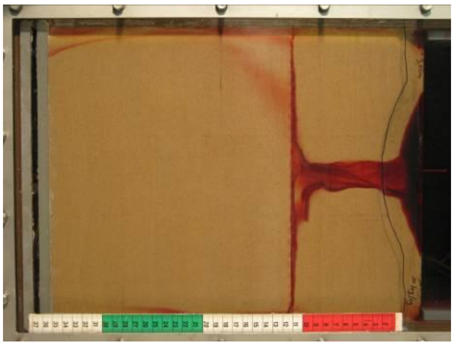
C
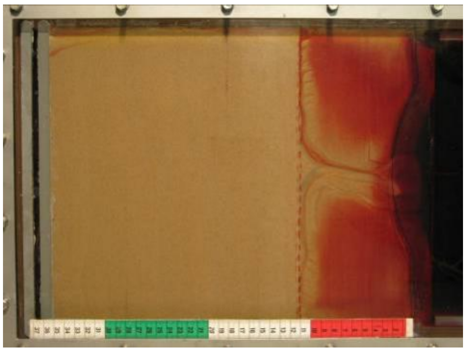
D

Figure 10 BioGrout preventing backward erosion channel growth

In experiment I-125, containing BioGrout and a clay lining, after initiation of the pipe, the pipe progressed towards the boundary of the BioGrout and then stopped. A further increase of head lead to growth of the pipe perpendicular to the flow direction, until the clay liners were reached. Here the increase of head did not result in failure. In test I-126 similar observations were made, although the pipe growth stopped after initiation (figure 11, left). When the head was raised 1 cm, the pipe grew further towards the BioGrout (figure 11, right). Both tests showed that the pipe did not grow along the clay liners, but remained in the middle of the sand sample.

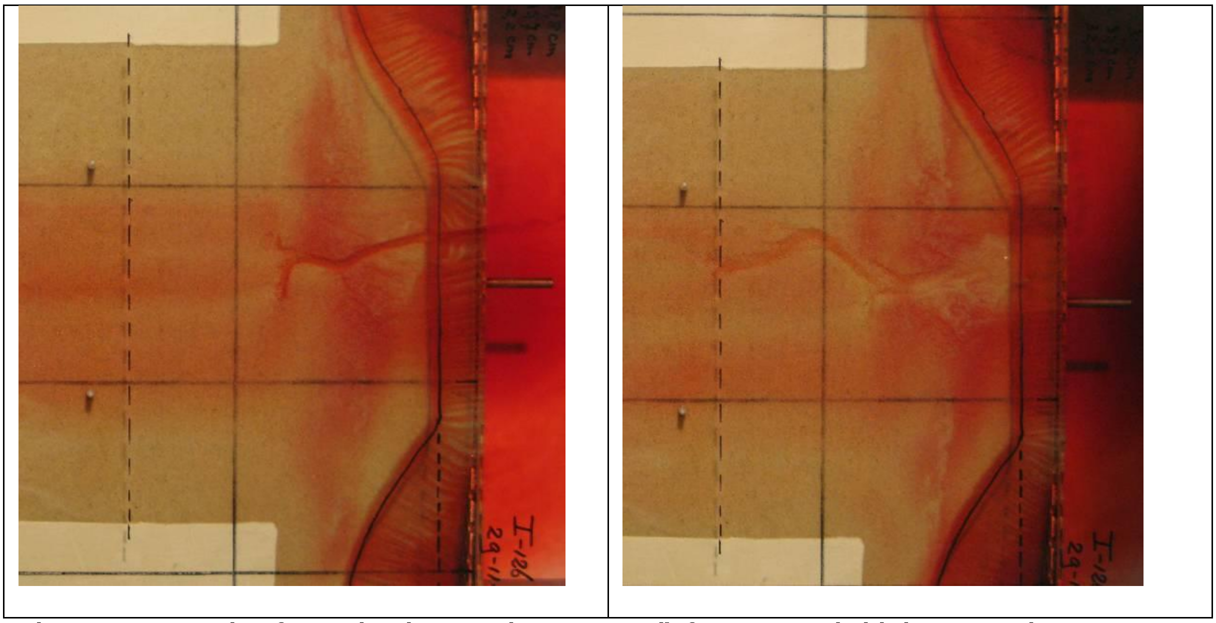

Figure 11 Pipe formation in experiment I-126 (left, H=0.20 m), (right, H=0.21).

Test I-127 was are petition of I-126 but with a wider clay liner, in an attempt to let the pipe grow along the clay liner. This did not succeed;, the pipe still developed in the middle of the sand sample. After initiation of the pipe, the water head needed to be increased several times to continue pipe growth up to the BioGrout. Subsequently, the pipe developed perpendicular to the flow direction, along the interface of loose sand and BioGrout. Breach did not occur.

In test I-128 and I-129 only a 1cm thick BioGrout layer was formed. Calcite dust decreased the overall permeability of sample I-128. After increasing the head a pipe initiated. After some time the pipe stopped growing and the head was increased with many steps before the pipe reached the BioGrout layer.

At this head, the pipe developed perpendicular to the flow direction, damaging the BioGrout (figure 12). Subsequently the pipe developed through the BioGrout shown in figure 13.

In test I-129, once a pipe was formed it immediately grew towards the BioGrout interface, where the pipe subsequently developed perpendicular to the flow direction. The head was increased several centimeters, but breach did not occur.

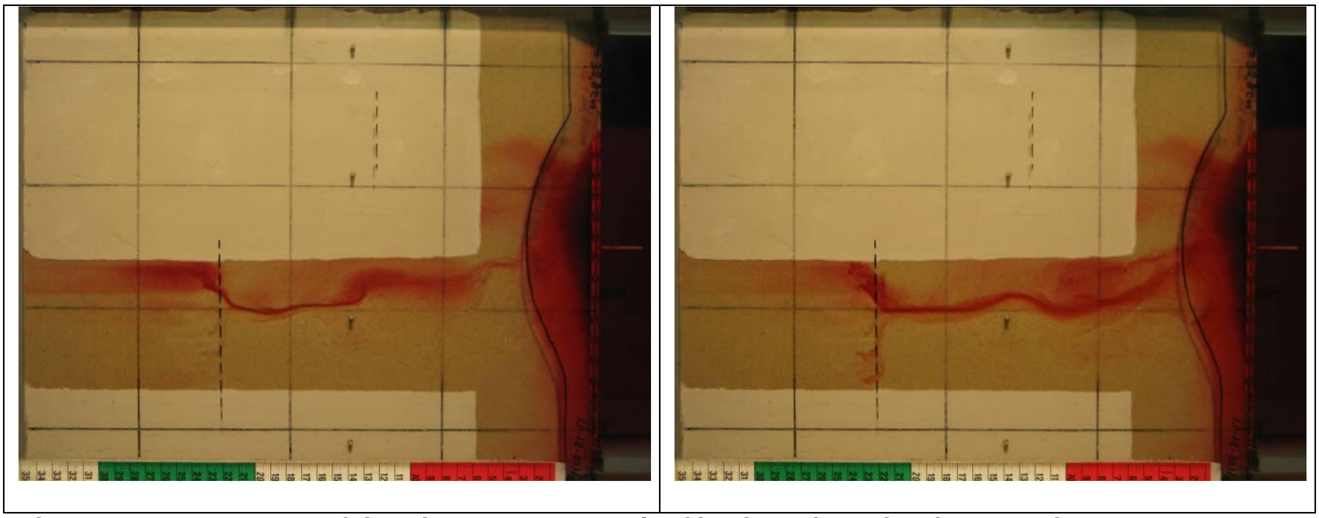

Figure 12 Damage of the BioGrout as a result of backward erosion (test I-128).

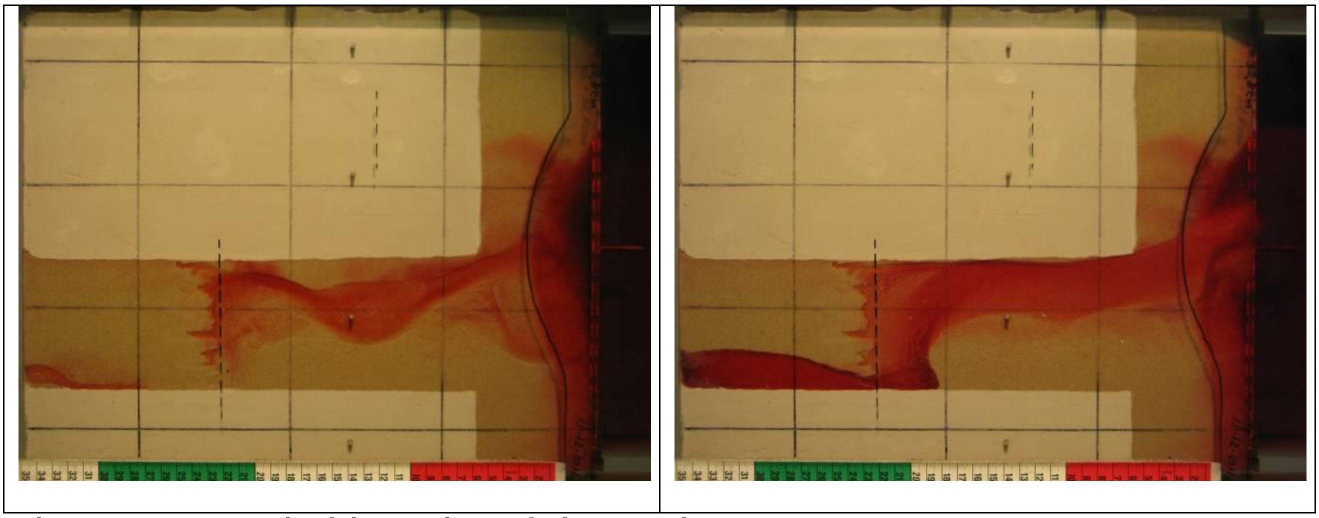

Figure 13 Breach of the sand sample (test I-128).

Noted from the observations in all experiments: the connection between BioGrout and the clay lining is sufficient against erosion.

With the medium-scale experiment (Itt-ms-15-bg), similar observations as in test I-127 were made. Even though the head was raised up to 0.50 m, the sample did not breach.

Table 9 summarizes the test results. For each test, the permeability, the head when the pipe initiated is noted (H_i), the head when the pipe progressed to the BioGrout-interface (H_p) and the head at which the sample failed (H_b).

Table 9 Overview small-scale test results

Test no:	K [m/s]	Hi [m]	Hp [m]	Hb [m]
I-124	1.7E-04	0.21	0.21	0.21
I-125	1.8E-04	0.15	0.15	>0.20*
I-126	1.5E-04	0.20	0.21	>0.50*
I-127	1.5E-04	0.19	0.26	>0.28*
I-128**	1.4E-04	0.20	0.27	0.27
I-129	2.2E-04	0.20	0.20	>0.25*
Itt-ms-15-bg	1.4E-04	0.298	0.337	>0.50*

(*sample did not fail, ** values corrected for clogged filter).

Analysis of the lab results

The model of Sellmeijer predicts the critical head for backward erosion in sand. The model is implemented in the ground water flow program MSeep, a 2D calculation model, to account for deviating configurations (Sellmeijer, 2006). For each experiment, this model was applied to calculate the critical head using the adjusted rule of Sellmeijer (Sellmeijer, 2011).

Table 10 Critical heads calculated with Sellmeijer's model for each experiment.

Experiment	Hc_Mseep [m]
I-124	0.144
I-125	0.141
I-126	0.156
I-127	0.149
I-128	0.153
I-129	0.132
Itt-ms-15-bg	0.443

As can be noted from the results in table 10, the calculated critical heads are lower than the critical heads reached in the experiments, even for the reference experiment. This might be related to the restriction of width due to the clay liners: the effect of width is not included in the 2D-calculation model. The width is usually expected to have a limited influence, as multiple channels will developed in parallel. However, when only one pipe can develop, which is the case for small-scale experiments, the width of the set up may influence the results.

It is unclear why the predicted critical head for the medium-scale experiment is higher than the experimentally obtained value. It is noted that there is only one test and a large spread of data is not uncommon for backward erosion experiments.

In all experiments, the BioGrout sample provided extra strength compared to the predictions, which was also observed. In each experiment the pipe stopped at the interface of BioGrout, indicating that this is a proper barrier. Experiment I-126 showed that for BioGrout at full depth the head can be increased to over 0.50 m without failure. Experiment I-128 is the only experiment in which the sample failed. In this experiment, BioGrout was removed to a limited depth of 1 cm, forming calcite dust in the sand sample causing a decrease in permeability. In reality this will not occur, BioGrout will be applied for a certain depth, and will not be removed forming calcite dust.

To analyze what these results mean for backward erosion resistance in practice, the failure mechanism for backward erosion in a BioGrout sample must be observed.

Two mechanisms are possible:

- Fluidization of sand underneath and around the BioGrouted part (similar to backward erosion in levees with a cut off)
- Breaking through the BioGrouted part.

Looking at the failure in experiment I-128, the latter seems more reasonable, although the experiment with full BioGrout depth shows greater strength than the experiment with partially grouted sand, indicating that the first mechanism might be important as well.

For both mechanisms calculations are performed.

Fluidization of sand

The fluidization of sand around a structure was studied to predict backward erosion in levees with a cut off. The most used criterion is of Terzaghi (1967), where the hydraulic gradient at the downstream part of the structure needs to be around 1. In the BioGrout experiment, a gradient of one is not reached easily as the BioGrouted sand is nearly as permeable as the sand layer.

For experiment I-128 the critical heads were calculated with MSeep, when fluidization gradient downstream of the BioGrout will become equal to one. The permeability of the BioGrouted part varied; the permeability of the sand was kept constant (1.4E-4 m/s). The head fall in the pipe was neglected, which is a conservative assumption.

Table 11 Critical heads using heave criterion for experiment I-128.

k_biogrout [m/s]	dHc [m]
1.40E-05	0.0718
1.26E-04	0.0707
7.00E-05	0.0707

The calculated heads show that fluidization should take place at a relatively low head difference (table 11). This head difference was easily exceeded in the experiments. Earlier experiments by Van den Ham (2009), in which the influence of a cut off wall on the backward erosion process and critical head was investigated in a similar set up, already showed that the occurrence of backward erosion in small-scale experiments with a cut off cannot be predicted very well by the model of Terzaghi. The most likely reason for this is the relative large influence of the head drop in the pipe on the vertical gradient downstream of the structure and the small size of the structure in relation to the particle size. In other backward erosion experiments, the method of Terzaghi has been proven successful to predict the critical head (Luijendijk, 2011).

The backward erosion resistance of a levee with a structure is very dependent on the depth of the structure. Figure 14 shows this dependency for a small-scale experiment. The permeability of the structure is also important, but to a lesser extent. The high permeability of the BioGrout has a small positive effect on the strength of the structure. The difference between the critical head for a complete permeable BioGrout structure and the head for an impermeable structure is about 20%.

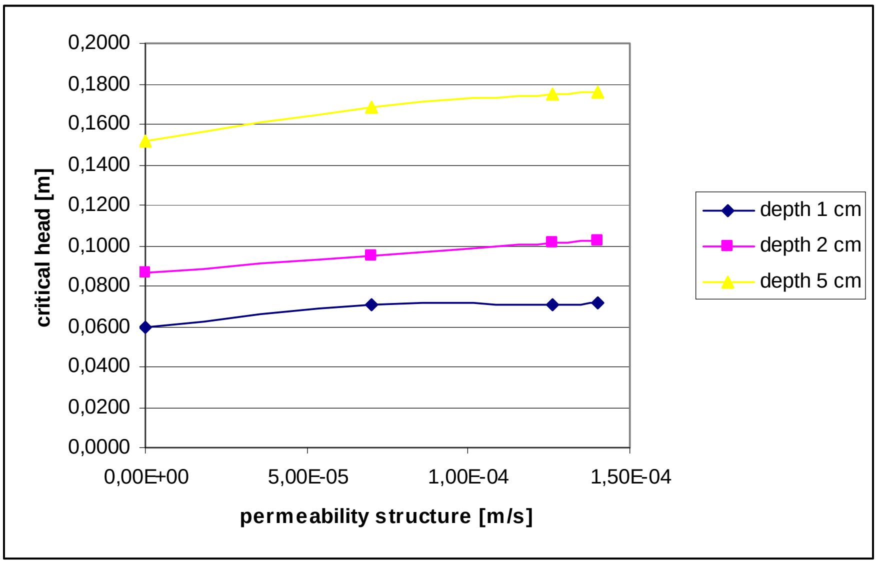

Figure 14 Influence of depth and permeability of the structure on critical head.

The medium-scale experiment has been evaluated similarly. The critical heads are calculated for a BioGrout sample 4 cm deep, with different permeability's (table 12). The calculation is conserved with respect to the head drop in the pipe; therefore the maximum applied head in the experiment (0.50 m) can be larger than the critical head listed in table 11.

Table 12 Critical heads using heave criterion for the medium-scale experiment

k_biogrout [m/s]	dHc [m]
1.40E-05	0.4350
1.26E-04	0.4291
7.00E-05	0.4029
1.00E-12	0.3350

Based on these results, fluidization downstream of the BioGrout structure is a likely failure mechanism, especially for situations where the depth of the BioGrout is limited.

Breaking through the BioGrout

The second failure mechanism is break-through of the pipe through the BioGrout sample. No calculation methods are available to calculate this failure. However, based on the experiments, an estimate can be given for the resistance of the sample. It is noted that for this failure mechanism the strength of the BioGrout sample determines the backward erosion resistance. This strength may vary with the size of the structure, as in a small BioGrout sample the chance for a weak spot is larger than for a larger sample. In addition, the variation in obtained strength may be larger in the field than in the laboratory.

To determine whether this failure mechanism is important several experiments need to be used. However, the only experiment in which failure took place was I-128. Here, the depth of cut off was relatively limited, indicating that fluidization could have been the dominant failure mechanism. In the other experiments failure did not occur, these experiments can be used to calculate a minimum value for the strength.

The model of Sellmeijer is used to calculate the progress of the pipe, not to determine the critical head for the BioGrout sample. With this model the critical head was determined by analyzing the grain equilibrium in the pipe (figure 15). It is assumed that the pipe will become longer when the grains in the pipe are transported. This assumption is not valid when a BioGrout structure is encountered.

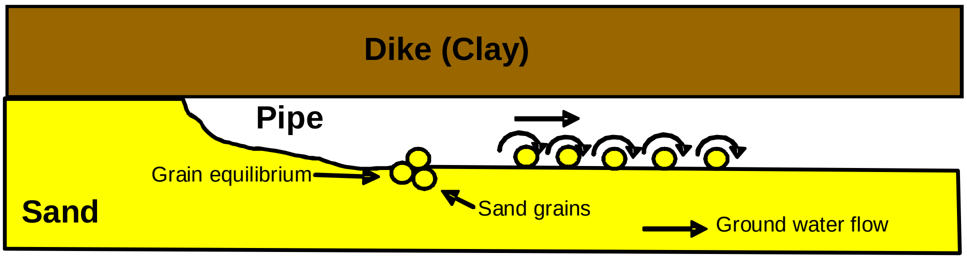

Figure 15 Schematization of pipe and grain equilibrium in Sellmeijer's model.

Breaking through the BioGrout sample therefore required a different approach. For continuation of the pipe at the interface of BioGrout and sand, the structure of the sample at the head of the pipe must be broken. To break the structure of BioGrout a certain flow velocity (v) or gradient (i) is required near the head of the pipe (illustrated in the figure 16). This gradient at pore scale is unknown, as it was determined by the size and head fall in the pipe.

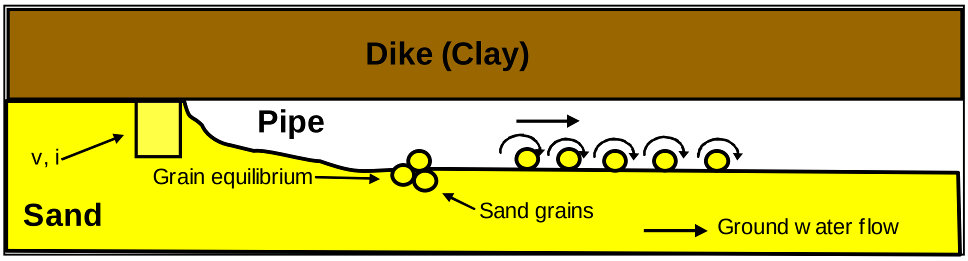

Figure 16 Schematization of pipe and criteria for growth at encounter of BioGrout sample.

To determine this local gradient, numerical calculations were performed using a mesh of 5 mm. The head drop in the pipe is neglected in these calculations. As the pipe develops parallel to the BioGrout boundary, a 2D situation is created which can be modeled in MSeep. Figure 17 shows the used configuration for the small-scale experiment. It was assumed that the BioGrout sample has the same permeability as the rest of the sand.

When applying a head of 0.25 m (corresponding to experiment I-129), a local velocity of 1.04E-3 m/s causes no damage to the sample, corresponding to a local gradient of 6.1.

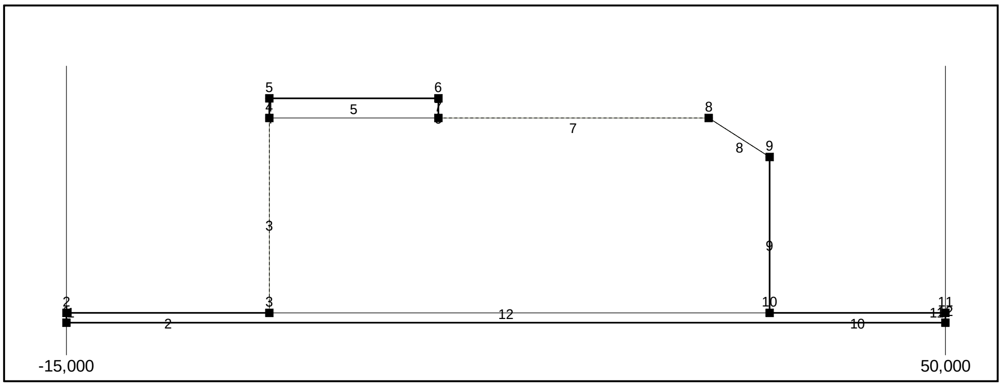

Figure 17 Input MSEEP showing boundary conditions.

The other experiments (except for I-128) have been evaluated in a similar manner. The local gradients calculated are listed in the table 13.

Table 13 Maximum local gradients near the head of the pipe (no failure).

Test no:	Hb [m]	local gradient [-]
I-125	>0,20	4.9
I-126	>0,50	12.2
I-127	>0,28	6.8
I-129	>0,25	6.1
Itt-ms-15-bg	>0,50	3.9

The experiments show that the BioGrout structure can withstand a local gradient of at least 3.9 - 12.2. The local gradient is smallest for the medium-scale test, whereas the head was raised to the same value as in test I-126. Scale effects caused this.

These scale effects were investigated when determining criteria for initiation of a pipe in an intact sample. Bezuijen and Steedman (2010) found that for configurations, similar to the small-scale set up, but with infinite depth, the critical overall gradient is related to the seepage length by $\frac{H_c}{L} \propto \frac{1}{\sqrt{L}}$. Van Beek and Förster (2012) determined a dependency of $\frac{H_c}{L} \propto L^{-0.46}$ for similar configurations with finite depth, which is very close to the relation found by Bezuijen and Steedman (2010). These relations can be used to calculate the critical head for breaking through a BioGrout sample in practice.

Implications for practice

The experiments have shown that two failure mechanisms can occur:

- Fluidization of sand underneath and around the BioGrouted part (similar to backward erosion in levees with a cut off)
- Breaking through the BioGrouted part.

For both mechanisms, a field situation was evaluated. The critical head was calculated for an arbitrary field situation with a single (dense) sandy layer, with the following characteristics:

Table 14 Case characteristics

d70 [um]	permeability [m/s]	D [m]	L [m]	Exit type	BioGrout
200	1.4E-4	10	50	Ditch	Downstream, depth of 2 m, width of 2 m

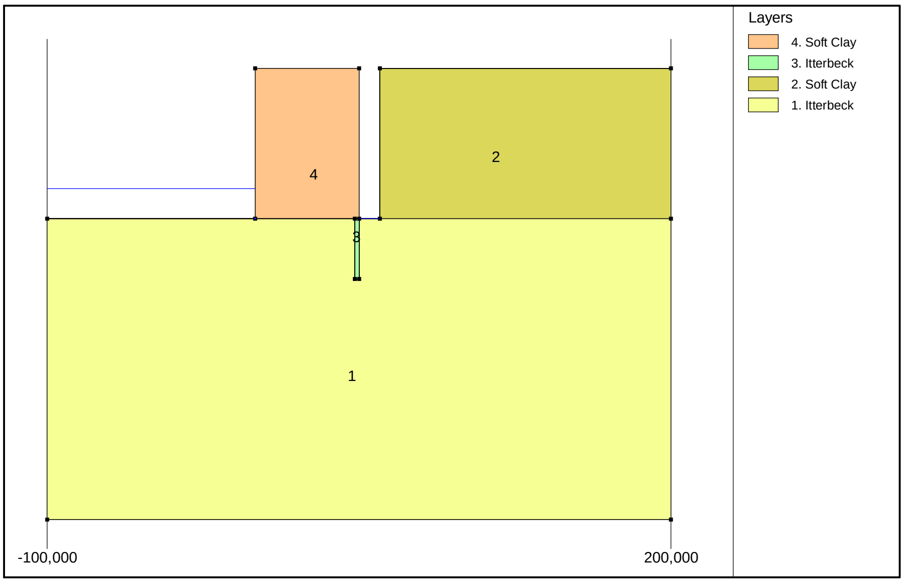

Figure 18 Input MSEEP (note the deviating x and y scale).

For this situation without BioGrout the critical head is 4.5 m according to the model of Sellmeijer. Using the failure criteria for breaking through the BioGrouted part, with a local gradient of 3.9 along a distance of 0.005 m at the boundary of the BioGrout, the allowable head is at least 4 m. With a local gradient of 12.2, the allowable head would be at least 12.5 m. Assuming that the BioGrout strength is higher for larger dimensions than for smaller dimensions, it seems justified to use the upper value of 12.2.

Using the heave criteria (downstream gradient of 1), the allowable head is 34.8 m. A completely clogged BioGrout sample would still be able to resist 26.6 m. BioGrout offers an adequate protection against backward erosion; the critical head is about 3 times higher with BioGrout than without. However, a few remarks must be made:

- It is noted that failure by backward erosion around the BioGrout might be a larger risk than failure through the BioGrout. This aspect is not investigated in this research.
- For each situation, new calculations must be made, because the influence of scale and geometry on the outcome.
- The calculations for break-through were based on criteria, which was derived from small-scale tests where failure did not occur. The applied scale effects are conservative, but speculative. It is assumed that there are no weak spots in BioGrout when applied in the field. Much will depend on the attained strength of BioGrout and its connection to the clay layer.
- No safety factors are included in the calculations.

5.3 Durability

Mechanical durability

The data was mainly processed in IGOR Pro 5.01 to determine deformation characteristics of the material during cyclic loading. The focus of interpretation was to verify the stress- strain behavior as well as degradation of stiffness in terms of change in the shear modulus and the driving factors and patterns of the degradation.

Stiffness properties

In theory, a soil subjected to cyclic loading will respond with so-called hysteresis to this kind of stress pattern (O'Reilly and Brown, 1991). During the course of the experiment, stress- strain curves show this characteristic hysteresis behavior with an increasing number of cycles. Figure 19 shows the stress- strain relation of S3 during cyclic loading for the initial 20.000 cycles (approx. 28h), representative for all conducted tests, since the behavior was very similar for all samples. The jumps in stress level depict the increase of load each hour. As the data processed in this graph is very dense, single ellipses are not visible. However, a constant creep across the strain axis can be clearly seen, indicating a damping (plastic deformation) of the material. The deformation of the sample, especially regarding the lower loads (100 or 200 kPa) representing stress levels induced by civil engineering applications, is in the range of 0.01 to 0.02%.

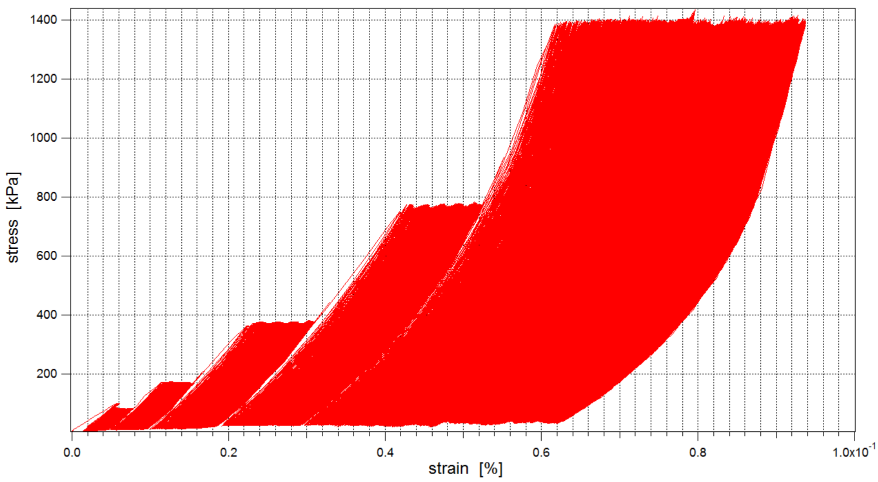

Figure 19 Stress- strain behavior of S3 for initial 20.000 cycles.

As already stated, the high density of data does not allow determining the development of ellipses themselves. Therefore, figures 20 and 21 only show a few single ellipses with a constant interval of 100 cycles and 2500 cycles respectively. As can be seen in figure 19, showing the development of hysteresis for load levels of 100, 200 and 400kPa, the increase in plastic strain becomes smaller with an increasing number of cycles in each load level. Figure 20 shows the same for a load amplitude of 1400kPa. Here it appears that the plastic strain only shows a very small increase until a sudden jump by approximately 0.8% of strain indicating failure of the sample has been initiated. This behavior indicates that it is rather hard to predict the failure of samples since there are no strong signs of increased weakening of the sample. As soon as the material showed a sudden increase in plastic strain it failed very rapidly. The deformation of the material was extremely low (figure 22). Tests of all samples have shown that the displacement in all cases has only reached a maximum range of approximately 1-2 mm before failure. S3 and S5, which did not fail during cyclic loading, showed a lower displacement of only 1.4 mm and 0.18 mm respectively.

Taking this into account it can be said that the material can withstand relatively high cyclic loads throughout a long period. However once deformation exceeds a certain point, the material fails very rapidly not giving room for any plastic deformation.

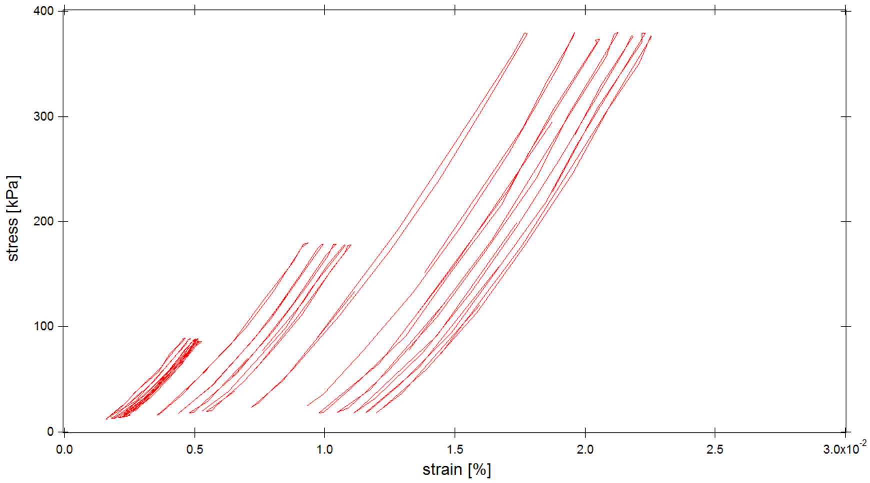

Figure 20 **Stress- strain behavior of S2, showed for load amplitudes of 100kPa, 200kPa and 400kPa, with a constant interval of 100 cycles.**

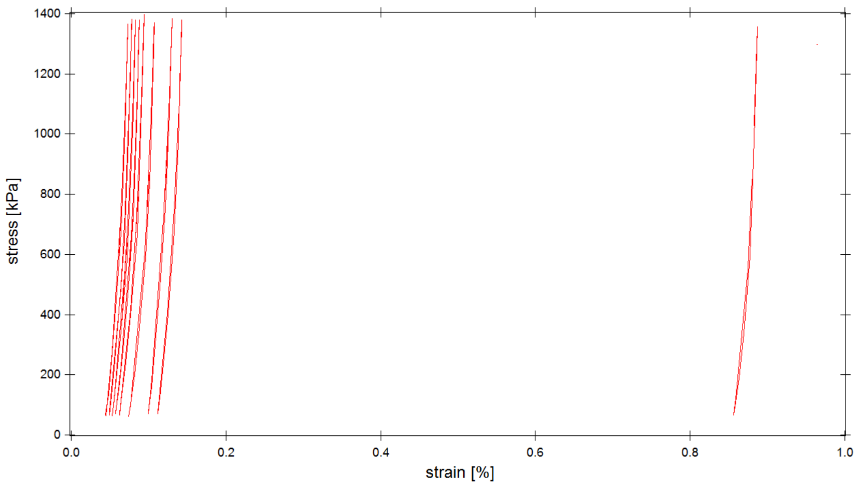

Figure 21 **Stress- strain behavior of S2, showed for load amplitude 1400kPa with a constant interval of 2.500 cycles.**

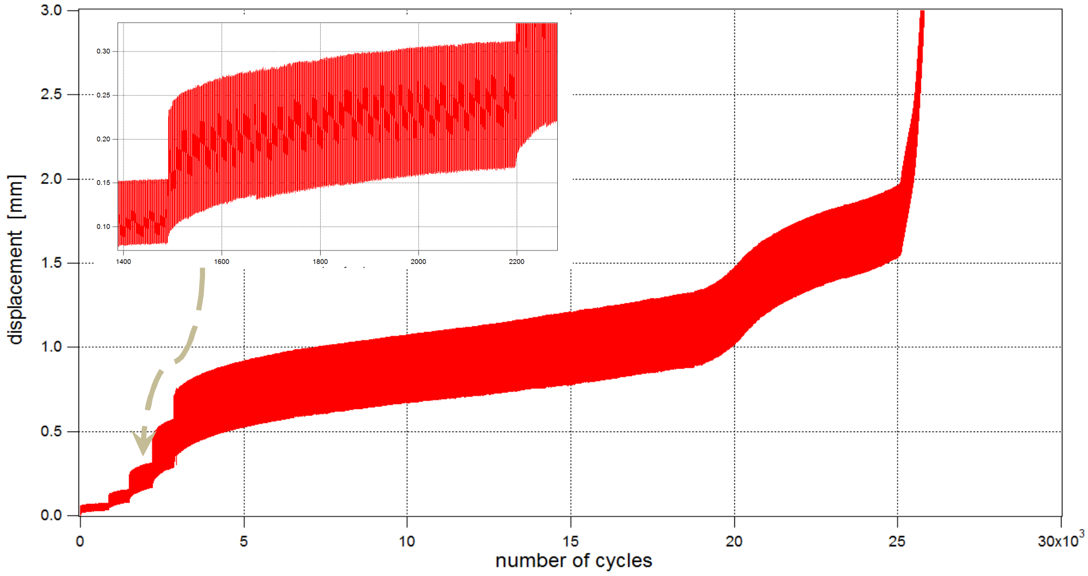

Figure 22 Displacement with increasing number of cycles upon failure for S2, with a zoom on the increase of displacement on load amplitude 400kPa.

Stiffness development

In the previous chapter we saw that the material does not only show a simple stiff behavior with increasing number of cycles, but seems to become stiffer with time on a low load amplitude. The actual failure or first signs of fatigue behavior of the samples occurred on a much larger load amplitude of those to be encountered in most civil engineering applications with a rather sudden event as was seen in figure 21. This can be confirmed by further examinations of the shear modulus, which was calculated according to figure 23.

The deviator stress q has been calculated according to $q = (\sigma_1 - \sigma_3)$ with σ_1 and σ_3 the major and minor principal stresses. Regarding single loops, the deviatoric cyclic stress q_c was obtained as stated in figure 23. Since the cyclic loading has been conducted under undrained conditions, the shear strain ϵ_s is equal to the main strain ϵ_1.

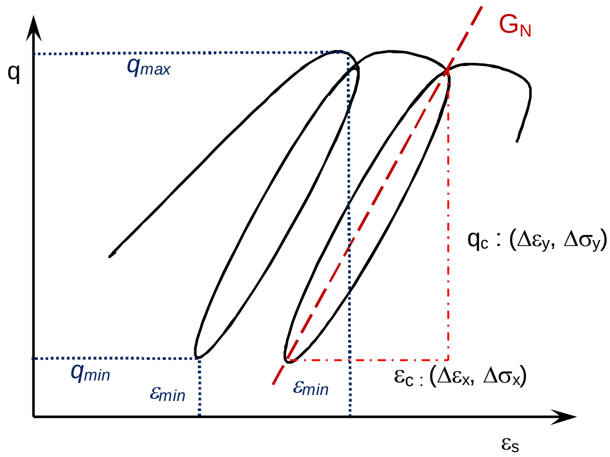

Figure 23 Scheme of calculating G- Modulus from stress- strain diagram, with Gn as the shear modulus depending on the number of cycles.

In order to make further examinations on the fatigue behavior first the unload reload paths of a single cycle regarding the shear modulus and deviatoric strain was compared (figure 24).

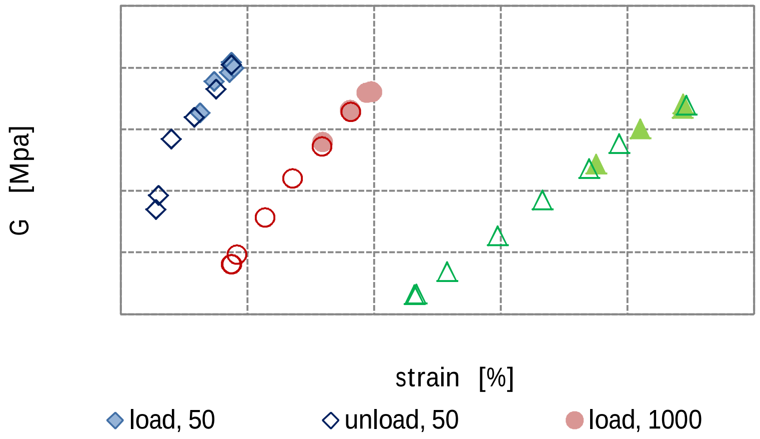

Figure 24 **Shear modulus for unload- reload parts of loops regarding to strain for S2, for 100kPa (blue), 200kPa (red) and 400kPa (green).**

Only a few data points for the reloading part were available, nevertheless it can be seen from the graph that the unload and reload part of a cycle follow the same path. Therefore no distinguishing difference is made between unload and reload parts of one cycle, considering both parts follow the same path. The reload part obviously reached higher values widening the range of values. This was the shear modulus and thus the stiffness can be further examined. Figure 25 (A) and (B) show the development of the shear modulus regarding to vertical applied stress for four and three cycles respectively. The values in these graphs were chosen to show the range of the initial 700 cycles on 100kPa vertical stress (A) and the range of the last cycles before failure on 1400kPa (B). From this a clear change in shear modulus with increasing stress and number of cycles can be seen. Both plots show that the shear modulus follows a linear trend within each loop for the minimum and maximum applied vertical stress. However when minimum stress is applied, the slope of the trend lines for the following cycles is nearly identical and the distance between them shows a small decrease with an increasing number of cycles. On the other hand in figure 25 (B), showing the same correlation for the maximum applied stress it can be seen that the behavior of the shear modulus with respect to the applied stress and number of cycles has changed. Overall, the amplitude of the shear modulus as well as the slope of the trend line which previously has been observed to be constant, have decreased and show a further decrease with increasing number of cycles on this particular stress level.

The correlation between shear modulus, applied stress and number of cycles found here corresponds with the previously shown stress-strain graphs. On the minimum applied stress level the slope of the curves was maximal and the distance between them in following cycles showed a small decreasing trend. This means within one cycle the stiffness increased during the loading part of the cycle and fell back to a lower value on the subsequent cycle. Decrease of stiffness on subsequent cycles seemed to decline with an increasing number of cycles. During maximum applied stress the shear modulus and thus the stiffness of the material is decreasing rapidly. This behavior was further examined, calculating the shear modulus in a cycle N (G_N) with respect to the shear modulus of the first cycle (G_1) for all cycles.

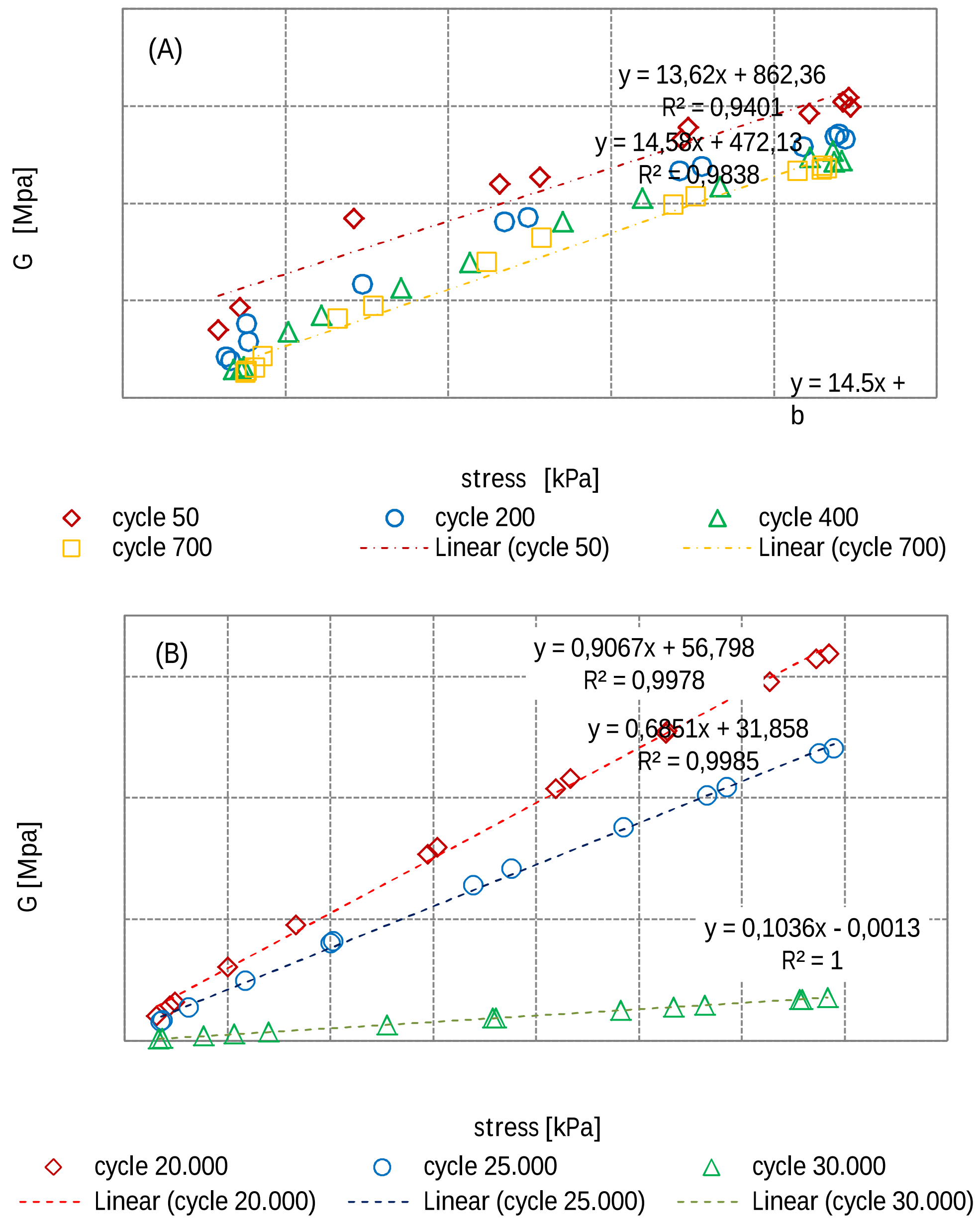

Figure 25 **Development of shear modulus against stress with increasing number of cycles for S2 at (A) 100kPa and (B) 1400kPa load amplitude.**

Degradation curves in figure 26 are shown for S1 and S3, resp. weakest and strongest sample, to demonstrate the different dimensions of stiffness and its degradation, which are nevertheless following the same trend. From figure 26 (A), results for S1, it can be observed that the shear modulus within one load amplitude remains on a constant level with minor variations, which are probably caused by inter granular movements. This means that with an increasing number of cycles on a comparably low stress level, the material does not undergo significant changes in stiffness. Only with the last increase of load amplitude, which led to failure of the sample, an immediate decrease in G_N was observed. Every increase in vertical stress yields a sharp increase in shear modulus, indicating a stiffer behavior on higher applied loads. Figure 26 (B) shows the same relationship for S3 as for S1. The inset zooms into the section of the figure at low ratios of G_N/G_1 revealing the same pattern as for S1.

Further comparing with S1, the range of shear modulus on low stress amplitudes is near zero, but shows the same sharp increases in G_N/G_1 as when the vertical stress was increased. At a load increased to 1400kPa, a large increase in G_N was measured. With an increase in the number of cycles, the G_N/G_1 eventually decreased indicating degradation in stiffness of this sample.

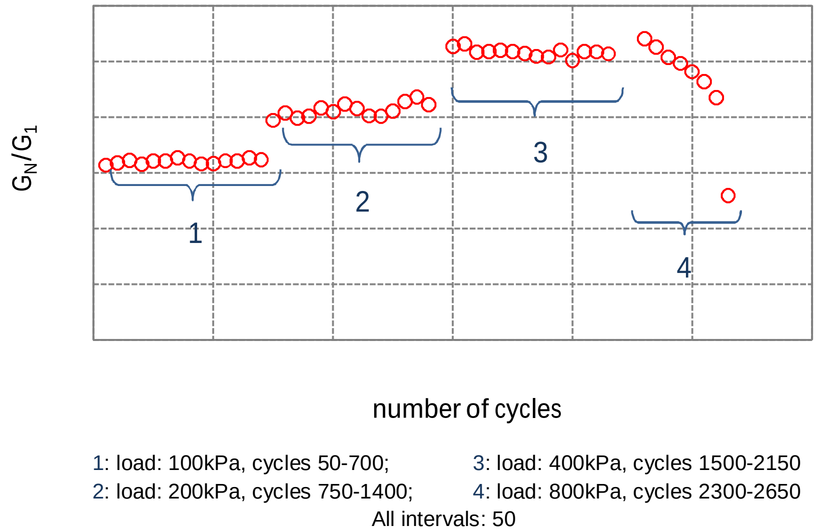

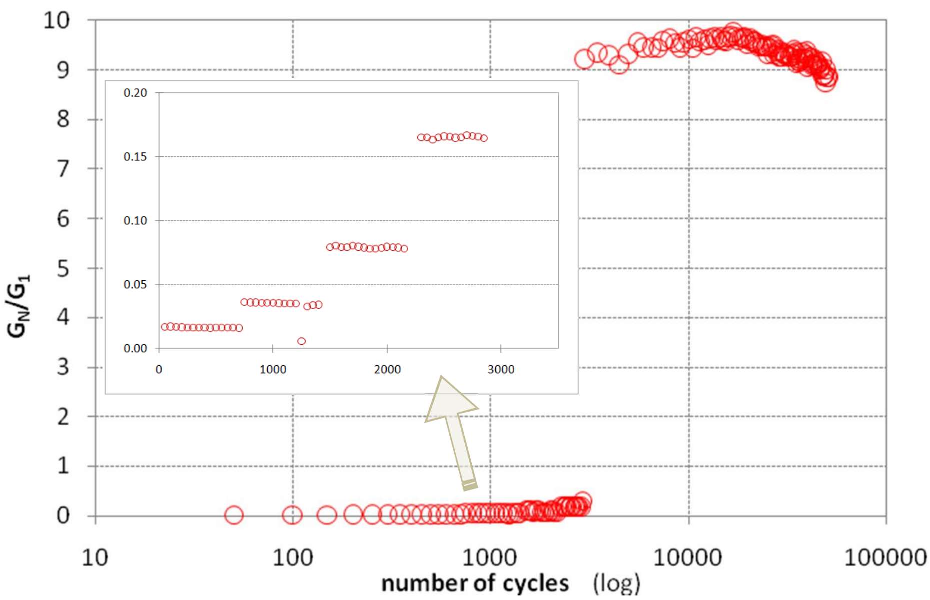

Figure 26 **Degradation of stiffness as shear modulus of cycle N (G_N) with respect to initial shear modulus (G_1), with increasing number of cycles for S3 (A) and S1 (B).**

From these correlations it was hard to determine what the exact effect is of the number of cycles on the stiffness of the material. Further investigations were made on the correlation between cyclic shear strain ϵ_c versus number of cycles (figure 27). For low cyclic loads ϵ_c follows a slowly decreasing pattern. From load amplitude 100kPa to 200kPa an increase in the slope of the declining strain can be seen. When the load increases to 400kPa the slope decreases again, indicating a change in stiffness behavior. The last increase to 800kPa shows an increase in strain with increasing number of cycles following an exponential trend line, eventually causing the sample to fail.

From this it can be concluded that on relatively low cyclic loads the strain of the material is decreasing in a very slow but stable manner throughout the entire time tested at a particular load. However, it can be assumed that the strain will not continue to decrease indefinitely, but reaches a yield value from which it will remain constant or start to raise. On higher loads such as in the ending phase of the test of this sample an immediate phase of softening is encountered. This correlation holds true for all other samples subjected to cyclic loading.

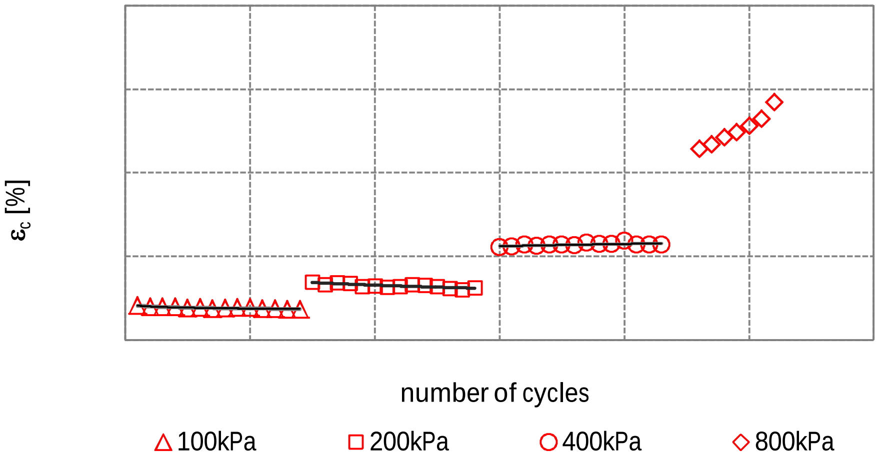

Figure 27 Strain within one cycle with respect to number of cycles for S1.

Since strain is the driving factor for stability of the material the normalized shear modulus (G_N/G_1) was plotted against the cyclic strain (ϵ_c) (figure 28). In figure 28A, degradation curves are plotted for S1, S2, S4 and S5 at cyclic load amplitudes of 100kPa to 800kPa for cycles 50-2900 with an interval of 50 cycles and for load amplitude 1400kPa with 3000 cycles upon failure with an interval of 500 cycles, except for S5 which had an interval of 1000 cycles. Figure 28 B is a zoom of the degradation curve for S1, S2 and S4 at a load amplitude of 100kPa. The plots show that all samples follow more or less the same pattern of degradation in stiffness. The vertical stress enforced on the samples obviously did not significantly influence the pattern of stiffness degradation. With each increase of vertical stress a sharp increase in shear modulus is observed, which is similar for strain shown in previous figures. In civil engineering applications mainly low cyclic stress levels occur, the degradation of stiffness follows an entirely linear trend (Figure 28B). The speed in which stiffness degrades caused by increased strain depends on the initial stiffness. High initial stiffness degrades faster than low initial stiffness. The data does not show any yield value of strain separating the initial stiffness from a start of substantial stiffness degradation as reported by Sharma and Fahey (2004).

Conclusion: the tested BioGrout shows a clear linear response to cyclic loading throughout all tested cyclic load amplitudes and number of cycles. Therefore it will be rather hard to distinguish and predict at which point the degradation of stiffness will be high enough to cause failure.

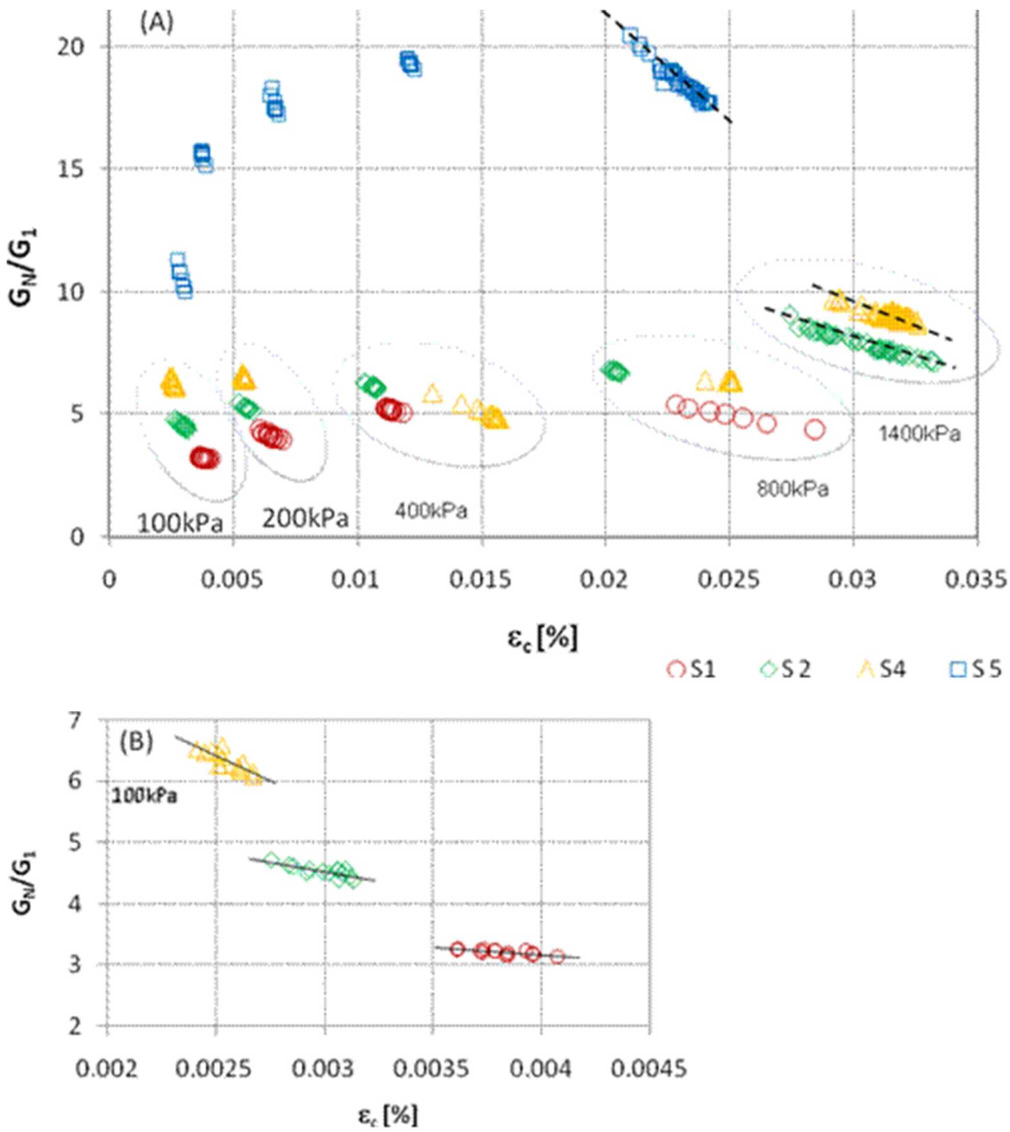

Figure 28 **(A) Degradation of stiffness with respect to cyclic shear strain and number of cycles, (B) shows a zoom into the degradation curves of S1, S2 and S4 on load amplitude 100kPa for initial 700 cycles.**

Chemical durability

The data clearly shows a decrease in compressive strength of all treated samples which can be related to dissolution processes inside the samples. During the experiment the pH, conductivity and $CaCO_3$ content increased in the effluent, indicating that dissolution reactions took place in the samples during flushing. Since the aim of this study was to determine the loss of strength due to chemical alteration caused by pore fluids, the chemical processes that took place were not investigated. However, the $CaCO_3$ content is clearly an important factor for the strength of calcareous soils and therefore its dissolution was looked at in more detail.

Measurements of $CaCO_3$ content showed an increase when flushing with artificial rain and demineralized water. Since values for both fluids are in the same range it was not possible to determine which fluid had a greater impact on the material. The artificial rainwater measurements show a higher scatter. The average dissolution rate of $CaCO_3$ was determined for each column. The dissolution rate of $CaCO_3$ for artificial rain water was around 10 mg/L with a high standard deviation (table 14).

The reason for the high deviation rate is probably because the fluid was artificially made in four batches leading to slight differences in composition and / or because the vessel, in which the influent was stored, was not constantly stirred. Measurements showed that the pH increased from the bottom to the top of the vessel. One can assume that also a gradient in $CaCO_3$ content and other components might have formed. Experiments with demineralized water showed a lower dissolution rate of 7 mg/L, with a small standard deviation. After flushing the columns with 260 pore volumes of fluid, the total dissolution of $CaCO_3$ was estimated between 3-4.5 % of the initial amount $CaCO_3$ (table 15 and figure 29).

Table 15 Details of dissolution of $CaCO_3$ for different samples.

$CaCO_3$		**CR 1**	**CR 4**	**CD 2**	**CD 3**
dissolution rate	[mg/L]	9.97	9.12	7.08	6.62
standard deviation	[mg/L]	2.42	2.42	2.42	2.42
density after treatment	[mg/cm³]	30.5	40.2	30.0	29.8
total amount after treatment	[g]	11.82	15.98	12.13	12.25
initial density	[mg/cm³]	31.93	41.43	30.92	30.62
initial content	[g]	12.373	16.472	12.500	12.586
total amount dissolved	[g]	0.555	0.488	0.370	0.336
total amount dissolved	**[%]**	**4.48**	**2.97**	**2.96**	**2.67**

As stated earlier, due to practical reasons the flow rate was lowered by half twice for approximately 65 hours during the experiment. However, the dissolution of $CaCO_3$ remained unaffected, indicating that the optimal dissolution was reached with a flow rate of 1 pore volume/h (figure 30).

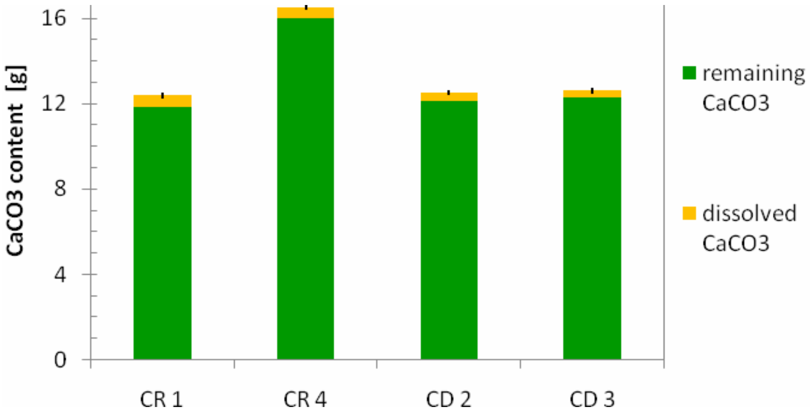

Figure 29 Initial $CaCO_3$ content of all samples with total amount of dissolved and remaining $CaCO_3$ content, including standard deviation (black dash).

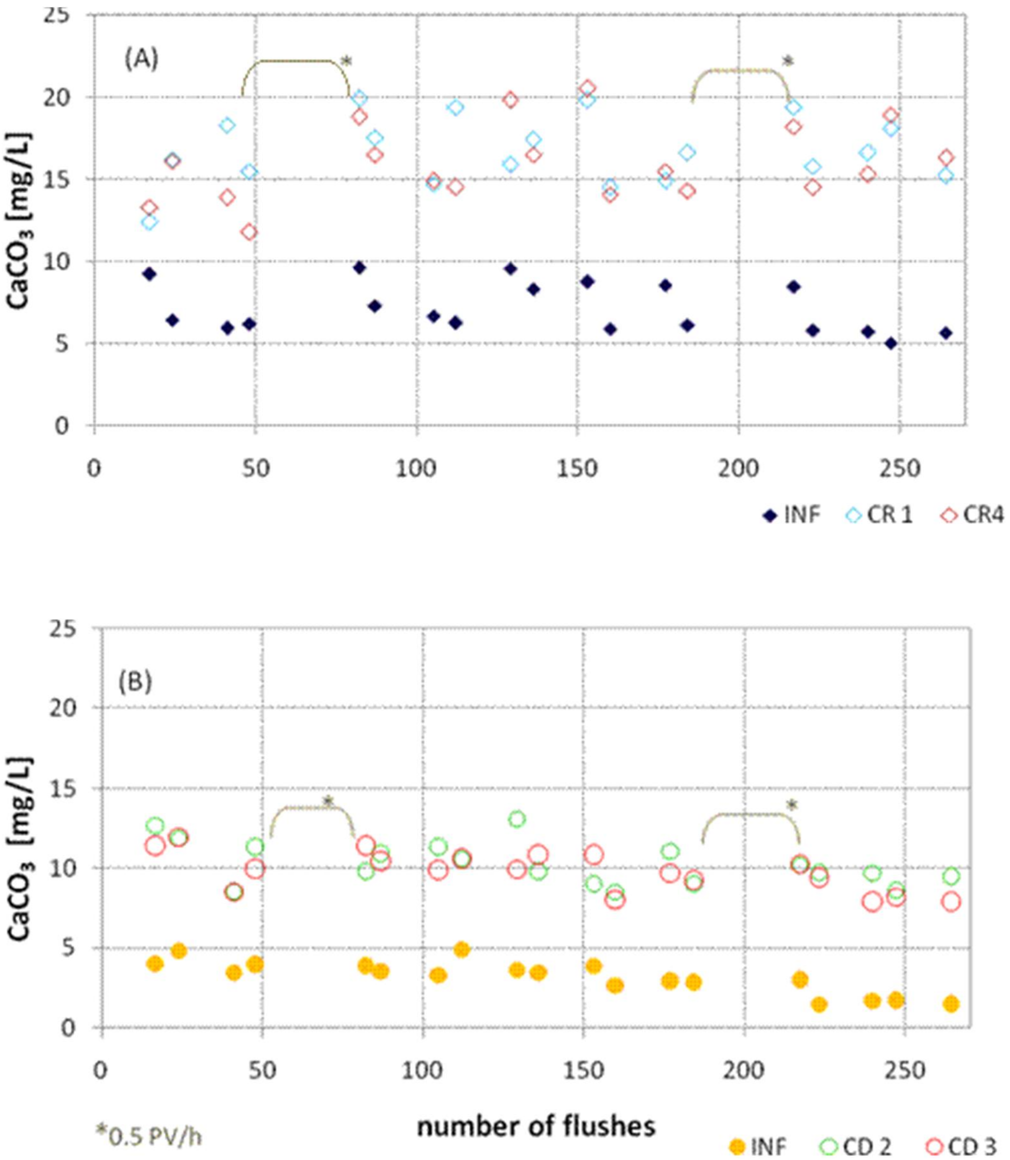

Figure 30 **Dissolution of $CaCO_3$ content for flushed through artificial rainwater (A) and demineralized water (B) during the experiment; the intervals marked with * indicate the period of lower flow rates during the weekends (0.5 PV/h).**

After flushing, the BioGrout samples were removed from the PVC tubes and their unconfined compressive strength (UCS) was tested. Due to the insufficient height of the samples the UCS tests were carried out on a 1:1 ratio and subsequently the standard values of 1:2 ratio according to ASTM D2938-86 were calculated. Details of the tested sand samples are shown in table 16.

The correlation with dry density and peak strength was determined (figure 30). The plot shows that all samples are below the estimated strength levels, also CB5 which should correlate with the predicted strength since it was not treated. The strength of the sample is probably lower due to a lower $CaCO_3$ content. Table 15 shows that the initial calcite content in CB5 was the lowest of all tested samples. The strength of the material was determined using the correlation between cementation and dry density. However, the correlation shown in figure 31 did not take into account the $CaCO_3$ content. Since both values of CB5 are very low compared with the treated samples it is understandable that its strength is around the same value as the treated samples.

Table 16 Details of precipitated sand columns prepared for unconfined compressive strength tests.

		CB 5	CR 1	CR 4	CD 2	CD 3
h_{prec}	[cm]	13.5	11.5	11.8	12	12.2
h	[cm]	5.37	5.25	5.44	5.15	5.23
d	[cm]	6.55	6.55	6.55	6.55	6.55
m	[g]	374.8	357.9	388.7	356.2	355.2
V	[cm³]	180.9	177.1	183.4	173.6	176.2
V_{mat}	[cm³]	122.3	118.2	129.8	119.7	118.9
m_{dry}	[g]	318.0	307.3	337.5	311.3	309.2
m_{sat}	[g]	376.6	366.2	391.1	365.2	366.5
V_{water}	[cm³]	58.59	58.91	53.59	53.87	57.30
ρ_{dry}	[g/cm³]	1.76	1.74	1.84	1.79	1.75
$CaCO_3$	[mg/cm³]	26.00	30.50	40.20	34.00	29.80
q_1	[kPa]	695	1034	1269	966	989
$q_{0.5}$	[kPa]	593	877	1086	815	838
q_{pre}	[kPa]	1333	1163	2184	1647	1306

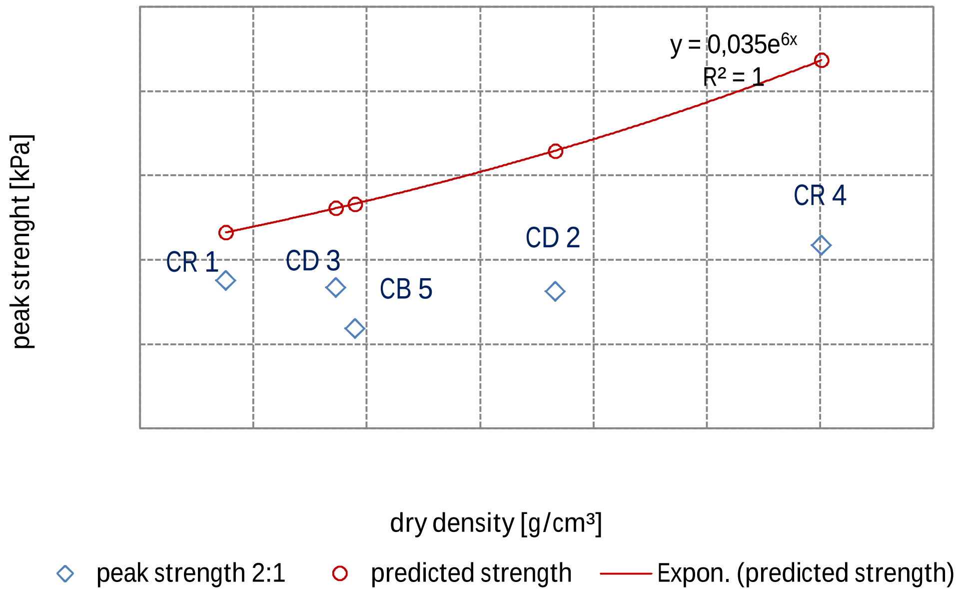

Figure 31 Predicted strength with respect to dry density calculated according to Van Paassen (2009) and measured peak strengths of the treated samples.

The focus of the experiment was to establish a correlation between the loss of $CaCO_3$ and the degradation in strength. Although tables 15 and 16 indicate a correlation with increasing amount of dissolved $CaCO_3$ the loss of strength decreases, the data available is not sufficient to set up a strong correlation (especially if we take samples CR1 and CD3 into consideration). Table 14 shows that CR1 encounters the highest amount of dissolution, whereas CD3 showed a minimum loss in $CaCO_3$. Yet CR1 shows a similar decrease in strength as CD3.

Conclusion: These tests are the first results on strength degradation of BioGrout due to chemical alteration caused by pore fluids. By flushing demineralized water as well as artificial rainwater through BioGrout samples a slight varying but overall constant dissolution of cementing material was found. Using a blank sample and the correlation between dry density and peak strength the unconfined compressive strength before treatment could be estimated. The UCS test showed a decrease in peak strength, yet no substantial correlation between the loss of $CaCO_3$ and decrease in strength could be established.

Taking into account only the absolute values obtained from the performed experiment: an aquifer consisting of BioGrout with an average ground water flow of 1m per day would encounter a loss of only 0.01% $CaCO_3$ in 50 years considering the fluid passing through the material had the same properties as the used demineralized water.

Freezing-thawing cycles

During the freeze- thaw cycles it was observed that in both samples some sand grains were crumbling off the surface of the core, despite the foil wrapped around. As pore fluids freeze concentrically towards the inside of the core, expansion of the fluid could cause grains at the surface to break off more easily. This means that the dimensions of the samples decreased slightly after treatment (table 17). As mentioned before, S06 broke at the middle with a more or less even plane during handling after completion of the freeze thaw cycles. Signs of weakening or cracks were not observed. The failure of the sample was probably due to inhomogeneity of the sample. The measured unconfined compressive strength for both samples is shown in table 17. The correlation of dry density and peak strength by van Paassen (2009) shows a decrease in strength for S10 by approximately 170kPa. However, for S06 the strength predicted is lower than the actual strength by 26kPa. This might be within the range of error for measurements and prediction.

Conclusion: Due to freeze and thaw a loss in strength was observed. However, more experiments are needed to establish a strong correlation.

Table 17 Details of samples before and after freeze- thaw cycles as well as peak strength measured during UCS test.

			S10	S06 *
before treatment	**d**	[cm]	6.42	6.40
	h	[cm]	13.20	13.56
	m	[g]	876.1	853.9
after treatment	**d**	[cm]	6.41	6.38
	h	[cm]	13.19	13.50
	m	[g]	874.3	841.2
	ρ_{dry}	[g/cm³]	1.88	1.66
	ф	[%]	0.231	0.232
	$CaCO_3$	[mg/cm³]	62.47	40.30
	q_{pre}	[kPa]	2824	759
	q	[kPa]	2657	785

5.4 Conclusions

- Two flushes with nutrients typically gives sufficient strength for preventing erosion (Hole erosion test)
- The difference between the critical head for a complete permeable BioGrout structure and the head for an impermeable structure is about 20%.
- Two possible failure mechanisms of the BioGrouted part of the sand can be distinguished: fluidization (heave), leading to backward erosion around the BioGrouted sand, and break-through. Calculations with a groundwater flow model and the model of Sellmeijer indicate that failure by backward erosion around the BioGrout might be a larger risk than failure through the BioGrout. This aspect has not been investigated in this research, as it is very dependent on local conditions (width of the structure and exit point geometry.
- The depth of the BioGrout structure has a bigger influence on the critical head, than permeability of BioGrout.
- From the durability experiments, it can be concluded that mainly freeze and thaw have an effect on the strength of BioGrout; however more experiments are needed to determine the correlation. The chemical durability of BioGrout is high: an aquifer consisting of BioGrout with an average ground water flow of 1m per day would encounter a loss of only 0.01% $CaCO_3$ in 50 years considering the fluid passing through the material had the same properties as the demineralized water used. The mechanical durability of BioGrout shows a linear response to cyclic loading. At low loads, as typically occur for most engineering activities, the material behaves elastically with a minimal decrease in stiffness.

6 Modelling results for application of BioGrout in practice

6.1 Location of BioGrout volume to prevent backward erosion – principles

Backward erosion is a potential failure mechanism for dikes and levees. Through this mechanism, particles are washed out from a sand layer at the surface level or up to a few metres below the surface. The driving mechanism is the head difference on both sides of the levee. If this becomes too high, the mechanism occurs (Figure 32). Backward erosion can be avoided by reducing the head difference (e.g. by increasing the level on the protected side, if the flood level cannot be influenced), or by increasing the resistance. This depends on the properties of the sand and the length of the seepage path. A well-known solution is the widening of levees, sometimes by placing a berm, thus increasing the distance between the entry point and the exit point. This is only possible if the local situation permits this, i.e. if there are no space limitations.

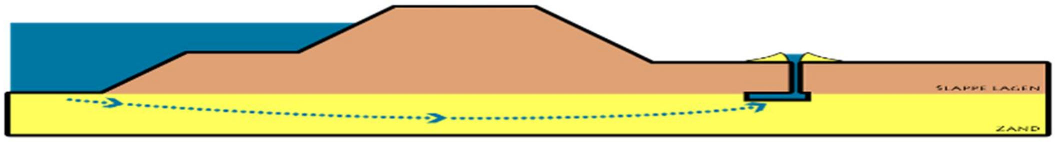

Figure 32 Schematic representation of backward erosion.

Installation of a screen, e.g. a sheet pile wall, is another possibility, through which the seepage path is enlarged vertically. This is usually expensive and future extensions are complicated or even impossible. Moreover, a closed screen only has a limited influence on the maximum head difference and the erosion process simply ‘dives’ under the screen.

Geometry of BioGrout

With BioGrout the permeability is hardly decreased, so most of the water still flows through the cemented volume. Backwards erosion downstream of the treated volume will still occur at the same head difference as before, but once the cemented grains are reached, the erosion will almost completely stop. When the head difference further increases, the erosion channel will be slightly enlarged, but because the main flow path remains unchanged, no alternative seepage flow, erosion path will develop as is the case with a sheet pile wall (or a “closed” volume of concrete, for example).

The geometry in figure 33 indicates the position and size of a BioGrout volume enabling a significant increase in head difference - with again the high water on the left side of the sketch.

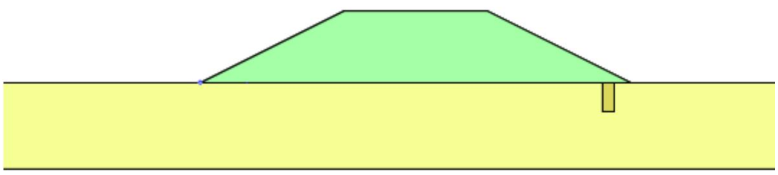

Figure 33 Schematic representation of the geometry of BioGrout in a flood defence system.

Several features can be noted:

- Position: an alternative seepage path through the toe of the levee should be avoided through the use of BioGrout. Although the reduction in permeability in the treated volume is likely to be small, this is still conceivable. If the toe mainly consists of clay, initially a thickness (of the toe) of 0.5 to 1.0 metre seems adequate;

- Thickness: theoretically, this solution is already sufficient when a continuous ‘wall’ of cemented sand grains is created with a thickness of less than 1 mm. In practice, other aspects should be considered too. First of all, the reliability of the solution: any hole through the treated volume will result in an abrasive flow of water and sand, quickly increasing the size of the hole. This should be avoided at all times. Secondly, other mechanisms, like local stability, come into play. A very thin cemented ‘wall’ with an eroded seepage path right behind it will cause shear stresses on this ‘wall’, which needs to be strong enough to withstand these stresses. For a very thin ‘wall’, this is not very likely. A more practical thickness is 30 centimetres.
- Depth: from small-scale seepage erosion tests with a volume of BioGrout extending to half the depth of the rather shallow sand layer, it appeared that the critical head difference could be doubled. The geometry of that test corresponded well to the geometry of the IJkdijk large scale backward erosion tests , with a sand layer thickness of 3 metres and a seepage length of 15 metres. With medium fine sand, the critical head appeared to be about 2.0 metres. Figure 33 reflects this geometry (to scale). With a BioGrout volume of 1 metre thickness, as sketched, a significant increase of the critical head may be expected.

.

6.2 (Optimal) injection strategies for BioGrout in the field

In this section, several injection and extraction strategies are proposed to obtain the geometry mentioned above in the field. These strategies were tried with the help of a model and should lead to a BioGrout body with a thickness of (at least) 30 cm and a height of (at least) 1 m. First, some constraints are given which should be taken into account when setting up an injection and extraction strategy. Several strategies for the placement of the bacteria are given and a set-up to investigate the influence of the density differences between the urea/calcium chloride solution and fresh water.

Constraints

In order to prevent backward erosion, there should be no gaps between the BioGrout body and the clay layer above it. Uncemented paths through the BioGrout body are also not allowed. With the BioGrout process the bacteria attach to the sand grains and they catalyse the reaction by which calcium carbonate is formed. If, however, the flow rate is too high, the bacteria are washed out and no calcium carbonate is formed. For that reason, the chosen flow rate should be small.

The urea/calcium chloride solution that is injected after the placement of the bacteria has a density which is larger than the density of water. The heavier fluid tends to sink. The residence time of the urea/calcium chloride solution should be short, such that no gaps appear between the BioGrout body and the clay layer above it. In other words, the horizontal flow velocity should be large, such that the vertical flow velocity (which is as a result of the heavier fluid density) is negligible. On the other hand, the flow velocity cannot be too high, in order to prevent wash out of bacteria. To meet both constraints, the distance between the injection and extraction lances should be small. In these tests, we choose 2.5 m as a distance between the injection and extraction lances.

Since the height of the BioGrout body should be 1 m, the length of the filters in the injection and extraction lances will also be 1 m.

Placement of the bacteria

In this subsection, several injection and extraction strategies were investigated. A tracer fluid was injected and examined to see whether the whole volume that should be BioGrouted was reached.

The porosity of the sand layer under the dike equals $\theta=0.4$ and its permeability equals $K=8x10^{-5}$m/s.
Figure 34 displays a part of the dike in top view. The row of lances is parallel to the dike. The lances are labelled with A, B, C, D and E.

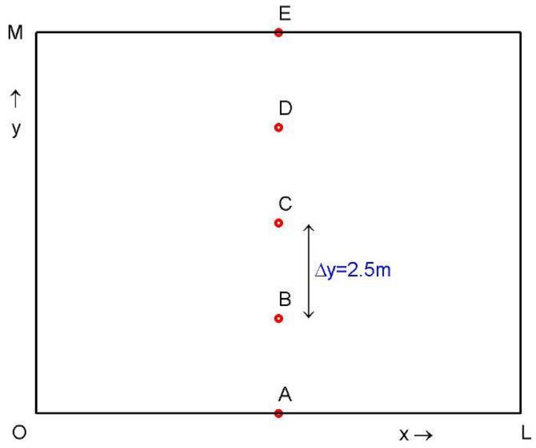

Figure 34 **Location of the injection and extraction lances, top view. The y-axis is parallel to the dike.**

The pore volume per injection lance (pv) is calculated by the formula L x W x H x θ, in which θ is the porosity, H the desired height of the BioGrout body (1m), B is the desired width of the BioGrout body (0.3m) and L is the length of the BioGrout body that is to be created from that specific lance (2.5m or 5.0m). The bacteria are injected with an activity of 2 mS/cm/min. The locations of interest are the locations where the activity is / has been at least 0.2 mS/cm/min.

In Table 18, four strategies are given for injection and extraction, including what fluid was injected. The flow rate at the injection and extraction lances was Q=0.6 m^3/h/lance. Injection was stopped when the injection fluids, as given in Table 18, were injected. Extraction started at the same time as injection and was maintained for 10 hours.

Table 18 **Injection and extraction strategy Strat1a, Strat1b, Strat2a and Strat2b. The difference between a en b is, that in b twice as much bacteria are injected than in a.**

name	*Injection/extraction strategy*	*Injection fluids*
Strat1a	Injection via lances B and D Extraction via lances A, C en E	1/5 pv bacteria 1/5 pv water 6/5 pv urea/calcium chloride (1pv=5*0.3*1*0.4=0.6m^3)
Strat1b	Injection via lances B and D Extraction via lances A, C en E	2/5 pv bacteria 1/5 pv water 6/5 pv urea/calcium chloride (1pv=5*0.3*1*0.4=0.6m^3)
Strat2a	Injection and extraction sequentially in couples of two lances: 1) injection B, extraction C 2) injection C, extraction D 3) injection D, extraction E	1/5 pv bacteria 1/5 pv water 6/5 pv urea/calcium chloride (1pv=2.5*0.3*1*0.4=0.3m^3)
Strat2b	Injection and extraction sequentially in couples of two lances: 1) injection B, extraction C 2) injection C, extraction D 3) injection D, extraction E	2/5 pv bacteria 1/5 pv water 6/5 pv urea/calcium chloride (1pv=2.5*0.3*1*0.4=0.3m^3)

Figure 35 shows another configuration. Two extra rows of lances are placed (labelled with 1 and 3), parallel to the existing row with lances. These extra lances are used for water injection and extraction in order to get a smaller BioGrout body than with the configuration in Figure 34.

The corresponding injection and extraction strategies are given in table 19. The flow rate at the injection and extraction lances is Q=0.6 m^3/h/lance for Strat3a and Strat3b and Q=0.3 m^3/h/lance for Strat4a and Strat4b. Again, injection is stopped when the injection fluids, as given in table 18, are injected. Extraction starts at the same time as injection and is performed for 10 hours.

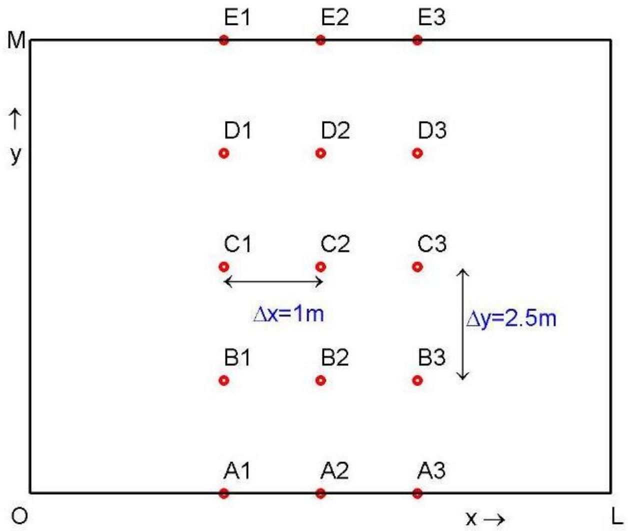

Figure 35 Location of the injection and extraction lances, top view. The y-axis is parallel to the dike.

Table 19 Injection and extraction strategy Strat3a, Strat3b, Strat4a and Strat4b. The difference between a en b is, that in b twice as much bacteria are injected than in a.

Name	Injection/extraction strategy for BioGrout liquids	Injection fluids for BioGrout	Water injection extra extraction during injection
Strat3a	Injection via lances B2 and D2 Extraction via lances A2, C2 and E2	1/5 pv bacteria 1/5 pv water 6/5 pv urea/calcium chloride (1pv=5*0.3*1*0.4=0.6m^3)	Injection: B1, B3, D1 and D3 Extraction: A1, A3, C1, C3, E1, E3
Strat3b	Injection via lances B2 and D2 Extraction via lances A2, C2 and E2	2/5 pv bacteria 1/5 pv water 6/5 pv urea/calcium chloride (1pv=5*0.3*1*0.4=0.6m^3)	Injection: B1, B3, D1 and D3 Extraction: A1, A3, C1, C3, E1, E3
Strat4a	Injection and extraction sequentially in couples of two lances: 1) injection B2, extraction C2 2) injection C2, extraction D2 3) injection D2, extraction E2	1/5 pv bacteria 1/5 pv water 6/5 pv urea/calcium chloride (1pv=2.5*0.3*1*0.4=0.3m^3)	Injection and extraction sequentially in couples of four lances: 1) injection B1, B3 extraction C1, C3 2) injection C1, C3 extraction D1, D3 3) injection D1, D3 extraction E1, E3
Strat4b	Injection and extraction sequentially in couples of two lances: 1) injection B2, extraction C2 2) injection C2, extraction D2 3) injection D2, extraction E2	2/5 pv bacteria 1/5 pv water 6/5 pv urea/calcium chloride (1pv=2.5*0.3*1*0.4=0.3m^3)	Injection and extraction sequentially in couples of four lances: 1) injection B1, B3 extraction C1, C3 2) injection C1, C3 extraction D1, D3 3) injection D1, D3 extraction E1, E3

As BioGrout is used as a backward erosion prevention method, it is likely that seepage occurs during the injection of the BioGrout fluid, too. This was neglected thus far. We repeated Strat1a, but now with seepage and call this situation Strat5a. For our calculations, we assumed a head difference of 3m over 15m. It is likely that the seepage will influence the BioGrout process. To prevent this, extra lances can be placed to pump away the seepage water, such that there is no flow in the region where BioGrout will take place. The BioGrout process will also cause a flow, of course. Pumping away the seepage water was done with one pump per 2.5 m (Strat6a) or with one pump per 10 m (Strat7a). For the effect of the BioGrout process, we repeated Strat1a.

The effect of density differences on the flow

After the placement of the bacteria, urea and calcium chloride are injected. While the solution with bacteria has approximately the same density as water, the solution of urea and calcium chloride is denser than water. It is likely that density flow will occur. To investigate the influence of the inflow and outflow velocity on the effect of density difference on the results, the configuration as given in Figure 36 was investigated.

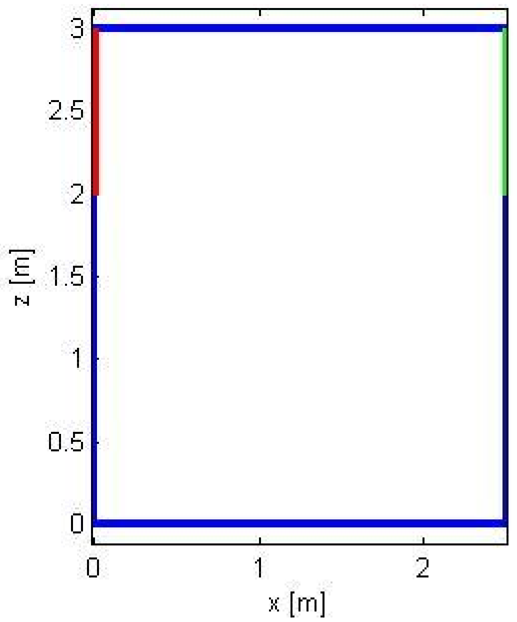

Figure 36 Configuration to investigate the effect of density differences on the flow.

This 2D configuration was placed vertically, such that density differences will have influence. Injection takes place at x=0m, between z=2m and z=3m (marked with a red colour). The extraction takes place at x=2.5m, also between z=2m and z=3m (marked with a green colour). The distance between injection and extraction has been taken as the distance that was used in the previous subsection, which is 2.5m. The flow rate and inflow concentration are varied. As a flow rate (pore water velocity) has been taken v=0.1 m/h, v=0.2m/h, v=0.3m/h, v=0.4m/h and v=0.5m/h. As an inflow concentration, c_{in}=1M and c_{in}=0.7M has been used.

The following formula has been used to calculate the injection time: T_{inj}= 0.48/v, in which v is the injection velocity. Extraction starts at the same time as injection, but continues when injection is stopped.

6.3 Results of the flow strategies model

In this section, several results of the various flow strategies are shown, in the first part on the placement of the bacteria and then by the effect of density differences on the flow.

Results for the placement of the bacteria

In this subsection, several results are shown for the placement of the bacteria. Since the bacteria provide the production of calcium carbonate, it is important that the bacteria are present at the locations that need to be reinforced. In this subsection the locations are shown where the activity of the bacteria was at least 0.2 mS/cm/min for some time for the various flow strategies.

In the appendices A to K some other results are shown, like the activity of the bacteria in the soil at several times, the pressure during injection and extraction and the pore water speed in the soil. To prevent bursting, the pressure can not be to high. The pore water speed should also be small enough, to prevent wash out of bacteria and backward erosion.

Figure 37 shows the results for the first eight strategies. The left column displays the results for the cases in which 1/5 pv of bacteria was injected, while in the right columns, twice as much bacteria were injected.

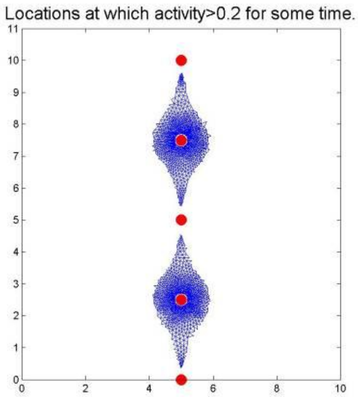 Strat1a	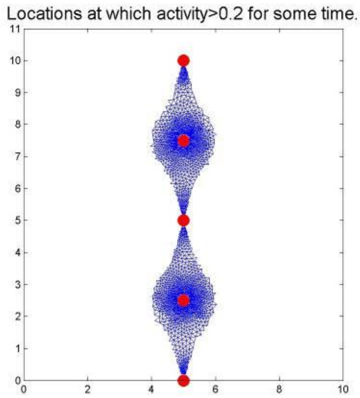 Strat1b
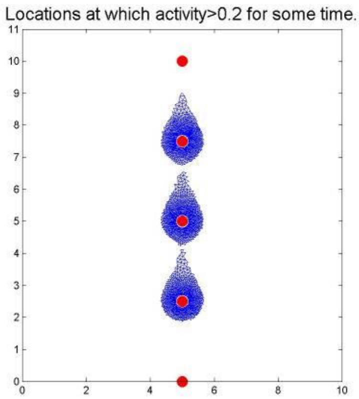 Strat2a	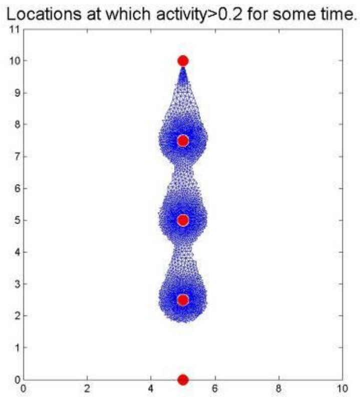 Strat2b

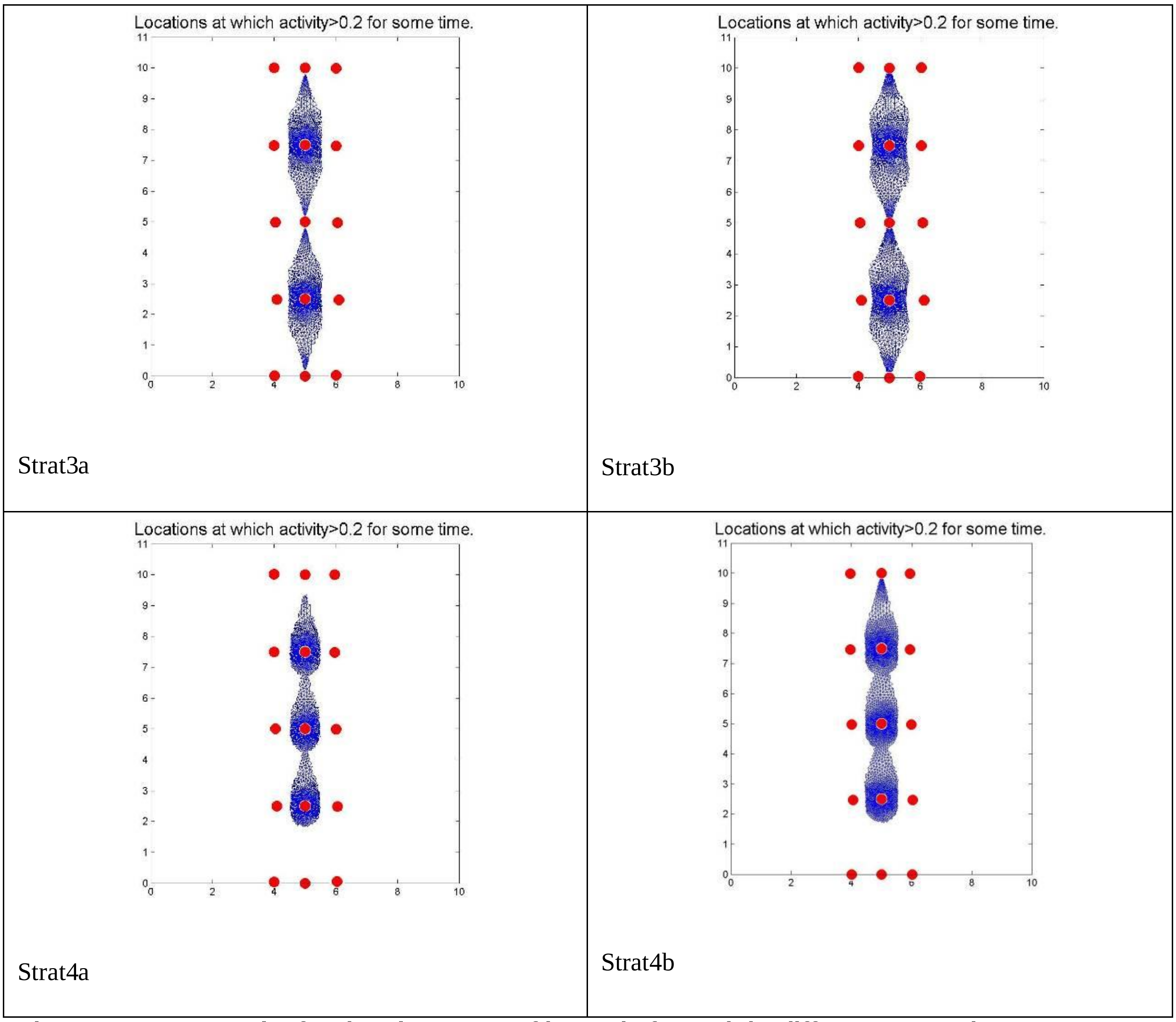

Figure 37 Results for the placement of bacteria from eight different strategies.

In Strat1a and Strat1b, the extraction points are weak zones, since the concentration of bacteria is not high enough (Strat1a) or only high enough in a very thin zone (Strat1b).

In Strat2a and Strat2b, the extraction points become injection points. Hence, the zones around the lances are strong zones. Enough bacteria should be injected , however, to get a closed BioGrout body, as is reached in Strat2b.

Strat1a, Strat1b, Strat2a and Strat2b are repeated, but extra lances are used in order to get a smaller and more homogenous BioGrout body. The extra lances are placed parallel to the existing row with lances used for water injection and extraction. This indeed results in a smaller and more homogeneous BioGrout body. The extraction points are now reached in all cases, although there are still weak zones in Strat3a, Strat3b and Strat4a.

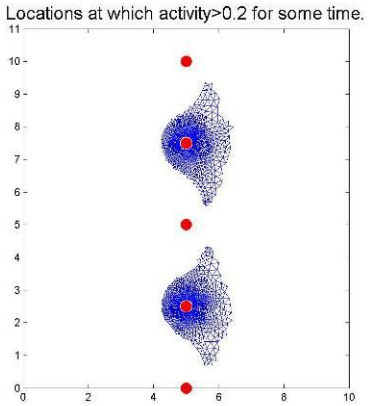

Strat5a

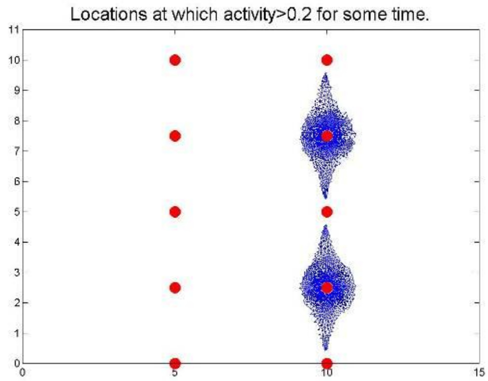

Strat6a

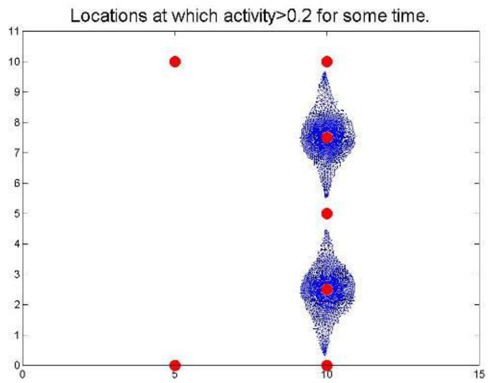

Strat7a

Figure 38 Repeated strategies, including influence of seepage.

In Strat5a, Strat1a is repeated, but now seepage is no longer neglected. The seepage influences the flow and results in large weak zones around the extraction wells. In order to get a zone without seepage in the region where BioGrout is adapted, extra lances are placed to pump away the seepage.

In Strat6a, four lances are used every 10 m, while in Strat 7a only one lance is used per 10 m. In both cases, the shape of the BioGrout body is the same as for Strat1a, as was desired (Figure 38).

The effect of density differences on the flow

In this subsection, some results are given of the investigation of the effect of density flow. Results are shown for several inflow velocities and concentrations (Figure 39).

The left plots in the following table display the locations where the concentration of urea/calcium chloride has been at least 0.2M. The right plots display the concentration at the top of the outflow filter (point (2.5; 3) as a function of time. This point has been chosen as a check to see if there is a gap between the BioGrout body and the clay layer above it. The inflow concentration equals c_{in}=1M and the inflow velocity is varied.

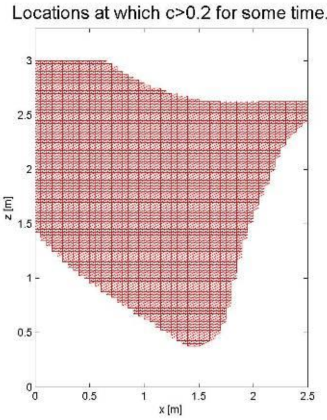 v=0.1m/h	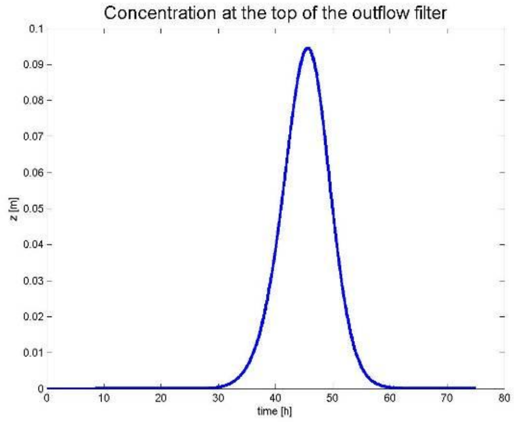
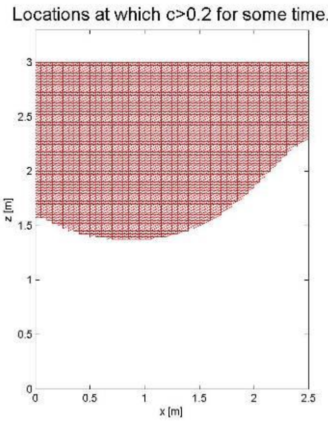 v=0.2m/h	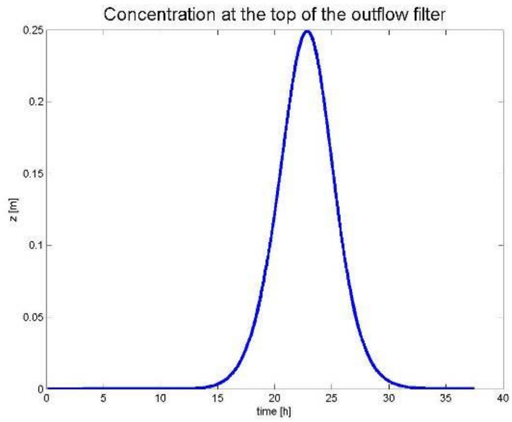

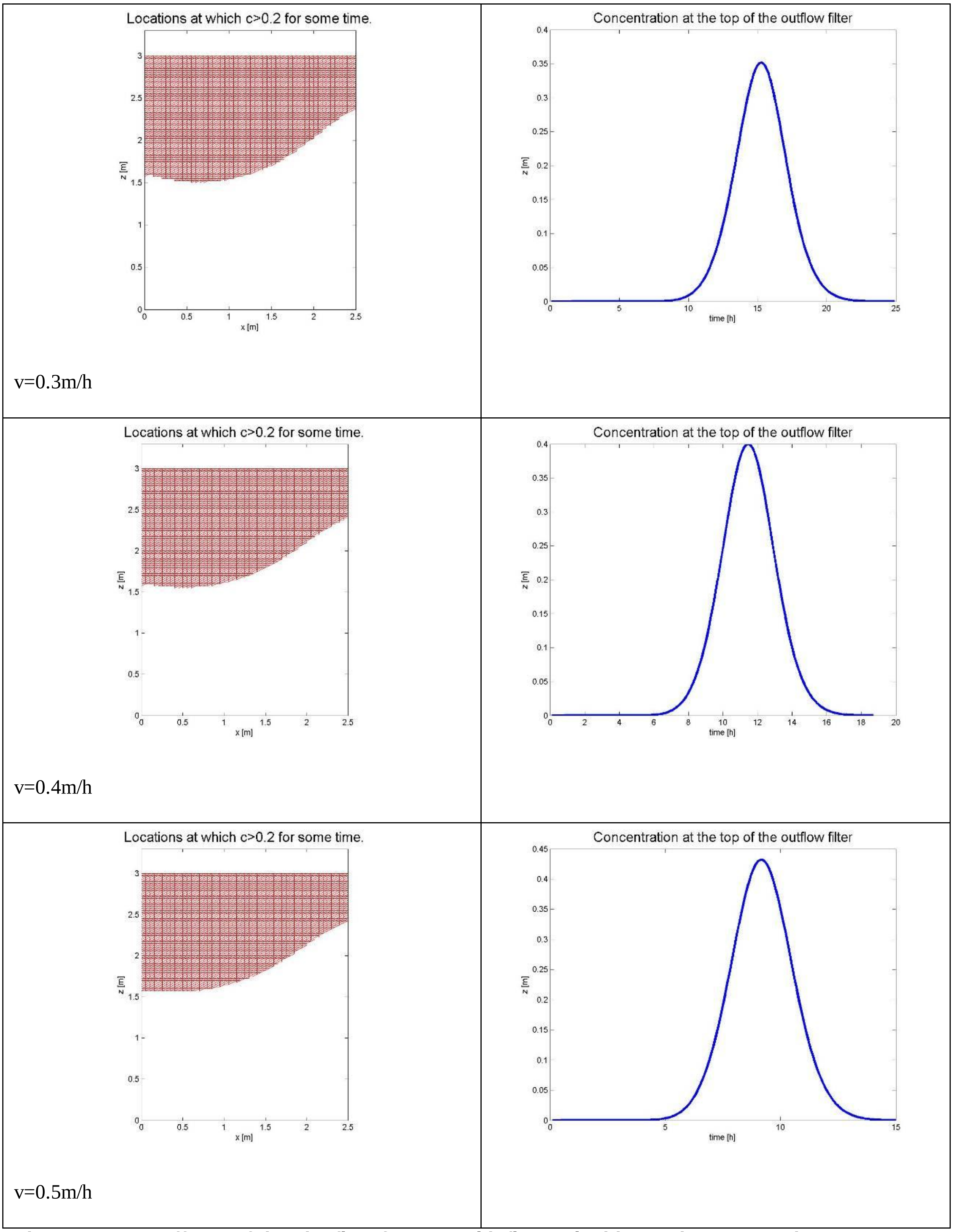

Figure 39　　Effects of density flow for several inflow velocities and concentrations.

If the injection and extraction flow rate is large, the residence time of the species is short and density flow only has a small influence. As a consequence, the maximal concentration at the top of outflow filter, directly below the clay layer, is high for a large inflow velocity.

The shape of the body that is reached with a sufficiently large concentration of urea and calcium chloride is comparable for v=0.2 to v=0.5 m/h, but significantly differs from the shape for v=0.1m/h. In the last case, the residence time is so large that the dense solution sinks away and only partly is pumped up.

Decreasing the concentrations will only decrease the density and hence, the density effect. The simulations above are repeated, but now for a lower inflow concentration. In these cases we have c_{in}=0.7M as an inflow concentration. The results are comparable, but especially for the inflow velocity v=0.1m/h, the density effect is smaller than for the inflow velocity c_{in}=1M.

From these figures, it can be seen that the flow velocity should be large enough. If the flow velocity is too small, the density differences will result in a gap between the top clay layer and the BioGrout body. The latter should be avoided since it has a risk of backward erosion.

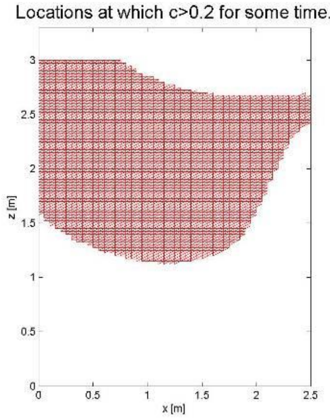

v=0.1m/h

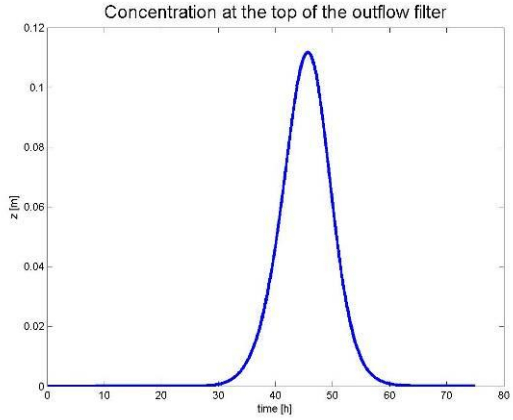

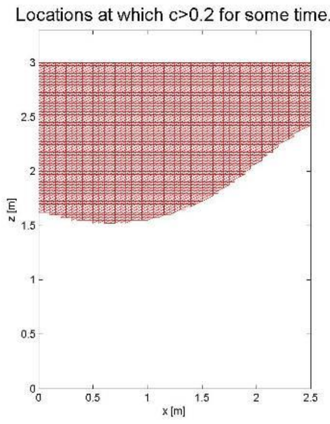

v=0.2m/h

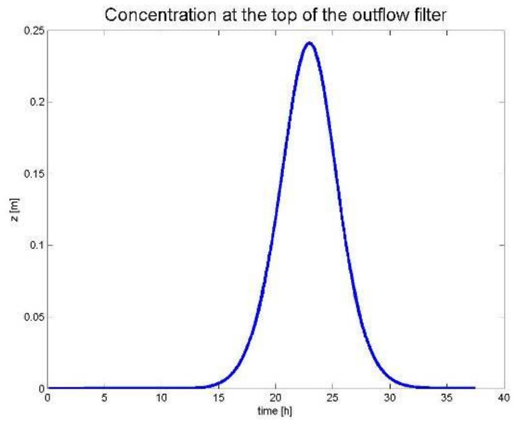

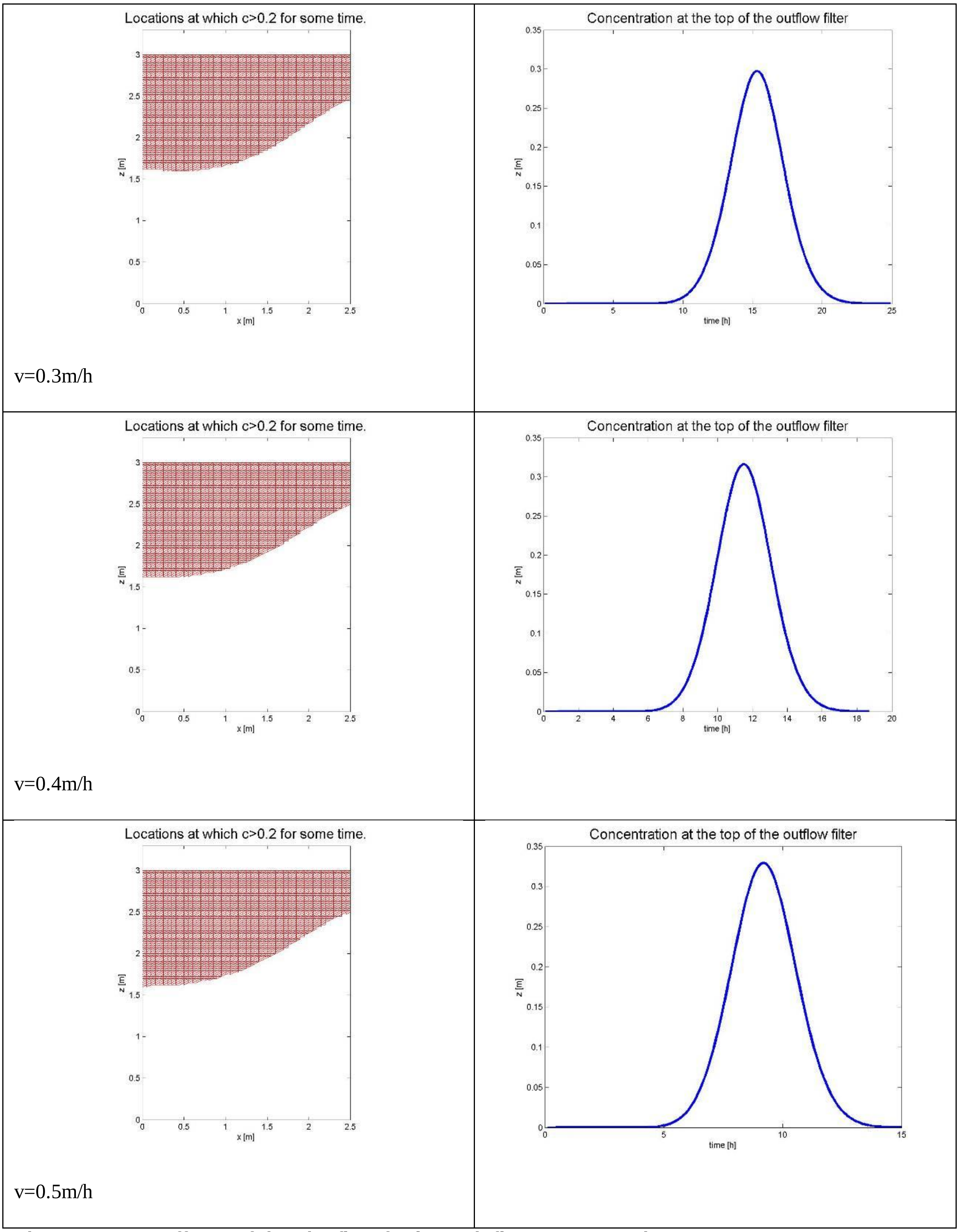

Figure 40 Effects of density flow for lower inflow concentrations.

6.3 Conclusions and Recommendations

The extraction lances are weak zones in the BioGrout body; see the results of Strat1a and Strat1b. A solution to this is to use the extraction lances later on as an injection lance or vice versa (Strat2a and Strat2b). Placing extra lances for water injection and extraction, left and right of the lances that are used for the BioGrout liquids, results in a smaller BioGrout body. The improvement is not very large, however and is probably outweighed by the costs of the extra lances. Injecting only 0.2 pore volumes of bacteria leads to a BioGrout body with holes or weak zones. At least 0.4 pore volumes is needed.

Seepage really should be taken into account during the injection of the BioGrout liquids, since it influences the flow. This influence can easily be so large that the BioGrout liquids do not reach the extraction points. As a result, the zone around the extraction points is not reinforced and will be sensitive to backward erosion. Placing extra lances upstream in the dike to pump away the seepage water is a good measure (Strat6a and Strat7a). It is not necessary to place these lances every 2.5 m. As can be seen from the results of Strat7a, one lance per 10 m is sufficient. It should be verified if the pressures and flow velocities that are calculated are feasible in practice.

The solution with bacteria has approximately the same density as water. The solution with urea and calcium chloride is denser than water and that can give a density effect. If the injection and extraction flow rate is small, the residence time of the species is long and density flow has a large influence. The urea and calcium chloride can sink away and will not reach the (top of the) extraction lance. As a consequence, there can be a gap between the BioGrout body and the top (clay) layer and that zone will be sensitive to backward erosion.

Decreasing the inflow concentration decreases the density difference and hence the density flow effect.

In the simulations that were done, a tracer fluid has been modelled. Reaction is not taken into account. Adsorption and desorption are important phenomena in the transport of bacteria. They result into retardation of the bacteria and it will take more time before the bacteria reach the outflow.

Another important phenomenon is fixation. When the bacteria come in contact with the fixation fluid, that is also injected, they are fixed onto the sand grains and they will not flow further. Clay can also influence the fixation process. It is important that the bacteria are spread in the whole region that has to be reinforced.

The reaction of urea and calcium chloride results in a reaction product that is less dense than the original liquid. This diminishes the effect of density flow. On the other hand, it is possible that all the urea and calcium chloride have reacted before the extraction is reached. Again, this will result in weak zones. It is important to take all of these reactions into account.

Furthermore, it is questionable if an extraction lance can be used later on as an injection lance or vice versa, since the filter might be clogged. Another question is if the calculated flow rates and pressures are feasible in the sense of bursting of the soil, pumping air in the soil around the extraction points and backward erosion.

Local instabilities can result in fingering of the denser fluid. If this happens, the density flow as calculated is underestimated. Furthermore, in reality there are short streamlines with a short residence time, but also long streamlines with a very long residence time. On the long streamlines, density differences play a large role. All these streamlines with the corresponding residence times should be taken into account. This can be done by doing 3D calculations.

It is strongly recommended that for at least one flow strategy a 3D calculation is carried out, including adsorption, desorption, fixation, reaction of urea and calcium chloride and density effects. Since it is very important that there are no holes in the BioGrout body, this should be monitored in some way. There should also be a good protocol, what to do if, for example, a lance is clogged and does not work any more.

7 Industrial application

This chapter summarises the main results of the laboratory experiments, and considers how these results can be considered for industrial application, including the costs for executing BioGrout.

7.1 Implication of the lab results for field application

The main conclusions of this research and its implication for industrial application are shown in table 20.

Table 20 Main research results and what this means for in the field.

Research Results	Implications for field application
Two flushes of nutrients are sufficient to prevent and stop backward erosion.	• Small amounts of ammonium chloride are produced and treated. • Small impact on the natural condition of the soil. • 2 weeks on site: 1 week flushing, 1 week (de)mobilisation.
No erosion develops along the BioGrout and clay boundary.	• The clay and sand boundary is probably the most sensitive area where erosion will start. This will be prevented with BioGrout.
Permeability is maintained.	• Water flow is hardly influenced; • Gaining 20% in critical head compared with impermeable structure.
With deeper BioGrout “walls”, the critical head increases.	• The deeper the BioGrout wall, the higher increase in critical head. • 1 m BioGrout is typically sufficient to prevent backward erosion.
Up to 1400 kPa loading, BioGrout reacts very elastic.	• “Normal” engineering activities produce small loading amplitudes, indicating that BioGrout will behave elastically to it and failure will not occur. • The exact influence of loading on BioGrout produced by two flushes in the soil must be tested.
Freeze and thaw influences the durability of BioGrout, no correlation however is found.	• Locations where <u>in the soil</u> strong freeze and thaw cycles occur, more research is needed to determine the exact impact on the durability of BioGrout.
Flushing with artificial rain and demineralized water had a small impact on the chemical durability of BioGrout.	• With an groundwater flow of 1 m /day, 0.01% $CaCO_3$ /50 years dissolves.
Position of BioGrout 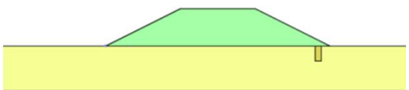	• BioGrout is good for use in locations where access is difficult or space for works limited. • Injection lances can be placed easily and will not cause damage to the flood defence.
Geometry BioGrout	• The BioGrout volume depends on the dike geometry, but the following geometry has been successfully tested in the lab: 0.3 m thick x 1 m deep x length “potential backward erosion”.
With modelling the injection strategy for in the field can be set up.	• Use models to define the injection strategy with 2D and 3D. • Monitoring is needed to determine if the BioGrout volume is treated evenly and no holes occur in the BioGrout volume.

7.2 Costs

Whether BioGrout will be applied in the field or not and to what extent, depends on two things: 1) does the technology work for preventing backward erosion? 2) What is the price for executing BioGrout? The first question can be answered positively. The lab results proove that BioGrout is a technology that is able to prevent backward erosion. The costs of a technology determine whether a technology is used and how often it is used. This paragraph gives some explanation about the costs for applying BioGrout. This is based on pilot tests and field tests that have been executed outside of the FloodProBE project.

The costs depend, as for other techniques, on the required volume of BioGrout, required depth and location. Therefore, it is hard to provide correct overall cost estimation. Costs can be divided into “project independent costs”, e.g. mobilization and demobilization, equipment and duration of treatment, and “project dependent costs”, like volume of the treated soil and required strength.

Assuming that the volume to be treated is 450 m^3, with 2 batches of 0.7M urea/$CaCl_2$ (0.5MPa), the costs will be:

- Project independent costs: € 60.000,
- BioGrout/m^3 costs € 450,-

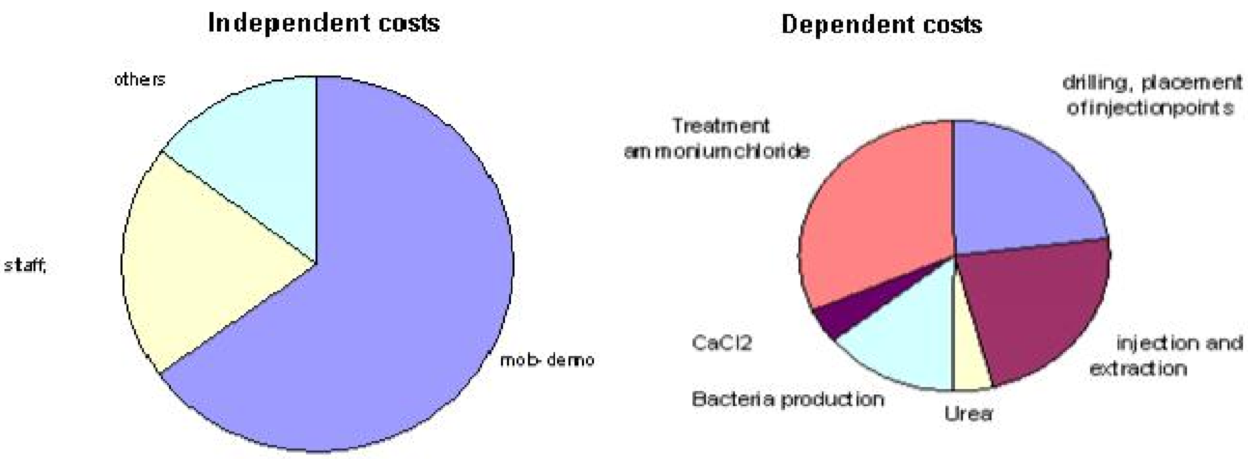

Figure 41 **Two diagrams showing the partition of costs for applying BioGrout. The independent costs are fixed costs, not influenced by volume, required strength. The dependent costs are variable costs, thus depending e.g. on volume and required strength.**

The main costs for applying BioGrout is the production of bacteria, the treatment of ammonium chloride and the mobilization and demobilization.

What should be kept in mind that this is a new technology, and therefore an optimisation process for application in the field must still be made. This will lower the cost price. However, in comparison to other solutions, the costs will still stay relatively high, making it a high-grade technology.

7.3 Connection to Water board

During the research programme a connection was made with four Dutch Water Board's and Stowa (Dutch Foundation for Applied Water Research, and stakeholder of FloodProBE). This was to be certain that the research done was applicable for in the field, and that the main questions stakeholders had before applying the technology in the field were answered. During four meetings the results of performed experiments were presented and discussed, and new experiments were planned. Not all questions could be investigated in the lab or in this project. The main issue was the connection of BioGrout with the topcoat, whish is tested extensive in the lab. Other questions were:

- Monitoring system needs to be set up to ensure that the total volume has the required minimum strength;
- What effect does BioGrout have on different materials occurring in the dike (e.g. wood, concrete)?
- What effect does the geometry of sand grains have on strength?
- Can cracks and fissures be created in the BioGrout due to vibrations? And can this be prevented?
- What effect does grass growing on the dike have on BioGrout?
- What effect does BioGrout have on grass growing on the dike?

After finishing the experimental programme, actions were undertaken to set up a pilot at the IJkdijk (North of the Netherlands), together with STOWA. Unfortunately, due to time pressure and shortage in budget this could not be executed.

7.4 Conclusions

Thus it can be concluded that BioGrout is a technology that can be used to prevent backward erosion under flood defence systems. It is suitable for flood defences where the water flow does not need to be stopped, but only erosion must be prevented. One must be aware that it can only be applied in permeable materials, so it cannot prevent erosion in clay/ peat formations. The main advantages of BioGrout as backward erosion method are: it is applied in situ, thus without disturbing the surroundings; only calcite is left in the soil; and it can be applied in poorly accessible locations, due to the use of light material. The durability of BioGrout is sufficient to endure "normal" activity around the treated soil. However, when large vibrations occur around the BioGrout volume, there is a chance that cracks will form in the BioGrout. Due to the costs it is a high-grade technology, and therefore it will not be applied to strengthen large volumes. It is very suitable for locations where other erosion prevention techniques cannot by used, due to a lack of space, restrictions on the disturbance of surroundings caused by vibrations, and areas not easily accessible.

It is recommended that a monitoring plan is defined for the first field tests, to ensure that the complete volume is BioGrouted, and no holes occur around the extraction zones. In areas/ countries where there is a warm summer and strong winter, where the soil regularly freezes and thaws, additional research is needed to determine the exact impact of these cycles on the durability of BioGrout.

BioGrout has a high potential to prevent erosion around hard structures in e.g. multifunctional flood defences. These locations are often inaccessible or inappropriate for traditional techniques.

8 References

Bezuijen, A., Steedman, R.S. (2010): Scaling of hydraulic processes, 7th int. conf. on Physical Modeling in Geotechnics, Zurich.

Bonelli, S., Brivois, O., Borghi, R, and Benahmed, N. (2006): On the modelling of piping erosion. Comptes Rendus de Mécanique, 8-9(334), pp. 555-559.

Boschloo, D.J., Stolk, A.P. (1999): Landelijk Meetnet Regenwatersamenstellingen, Meetresultaten 1995. RIVM Rapport 723101046 Rijksinstituut voor volksgezondheid en milieu national institute of public health and the environment.

Castanier S, Le Metayer-Levrel G, Orial G, Loubiere JF and Perthuisot JP. (2000): Bacterial carbonatogenesis and applications to preservation and restoration of historic property. Of microbes and art. Ciferri O, P Tiano and G Mastromei. New York, Kluwer Academic / Plenum Publishers: 203-218.

Hale, P.A., Shakoor, A. (2003): A laboratory investigation of the effects of cyclic heating and cooling, wetting and drying, and freezing and thawing on the compressive strength of selected sandstones. Environmental & Engineering Geoscience, Vol. IX, No. 2, pp. 117-130.

Ham, G.A. van den (2009): SBW Piping Kunstwerken – KW9. Analyse kleine schaalproeven, Deltares report 1200675-002-GEO-0001.

Harkes, M. P., J. L. Booster, et al. (2008). Microbial induced carbonate precipitation as ground improvement method – bacterial fixation and empirical correlation CaCO3 vs strength. International conference on BioGeoCivil Engineering, Delft.

Harkes, M.P., Van Paassen, L.A., Booster, J.L., Whiffin, W.S., Van Loosdrecht, M.C.M. (2009): Fixation and distribution of bacterial activity in sand induce carbonate precipitation for ground reinforcement. Ecological Engineering 36, 112-117

Lo Presti, D.C.F., et al (1997): Shear modulus and damping of soils. Géotechnique, 47(3), pp. 603-617

Luijendijk, S. (2011): SBW Piping Kunstwerken 4. Bureaustudie inventarisatie problemen en oplossingen piping bij historische kunstwerken, Deltares rapport 1204201-004-GEO-0001.

O'Reilly, M.P., Brown, S.F. (1991): Cyclic Loading of Soils: from theory to design. Blackie and Son Ltd

Samuels, P.G ., Burt, T.N. (2002): A new joint probability appraisal of flood risk, Proceedings of the Institution of Civil Engineers, Water & Maritime Engineering, Vol.154 (2), pp109-115.

Sellmeijer, J. B., (2006): Numerical computation of seepage erosion below dams (piping): Third International Conference on Scour and Erosion, p. 596-601.

Sellmeijer, J. B., Lopez De La Cruz J., Beek V.M. van, Knoeff J.G. (2011): Fine-tuning of the piping model through small-scale, medium-scale and IJkdijk experiments, European Journal of Environmental and Civil Engineering, vol 15/8 2011 pp.1139-1154.

Sharma,S.S., Fahey, M. (2004): Deformation characteristics of two cemented calcareous soils. Canadian Geotechnical Journal: (41):1139-1151

Terzaghi, K., Peck, R.B. (1967): Soil mechanics in engineering practice. John Wiley and Sons, New York.

Van Beek, V., Förster, U. (2012): SBW Piping: 2B. Bureaustudies fysische onderbouwing aangepaste rekenregel, tijdsafhankelijkheid en heterogeniteit, Deltares rapport 1204201-002-GEO-0001.

Van Paassen L.A., Daza C.M., Van Loosdrecht M.C.M., Kleerebezem R., Van der Star W.R.L. and Van der Zon W.H. (2007): Patent WO2007069884. Stichting GeoDelft.

Van Paassen L.A. (2009): Biogrout, Ground improvement by microbially induced carbonate precipitation. Ground Improvement Journal. Delft, Delft University of Technology. PhD 202.

Van Paassen L.A., Ghose R., Van der Linden T.J.M., Van der Star W.R.L. and Van Loosdrecht M.C.M. (2010a): Quantifying biomediated ground improvement by ureolysis: Large-scale BioGrout experiment. J Geotechn Geoenv Eng 136(12): 1721-1728.

Van Paassen L.A., Pieron M., Mulder A., Van der Linden T.J.M., Van Loosdrecht M.C.M. and Ngan-Tillard D.J.M. (2010b): Strength and deformation of biologically cemented sandstone. in Vrkljan, Ed. ISRM Regional conference EUROCK 2009 – Rock engineering in difficult ground conditions – Soft rocks and karst, Dubrovnik, Croatia Taylor and Francis Group 405-410.

Van Paassen L.A. (2011): Bio-mediated ground improvement: From laboratory experiment to pilot applications. Geofrontiers Congress 2011: Advances in Geotechical Engineering.

M.A. Van, G.A. van den Ham, M. Blauw, M.Latil, N. Benahmed, P. Philippe, 'Preventing Internal Erosion Phenomena with the BioGrout process', Proceedings of the 15th European Conference on Soil Mechanics and Geotechnical Engineering, A. Anagnostopoulos et al. (Eds.), IOS Press, Athens, 2011.

Whiffin V.S. (2004): Microbial $CaCO_3$ Precipitation for the production of Biocement. Science and Engineering, School of Biological Sciences & Biotechnology Perth, Western Australia, Murdoch University. Ph.D thesis 154.

Whiffin V.S., Van Paassen L.A. and Harkes M.P. (2007): Microbial Carbonate Precipitation as a Soil Improvement Technique. Geomicrobiol J 24(5): 417-423.

Appendixes

A Extra results for Strat1a

The figures show the concentration of bacteria at several times, the pressure during injection and during extraction and the pore water velocity as a function of location for Strat1a.

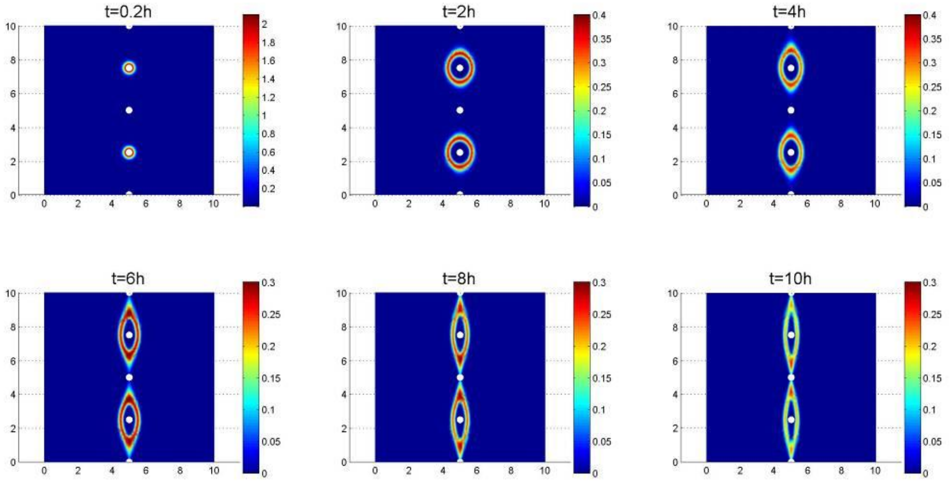

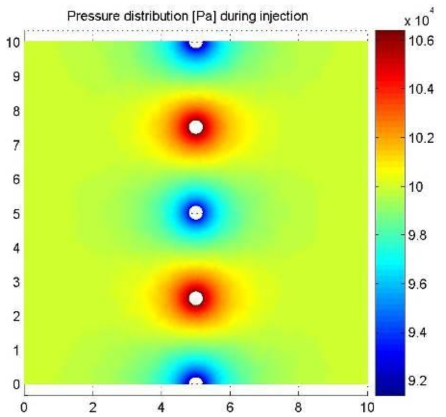

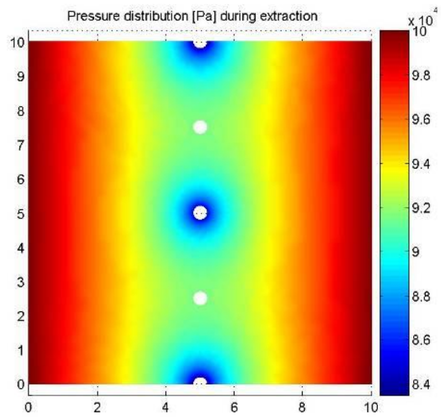

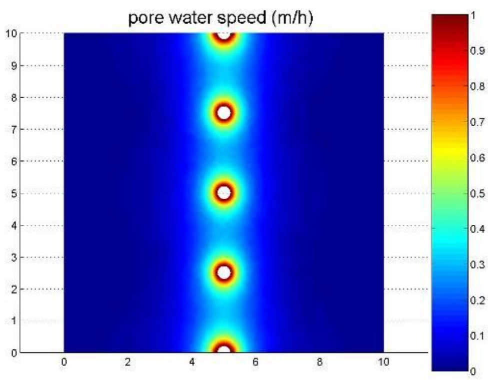

B Extra results for Strat1b

The figures show the concentration of bacteria at several times, the pressure during injection and during extraction and the pore water velocity as a function of location for Strat1b.

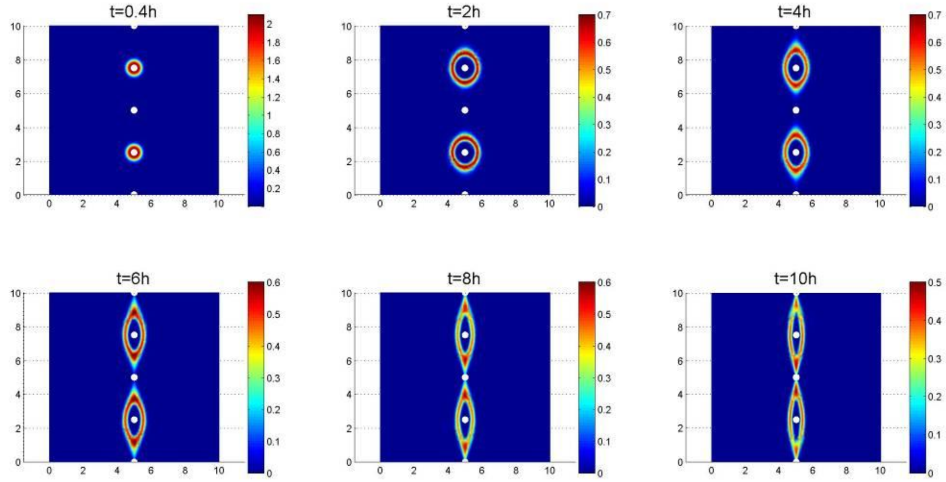

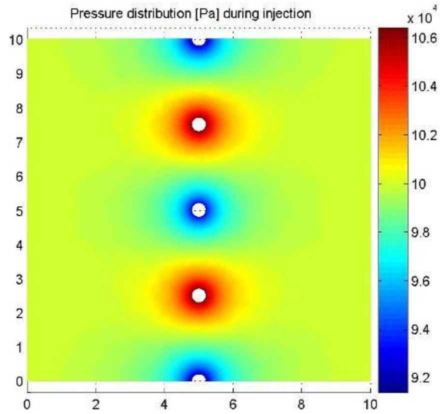

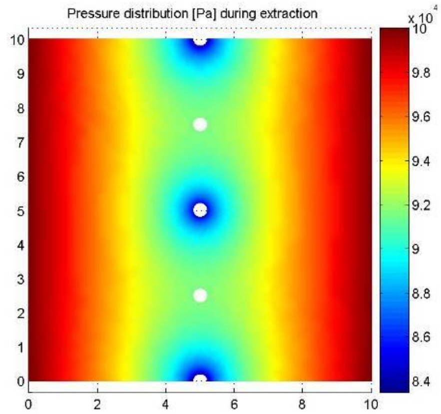

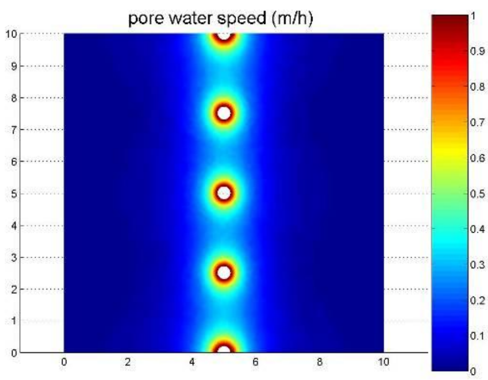

C Extra results for Strat2a

The figures show the concentration of bacteria at several times, the pressure during injection and during extraction and the pore water velocity as a function of location for Strat2a.

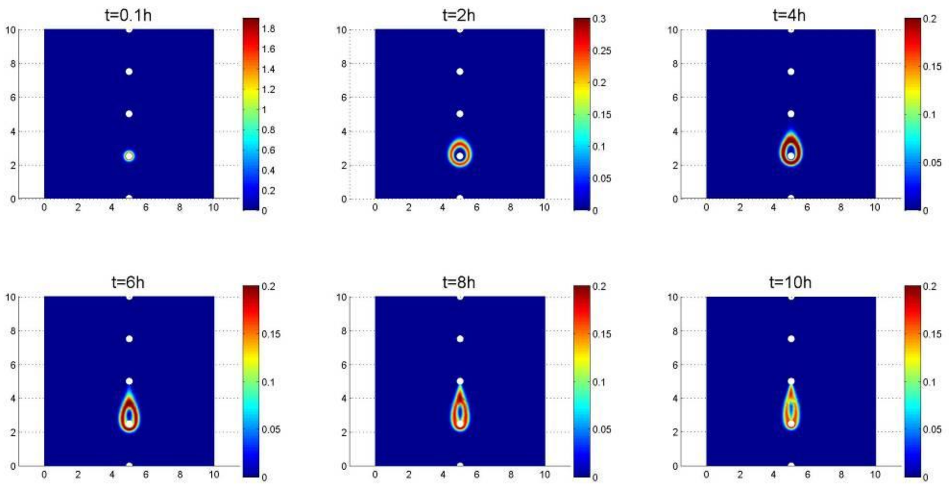

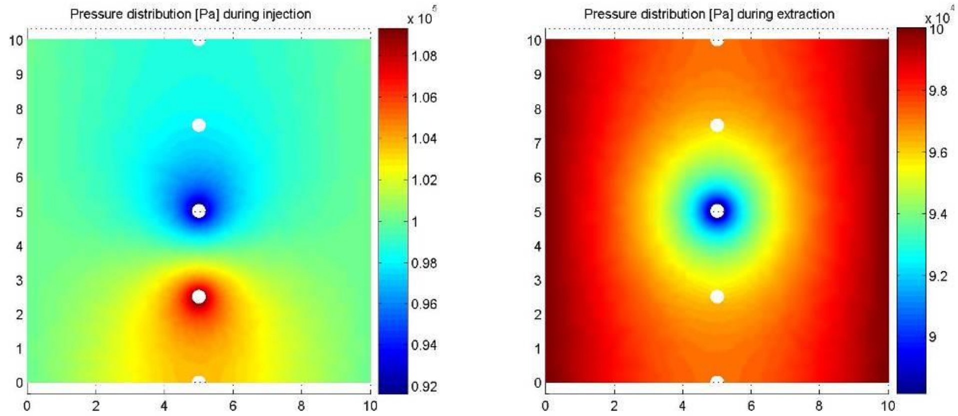

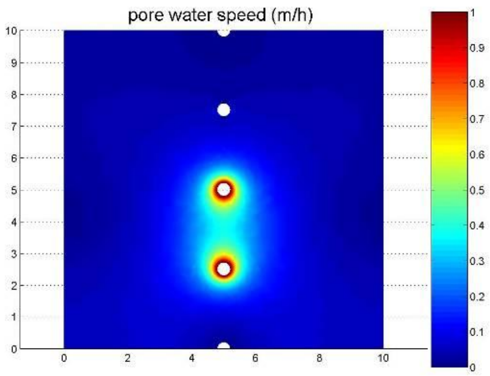

D Extra results for Strat2b

The figures show the concentration of bacteria at several times, the pressure during injection and during extraction and the pore water velocity as a function of location for Strat2b.

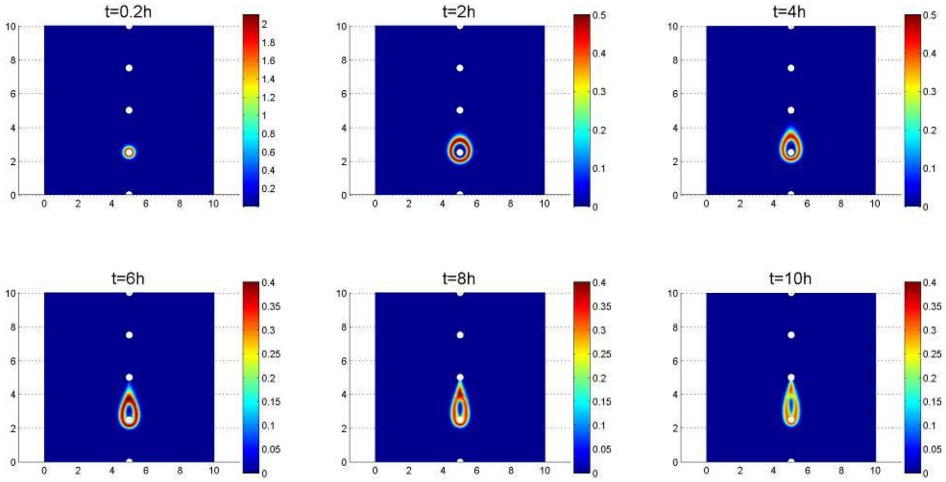

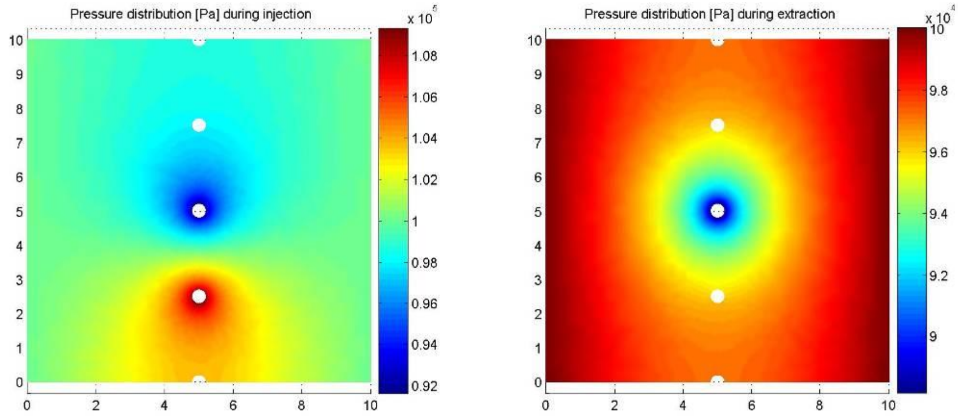

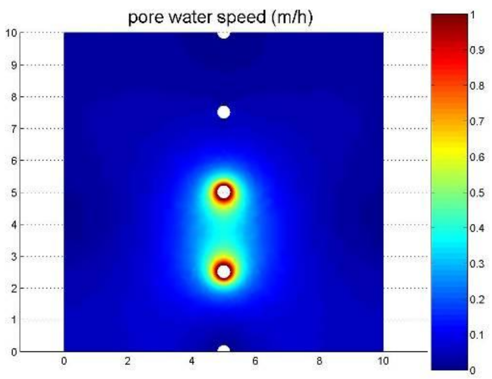

E Extra results for Strat3a

The figures show the concentration of bacteria at several times, the pressure during injection and during extraction and the pore water velocity as a function of location for Strat3a.

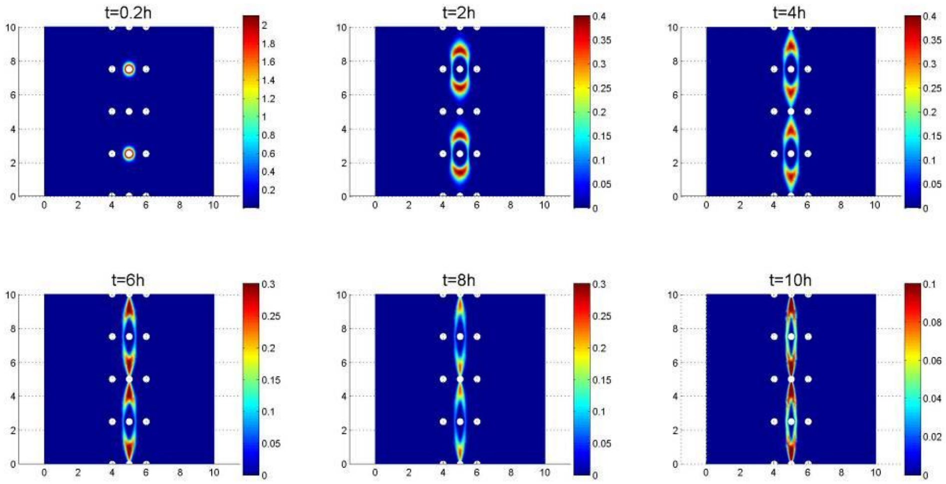

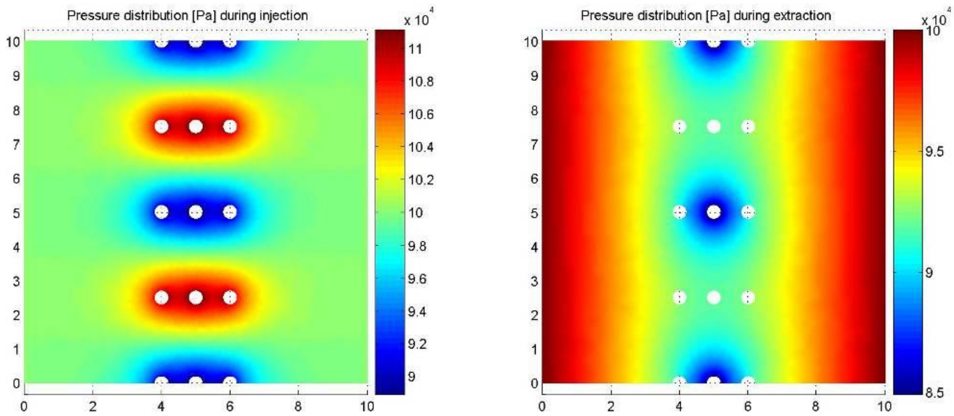

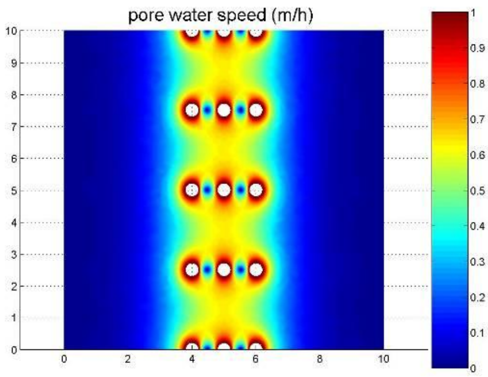

F Extra results for Strat3b

The figures show the concentration of bacteria at several times, the pressure during injection and during extraction and the pore water velocity as a function of location for Strat3b.

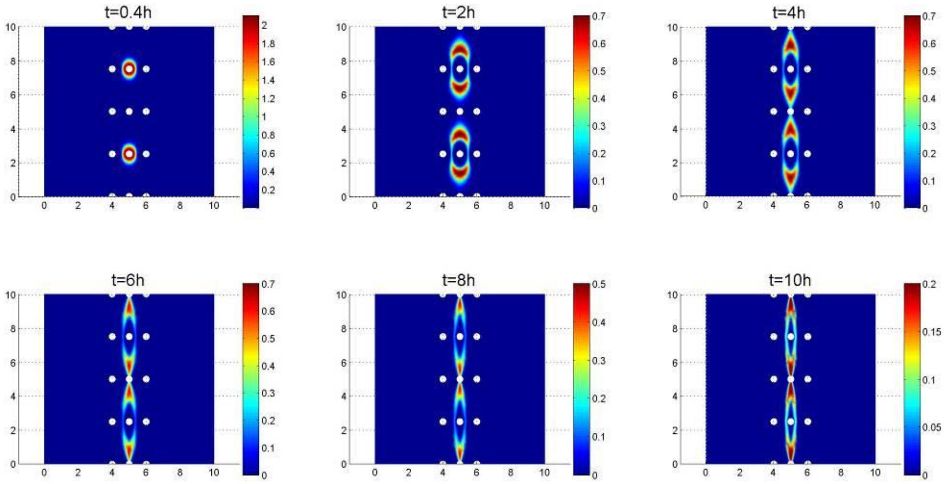

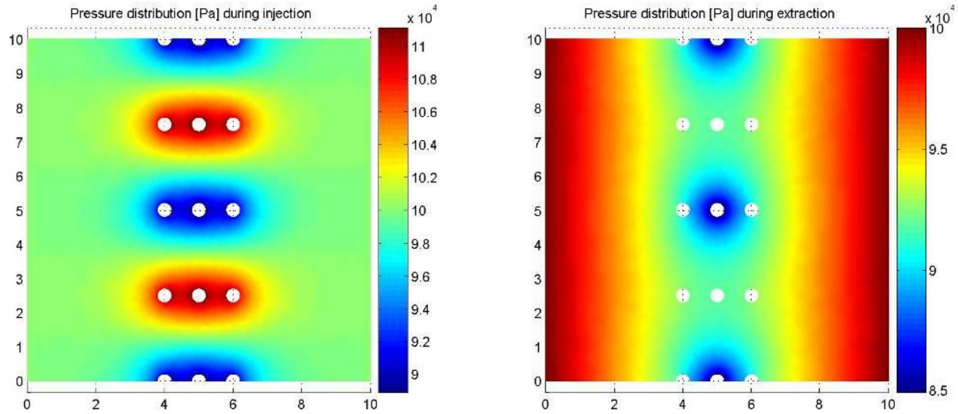

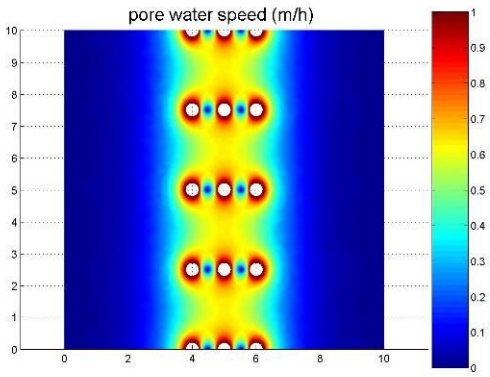

G Extra results for Strat4a

The figures show the concentration of bacteria at several times, the pressure during injection and during extraction and the pore water velocity as a function of location for Strat4a.

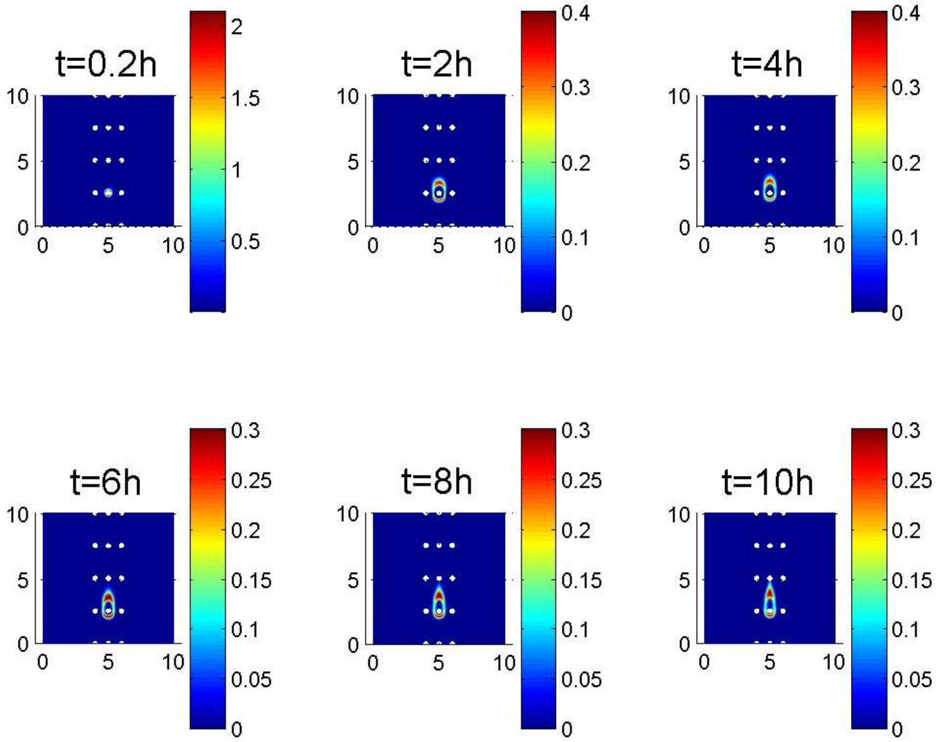

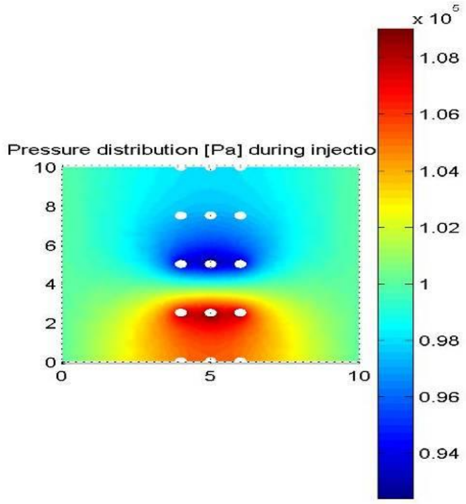
Pressure distribution [Pa] during injectio
x 10^5

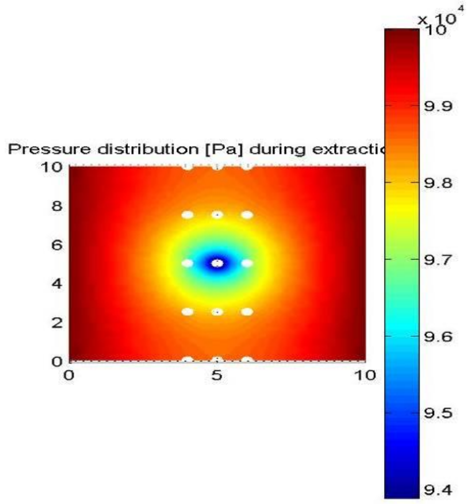
Pressure distribution [Pa] during extractio
x 10^4

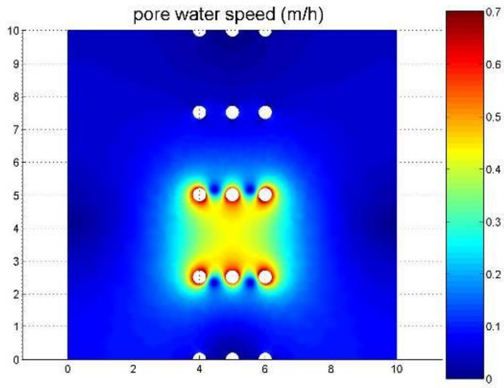
pore water speed (m/h)

H Extra results for Strat4b

The figures show the concentration of bacteria at several times, the pressure during injection and during extraction and the pore water velocity as a function of location for Strat4b.

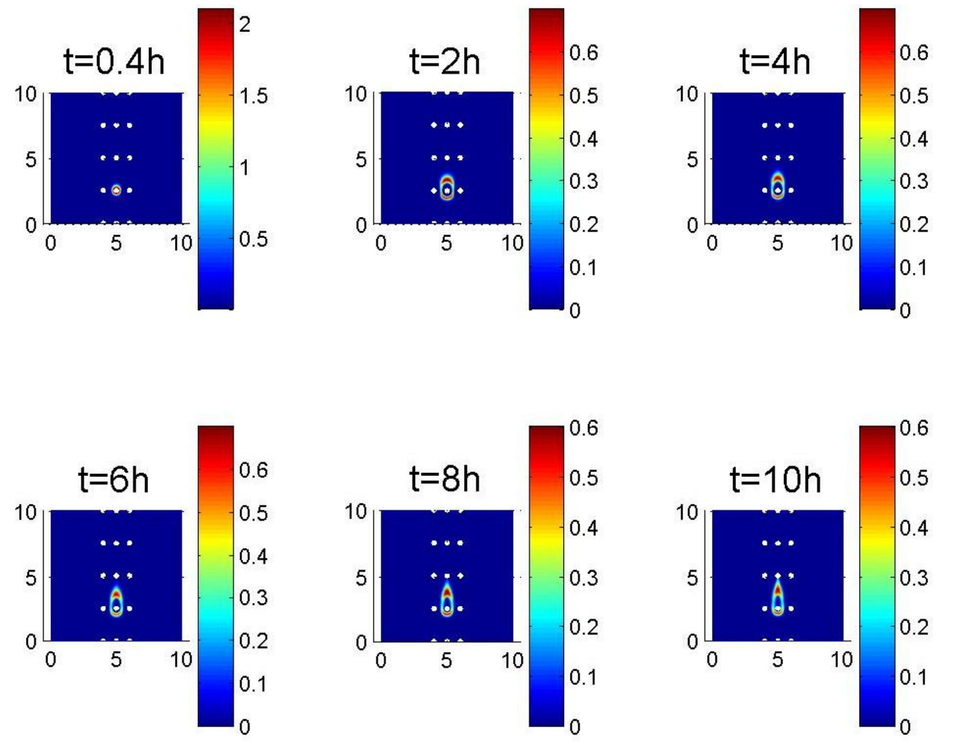

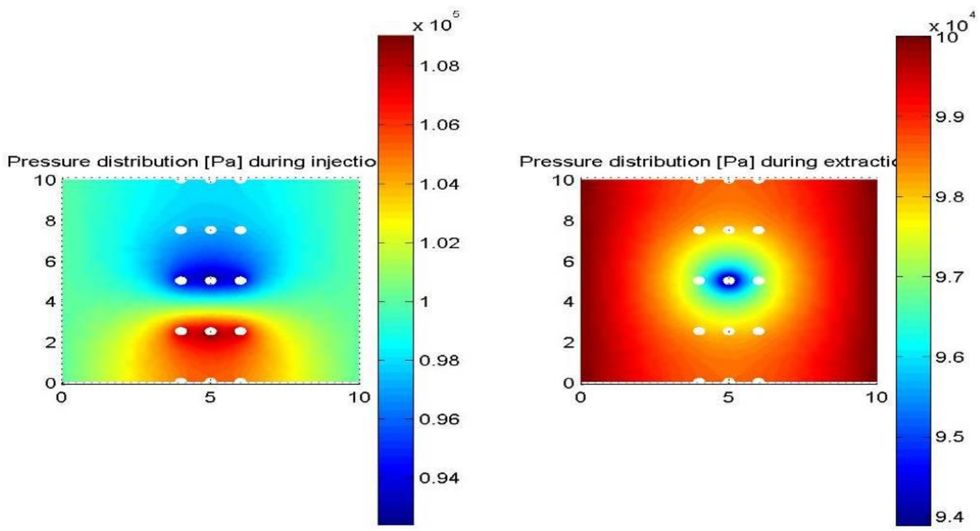

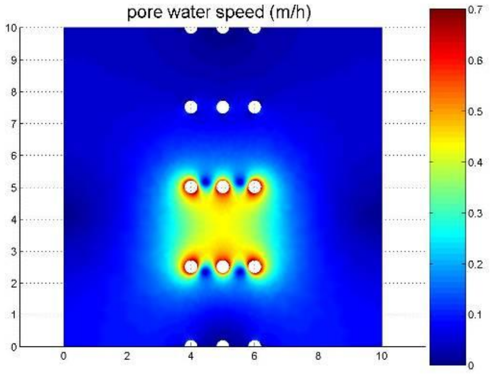
pore water speed (m/h)
0
1
2
3
4
5
6
7
8
9
10
0
2
4
6
8
10
0.7
0.6
0.5
0.4
0.3
0.2
0.1
0

I Extra results for Strat5a

The figures show the concentration of bacteria at several times, the pressure during injection and during extraction and the pore water velocity as a function of location for Strat5a.

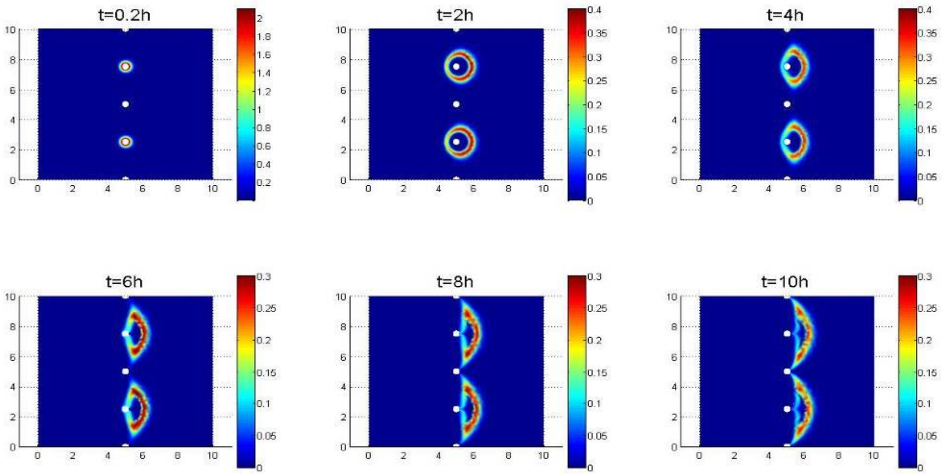

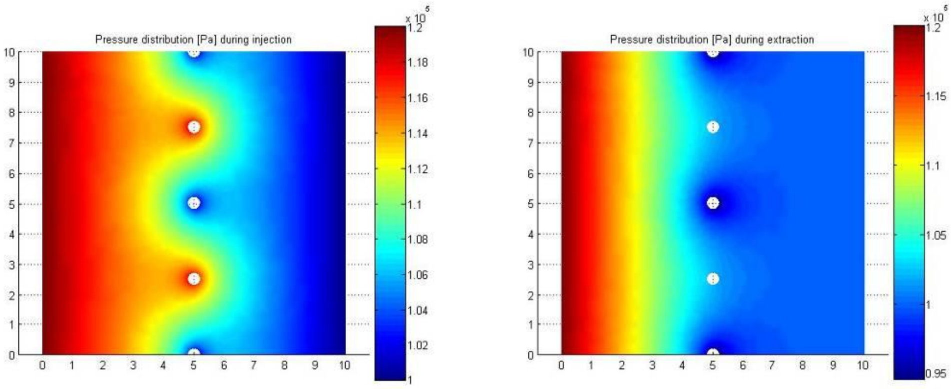

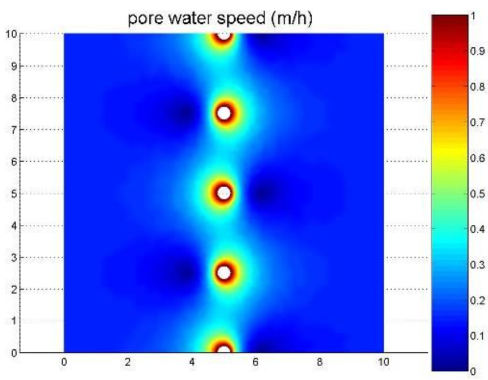

J Extra results for Strat6a

The figures show the concentration of bacteria at several times, the pressure during injection and during extraction and the pore water velocity as a function of location for Strat6a.

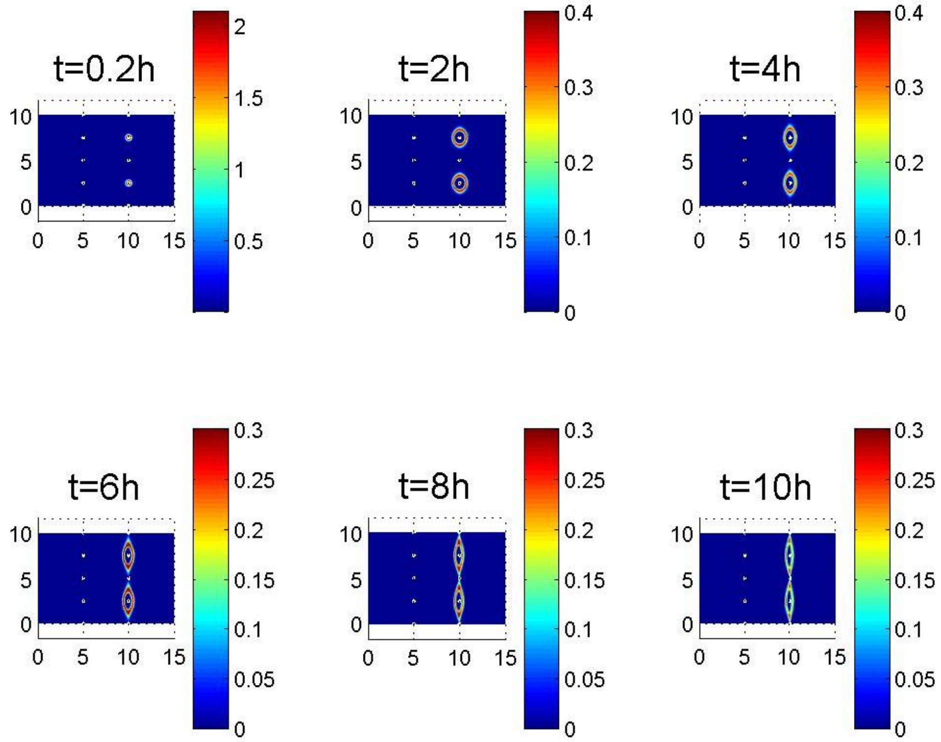

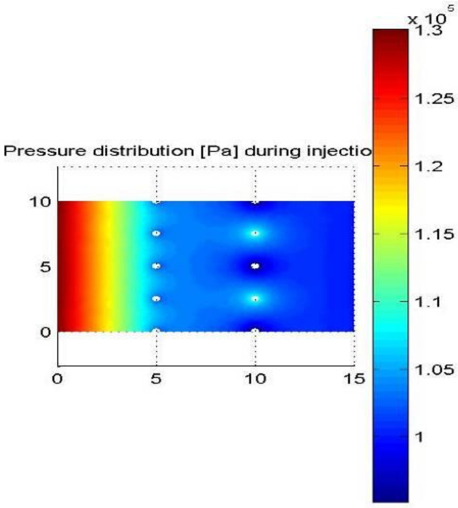
Pressure distribution [Pa] during injectio
x 10^5
1.3
1.25
1.2
1.15
1.1
1.05
1
10
5
0
0 5 10 15

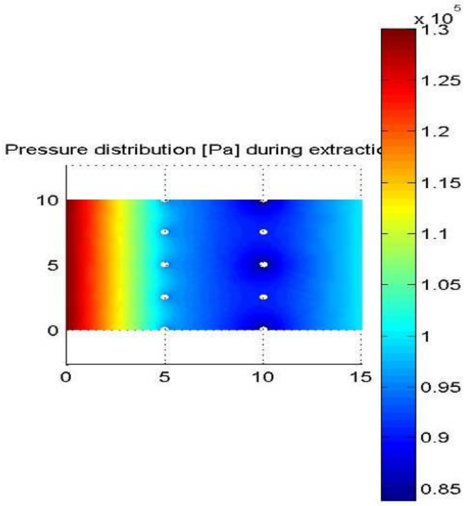
Pressure distribution [Pa] during extractio
x 10^5
1.3
1.25
1.2
1.15
1.1
1.05
1
0.95
0.9
0.85
10
5
0
0 5 10 15

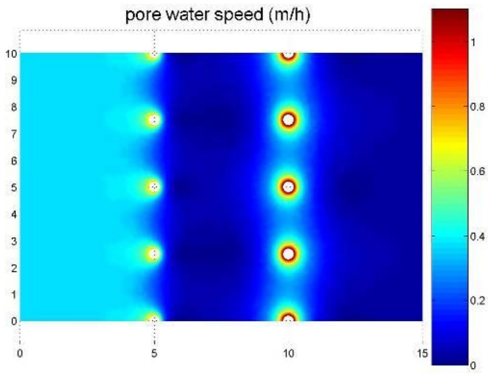
pore water speed (m/h)
1
0.8
0.6
0.4
0.2
0
0 5 10 15

K Extra results for Strat7a

The figures show the concentration of bacteria at several times, the pressure during injection and during extraction and the pore water velocity as a function of location for Strat7a.

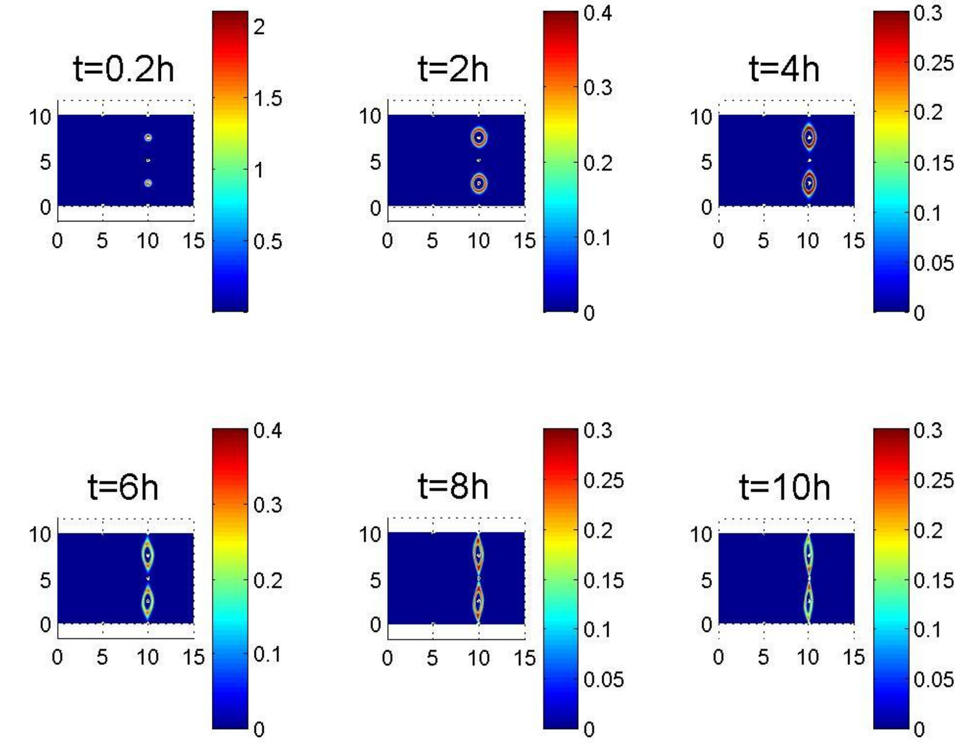

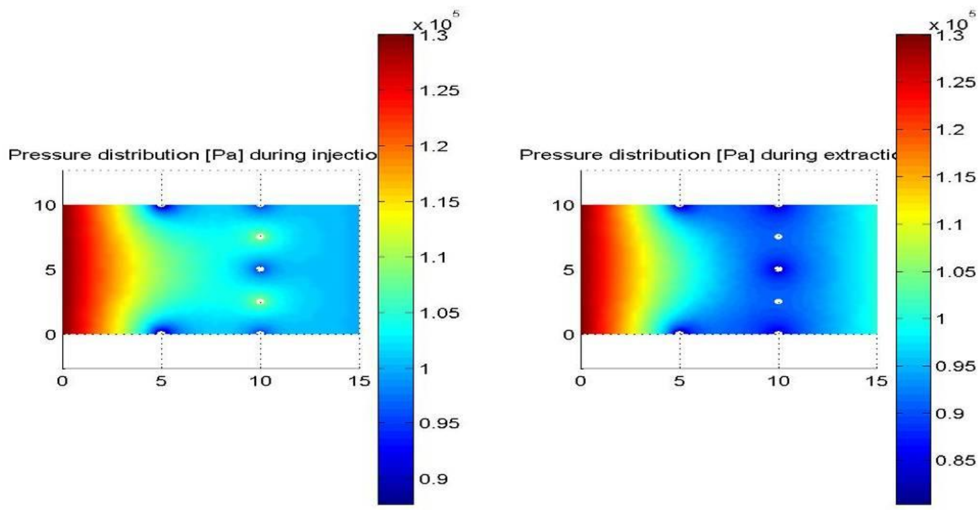

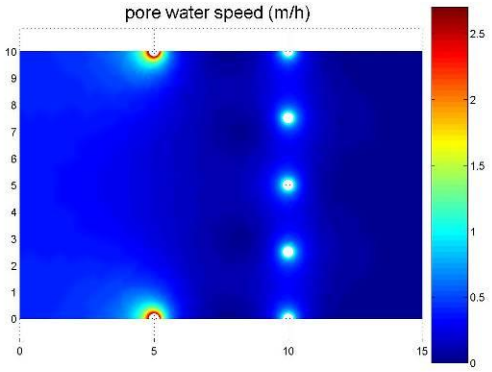
pore water speed (m/h)
0
1
2
3
4
5
6
7
8
9
10
0
5
10
15
0
0.5
1
1.5
2
2.5